Identification and characterization of cancer stem cells in cutaneous malignant melanoma

Dissertation zur Erlangung des akademischen Grades des Doktors der Naturwissenschaften (Dr. rer. nat.)

eingereicht im Fachbereich Biologie, Chemie, Pharmazie der Freien Universität Berlin

vorgelegt von

Yvonne Welte
aus Altdöbern

2013

1. Gutachter: Prof. Dr. Hans Lehrach,
Max-Planck-Institut für Molekulare Genetik

2. Gutachter: Prof. Dr. Petra Knaus,
Freie Universität Berlin

Disputation am 23.04.2013

Acknowledgment

An erster Stelle möchte ich meinem Mentor Dr. Christian RA Regenbrecht danken, durch dessen Engagement das vorliegende Projekt ins Leben gerufen wurde und dessen Unterstützung in den vergangenen Jahren unschätzbar war.

Für die konstruktiv kritische Begutachtung meiner Arbeit und Erstellung des Erstgutachtens sowie die Möglichkeit meine Doktorarbeit zwei Jahre am MPI für molekulare Genetik durchzuführen gilt Prof. Hans Lehrach besonderer Dank.

Frau Prof. Petra Knaus danke ich ganz herzlich für die Übernahme des Zweitgutachtens und den interessanten und wertvollen wissenschaftlichen Austausch vor allem während der Doktorandensymposien sowie die Zeit für persönliche Gespräche.

Ein großes Dankeschön geht an Dr. Gabriele Zybarth für die Korrektur und Unterstützung bei der Anfertigung meiner Dissertation sowie für viele Tipps und Anregungen bezüglich wissenschaftlicher Fragestellungen.

Für das große Interesse an den wissenschaftlichen und methodischen Fragestellungen dieser Doktorarbeit und die bereichernden Diskussionen insbesondere auf dem Gebiet der humanen Stammzellen möchte ich ebenfalls Dr. James Adjaye danken.

Besonderer Dank gilt allen Kollegen unserer Arbeitsgruppe Tumorstammzellen für die gute Zusammenarbeit und das gute Arbeitsklima. Erwähnen möchte ich v.a. Janne Saint-Paul, die leider viel zu kurz für tatkräftige Unterstützung und viel Sonnenschein in unserer Arbeitsgruppe gesorgt hat und Wasco Wruck, der die Genexpressions- und Sequenzierungsdaten ausgewertet und für mich verständlich erklärt hat sowie Dr. Torben Redmer, Isabel Walz und Dorothea Przybilla.

Auf diesem Wege möchte ich mich außerdem bei allen ehemaligen Kollegen aus der Dermatologie sowie den Kollegen aus der Tumorpathologie bedanken für die nicht zuletzt auch seelische Unterstützung, Motivation und die angenehme Zusammenarbeit während der letzten Jahre.

Für das fortgesetzte wissenschaftliche Interesse und die Möglichkeit diese Arbeit am Institut für Pathologie erfolgreich abzuschließen, gilt dem TREAT 20 Konsortium, insbesondere Prof. Manfred Dietel und Prof. Reinhold Schäfer, großer Dank.

Ein großes Dankeschön geht natürlich auch an unsere Kooperationspartner aus Buxtehude Beate Volkmer, Rüdiger Greinert und Alexandra Faust für die höchst angenehme und fruchtvolle Zusammenarbeit.

Für die Unterstützung bei den Durchführungen der Sequenzierungen und Genexpressions-analysen danke ich Bernd Timmermann und Aydah Sabah.

Ein großes Dankeschön gilt außerdem den Mitarbeitern der EPO GmbH für die Durchführung der *in vivo* Versuche und den Mitarbeitern der FACS Facility am DRFZ für das Sortieren der Melanomzellen.

Ausgesprochen großer Dank gilt meinen Freunden und meiner Familie, insbesondere meinen Eltern, die mich in allem, was ich bisher angepackt habe, bedingungslos unterstützten, auch wenn ich keine Frau Dr. Wachtel mehr wurde.

Nicht zuletzt möchte ich Markus Welte ganz besonders danken. Seine stetige Unterstützung, Motivation und Ablenkung, seine unendliche Geduld und sein Humor waren und sind unschätzbar. Merci pour tout!

Contents

Abbreviations

µg	micrograms
µl	microlitres
µm	micrometer
µM	micromol
Ab	antibody
ABC transporter	ATP-binding cassette transporters
ALM	acral lentiginous melanoma
AP	alkaline phosphatase
ATP	adenosine triphosphate
a.u.	arbitrary unit
bFGF	basic fibroblast growth factor (synonyms FGF2, FGF-β)
bp	base pairs
BSA	bovine serum albumin
°C	degree Celsius
cAMP	cyclic adenosine monophosphate
cDNA	complementary desoxyribonucleic acid
cm	centimeter
Ct	threshold cycle
CTP	cytidine triphosphate
d	day(s)
DAPI	4′,6-Diamidino-2-phenylindole dihydrochloride
dH_2O	double destilled water
DMEM	Dulbecco's modified Eagle's medium
DMSO	dimethyl sulfoxide
DNA	deoxyribonucleic acid
dNTP	deoxyribonucleotide triphosphate
ds	double stranded
ECL	enhanced chemoluminescence analysis
E. coli	*Escherichia coli*
EDTA	ethylenediaminetetraacetic acid
EGFP	enhanced green fluorescent protein
ELISA	enzyme-linked immunosorbent assay
EMT	epithelial-to-mesenchymal transition
ERK	extracellular signal-regulated kinase
et al. (*lat.*)	et altera; and others
FACS	fluorescence-activated cell sorting
FCS	fetal calf serum
g	gram / gravity
GO	Gene Ontology
GTP	guanosine triphosphate
h	hour
HE	hemotoxilin/eosin
hESC	human embryonic stem cells
HEPES	(4-(2-hydroxyethyl)-1-piperazineethanesulfonic acid)
HH	hedgehog
IC_{50}	half maximal (50%) inhibitory concentration (IC) of a substance
kb	kilobase
KEGG	Kyoto Encyclopedia of Genes and Genomes
l	liter
LB medium	lysogeny broth medium
LMM	lentigo maligna melanoma
µ	micro
M	molar

MACS	magnetic-activated cell sorting
MAPK	mitogen-activated protein kinase
MCS	multiple cloning site
MET	mesenchymal-to-epithelial transition
mg	milligram
min	minute
ml	millilitre
mM	millimolar
mRNA	messenger-RNA
MTT	3-(4,5-Dimethylthiazol-2-yl)-2,5-diphenyltetrazolium bromide
NA	not available
NaN	not a number (undefined value)
nd	not determined
NEAA	non-essential amino acids
ng	nanogram
nm	nanometer
NM	nodular melanoma
NOD/SCID	none-obese diabetic / severe combined immunodeficiency
NSG	NOD/SCID gamma (NOD/SCID mice lacking the interleukin 2 receptor gamma chain)
PBS	phosphate buffered saline
PBST	phosphate buffered saline with 0.1% Tween 20
PCR	polymerase chain reaction
PFA	paraformaldehyde
pH	negative decimal logarithm of the hydrogen ion activity in a solution
PI	propidium iodide
PI3K	phosphatidylinosytol-3-kinase
POMC	pro-opiomelanocortin
PS	penicillin streptomycin
Q263	Quantum 263 medium
RNA	ribonucleic acid
ROS	reactive oxygen species
rRNA	ribosomal RNA
rpm	rounds per minute
RT	reverse transcription
s	second
SAM	Sequence Alignment/Map
SDS	sodium dodecyl sulfate
SDS-PAGE	sodium dodecyl sulfate polyacrylamid gel electrophoresis
SIFT	sorting intolerant from tolerant
SP	side population
SR	serum replacement
SSM	superficial spreading melanoma
TBS	Tris-buffered saline
TBST	Tris-buffered saline with 0.05 % Tween-20
TE	Tris/EDTA
TEMED	tetramethylethylenediamine
TGF-β	transforming growth factor β
TTP	thymidine triphosphate
UTR	untranslated region
UV	ultraviolett
V	volt
vs	versus
WHO	World health organization

List of figures

List of tables

Abstract in English

Cutaneous malignant melanomas result from neoplastic growth of melanocytes and are the most severe type of skin cancer. To improve overall survival, a better understanding of melanoma tumorigenesis is needed. Recent findings suggest that within almost all solid tumors in anology to hematopoetic tumors a small subpopulation of tumor cells exculsively have tumor initiating and propagating capacity. These so called cancer stem cells (CSCs) might also be the reason for the high rate of therapy failure, tumor relapse and metastasis.

This study was aimed at establishing useful methods and identifying markers or combinations of markers to characterize CSCs in low-passage melanoma cells. After establishing primary melanoma cell cultures I identified subpopulations of melanoma cells that express CD133, which is correlated with asymmetric cell division and downregulated upon cell differentiation and OCT4A the master regulator of pluripotency. I enriched $CD133^+$ as well as $OCT4A^+$ cells from the bulk and found that crucial regulatory pathways related to oncogenesis and stemness such as Wnt, Hedgehog and Notch signaling are significantly overexpressed in the respective positive populations. I validated these results for the TGF-β signaling pathway, which is crucial to maintain the undifferentiated state in human embryonic stem cells (hESCs) on the protein level. I found this cascade exclusively activated in $CD133^+$ melanoma cells. In addition, an overlap of both putative CSC populations was indicated by the overexpression of OCT4A in the $CD133^+$ subpopulation compared to $CD133^-$ melanoma cells and vice versa. *In vivo* experiments showed enhanced tumor growth capabilities of $CD133^+$ and $OCT4A^+$ melanoma cells compared to their negative counterparts. Thus, $CD133^+$ and particularly $OCT4A^+$ melanoma cells comprise both the characteristics of stem-like cells and malignant tumors and provide strict criteria for self-renewal and asymmetric cell division to hold up the term of CSCs in solid tumors. Targeting these cells may lead to a more successful tumor intervention in the future. The dynamic conversion of tumor cell phenotypes that I have observed in my work could substantially hamper a successful therapeutic intervention. Until recently it was believed that tumor heterogeneity was due to a strict hierarchical order where only dedicated CSCs could fuel tumor-development and -fate in an unidirectional manner. My results indicate that a dynamic plasticity between both CSC and bulk tumor populations exists, which would explain tumor survival and rapid adaptation to unfavorable microenvironments like chemo- and radiotherapy. Further characterization of melanoma cancer stem cells and elucidation of the interconversion between tumor cell populations will be an important prerequisite for a lasting prevention of tumor recurrence and metastasis and may pave the way for better understanding tumor biology.

Abstract in German

Das kutane maligne Melanom, eine bösartige Entartung der Melanozyten, stellt die gefährlichste Form von Hautkrebs dar. Um die Gesamtüberlebenszeit der Melanom-patienten zu verlängern, ist ein besseres Verständnis der Mechanismen der Melanom-Tumorigenese notwendig. Studien legen nahe, dass fast alle soliden Tumore genau wie hämatopoetische Tumoren eine kleine Subpopulation von Tumorzellen enthalten, die ausschließlich die Fähigkeit zur Tumorinitiierung und Selbsterneuerung besitzen. Diese sogenannten Krebsstammzellen stellen vermutlich auch die Ursache für das häufige Therapieversagen, sowie das Auftreten von Tumorrezidiven und Metastasen dar.

Ziel dieser Arbeit war die Etablierung geeigneter Methoden und Identifizierung eines geeigneten Markers oder einer Markerkombination für die Charakterisierung von Krebsstammzellen in primären, niedrig-passagigen Melanomzellen. Nach Etablierung primärer Melanom-Zellkulturen habe ich Subpopulationen von Melanomzellen identifiziert, die CD133 exprimieren, einem Marker, der mit asymmetrischer Zellteilung korreliert und während der Zelldifferenzierung herunterreguliert wird, sowie OCT4A, den wichtigsten Regulator der Pluripotenz. Ich habe $CD133^+$ und $OCT4A^+$ Zellen aus den Melanomkulturen isoliert und herausgefunden, dass wichtige regulatorische Entwicklungs- sowie krebsbezogene Signalwege wie Wnt, Hedgehog und Notch signifikant in diesen Marker-positiven Populationen hochreguliert sind. Für den TGF-β-Signalweg, der in humanen embryonalen Stammzellen essenziell ist, um den undifferenzierten Zustand zu erhalten, habe ich diese Ergebnisse auf Proteinebene validiert. Die TGF-β-Kaskade war ausschließlich in $CD133^+$ Melanomzellen aktiviert. Eine Überschneidung von beiden putativen Krebsstammzell-Populationen wurde außerdem durch Überexpression von OCT4A in der $CD133^+$ Subpopulation im Vergleich zur $CD133^-$ Fraktion und vice versa angezeigt. *In vivo* Experimente zeigten schließlich, dass $CD133^+$ und $OCT4A^+$ Melanomzellen stärkere Tumor-initiierende und -propagierende Eigenschaften besitzen als $CD133^-$ und $OCT4A^-$ Zellen. Somit weisen $CD133^+$ und $OCT4A^+$ Melanomzellen sowohl die Eigenschaften von Stammzellen als auch malignen Tumorzellen auf und bieten strenge Kriterien für Selbsterneuerung und asymmetrische Zellteilung, um dem Begriff Krebsstammzellen in soliden Tumoren gerecht zu werden. Auf diese Zellen gerichtete Therapien könnten in der Zukunft effizientere Strategien zur Heilung von Melanompatienten darstellen. Die dynamische Konversion von Tumorzell-Phänotypen, die ich während meiner Doktorarbeit beobachtet habe, könnte eine erfolgreiche therapeutische Intervention jedoch erschweren. Bis vor kurzem wurde angenommen, dass die Heterogenität in Tumoren einer strikten Hierarchie unterliegt, in der nur

Krebsstammzellen die Tumorentwicklung und das Tumorschicksal in einer streng unidirektionalen Weise steuern. Ich habe gezeigt, dass stattdessen eine dynamische Plastizität zwischen Krebsstammzell- und nicht-stammzellartigen Populationen existiert, die das Tumorüberleben und eine rasche Adaption an Veränderungen im Tumorumfeld wie bei Chemo- und Strahlentherapie erklären. Eine weitere Charakterisierung der Melanom-Krebsstammzellen und Aufklärung der gegenseitigen Umwandlung von Tumorzellpopulationen wird die Voraussetzung für eine langanhaltende Verhinderung von Tumorrezidiven und Metastasen sein und den Weg für ein besseres Verständnis der Tumorbiologie ebnen.

1 Introduction

1.1 Human skin

The skin is the largest multifunctional organ of the human body. It provides sensation, thermoregulation, metabolic, and immune functions as well as protection from dehydration, microorganisms and physical and chemical injury (Wysocki 1999). It consists of two layers, the epidermis and dermis, separated by the basement membrane. The schematic structure of the skin with its most important components is shown in Figure 1.1. The epidermis, a stratified squamous epithelium, represents the outer layer of the skin and is composed of five sublayers, the stratum basale, stratum spinosum, stratum granulosum, stratum licidum and stratum corneum. Within the epidermis four types of specialized cells are located: keratinocytes which regulate immune and inflammatory responses in the skin (Shirakata 2010); melanocytes which produce the pigment melanin; Langerhans cells which are a prerequisite for T cell antigen presentation (Kaplan 2010) and Merkel cells which act as mechanoreceptors (Lucarz *et al.* 2007).

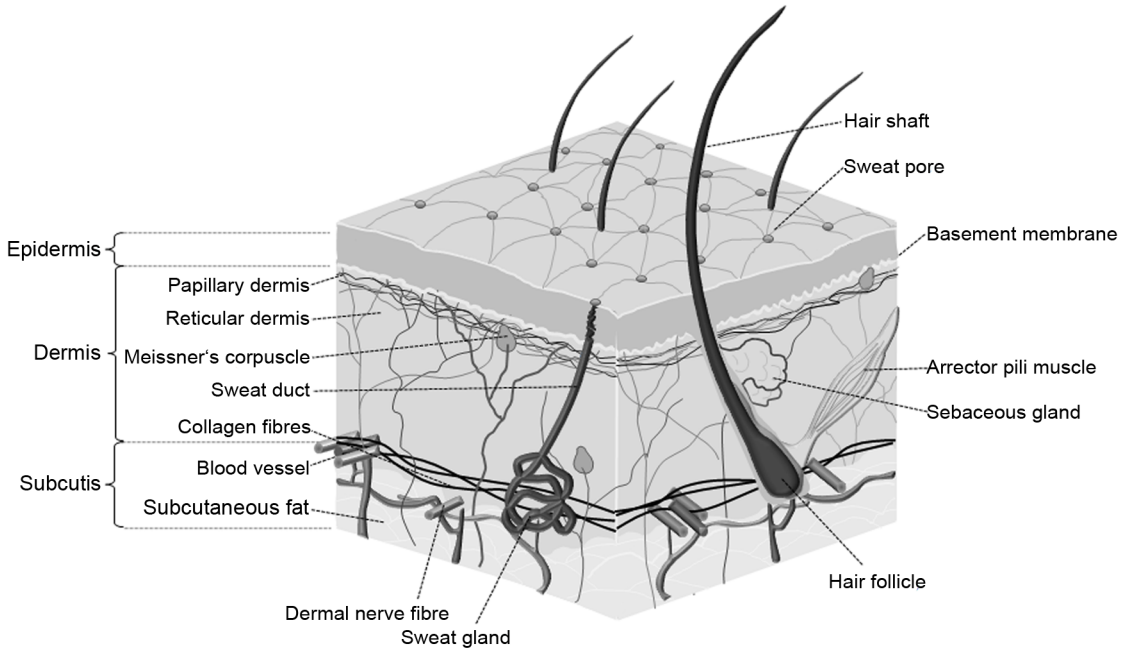

Figure 1.1: Schematic structure of the human skin.
Shown are the two layers of the skin, the epidermis and dermis as well as the subcutis with its most important components like collagen fibres, sweat glands, nerves and hair follicles.

The epidermis is maintained by mitosis of cells within the stratum basale. Differentiating cells delaminate from the basement membrane and are displaced outwards through the epidermal layers. Finally, these cells flatten, die and are repelled as corneocytes. In this way, the entire epidermis is renewed about every 28 days (Hoath *et al.* 2003). The dermis

possesses important functions like stabilization of the skin and immune defense and consists of the papillary and reticular layer. These layers in turn, contain collagen fibres, immune cells, blood vessels and nerves. The subcutis is a layer of fat and connective tissue below the dermis that comprises larger blood vessels, hair follicles, sweat glands and nerves. This layer is important for the temperature regulation of the skin itself and the body.

1.1.1 Melanogenesis

About 2000 melanocytes per mm^2 are located in the stratum basale of the epidermis (Fukunaga-Kalabis *et al.* 2006, Hoath *et al.* 2003). They originate from highly migratory embryonic cells of the so called neural crest (Uong *et al.* 2010). The cutaneous melanocyte homeostasis as well as melanocyte migration to the epidermis, function, and its survival are all dependent on the interaction of the stem cell factor (SCF) with its tyrosine kinase receptor, C-KIT (Grichnik *et al.* 1998). In specific cytoplasmic organelles called melanosomes melanocytes synthesize and deposite the pigment melanin. Melanocytes produce two main types of melanin, the dark brown to black eumelanin and the reddish-yellow pheomelanin. The ratio of eumelanin and pheomelanin determines the color of the human skin and hair. The higher the eumelanin/pheomelanin ratio the darker the skin (Jimbow *et al.* 1993). Melanin is a polymere of dihydroxyindolecarboxylicacids, and their reduced form is synthesized from the amino acid tyrosine using the enzyme tyrosinase (Orlow 1995). When skin is exposed to UV light the tumor suppressor protein p53 is stabilized in keratinocytes and, in turn, transcriptionally activates the expression of pro-opiomelanocortin (POMC) followed by the production of the melanocytes-stimulating hormone (MSH). Subsequently, MSH is released by keratinocytes to act on resting melanocytes via the melanocortin 1 receptor (MC1R) (Cui *et al.* 2007). Activation of MC1R leads to elevation of cAMP levels within melanocytes, which in turn increases transcription of microphthalmia-associated transcription factor (MITF). In response, tyrosinase is upregulated, the melanocytes proliferate, the number of melanosomes increases and the synthesis of melanin from tyrosine starts (Garibyan *et al.* 2010). Melanin pigment synthesized by each melanocyte is packed in melanosomes and transferred back to an average of 36 keratinocytes. The transferred melanin then forms a cap at the top of the nucleus of mitotically active basal cells, prevents the ultraviolet injurious effects on the genomic DNA and results in tanning of the skin (Bandarchi *et al.* 2010) (compare **Figure 1.2**).

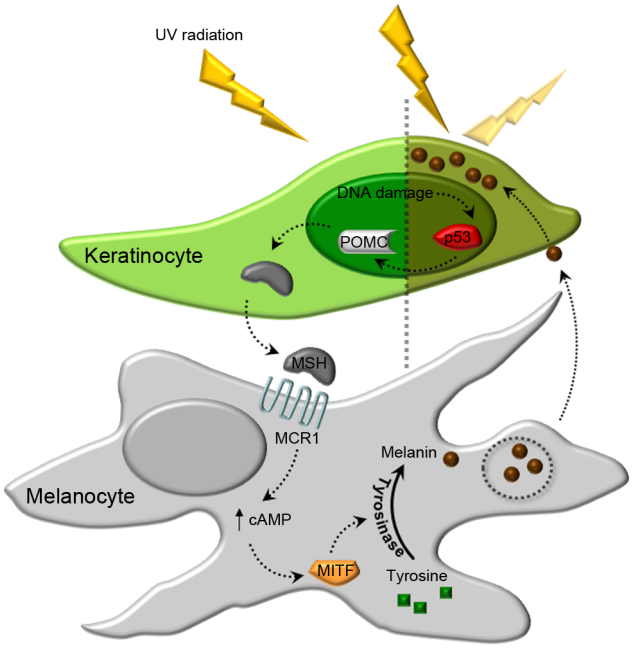

Figure 1.2: Keratinocyte-Melanocyte-Interaction.
Modified from Garibyan *et al.* 2010. UV radiation induced DNA damage leads to stabilization of p53 in keratinocytes, which activates the expression of POMC followed by the production of MSH. MSH is released and activates resting melanocytes via the receptor MC1R. After elevation of cAMP within melanocytes, which in turn increases transcription of MITF, tyrosinase gets upregulated, and the synthesis of melanin from tyrosine starts. Melanin is packed in melanosomes and transferred back to keratinocytes where it forms a cap at the top of the nucleus. This melanin accumulation results in tanning of the skin and protects the cells from further UV induced DNA damage.

1.2 Malignant melanoma

Malignant melanomas represent the neoplastic growth of melanocytes. During the following sections epidemiology, etiology, pathophysiology, diagnosis, classification and therapy of malignant melanoma will be described.

1.2.1 Epidemiology and etiology

The risk factors associated with melanoma include external factors such as exposure to UV radiation and host factors such as family history, history of dysplastic nevi, and high number of nevi (Cho *et al.* 2010). Chronic exposure to UV radiation, particularly during the childhood, as well as intermittent UV exposure causing severe sunburns increases the risk of melanoma development dramatically (Diepgen 2005). In 1992 the International Agency for Research on Cancer (IARC) classified UV radiation from sunlight as a human carcinogen. Upon reaching the skin, photons of UVR are absorbed by electrons of DNA producing excited electron states and leading to DNA damage. UVR can also lead to generation of toxic by-products, which then indirectly damage DNA. A photochemical reaction that takes place after DNA is exposed to UVB usually occurs between pyrimidine dimers and leads to formation of photoproducts known as cyclobutane pyrimidine dimers (CPDs) and pyrimidine 6-4 pyrimidone. Although, for the most part DNA repair enzymes are able to correct this damage, this is an error-prone process. Incorrect repair leads to mutations in epidermal cells, thus initiating the development of cancer. Furthermore, there is growing evidence of the involvement of UVA radiation in development of skin cancer. Upon reaching the skin, UVA radiation that is also used in tanning beds, can generate reactive oxygen species (ROS) capable of causing oxidative DNA damage

(Garibyan *et al.* 2010). Studies showed that exposure to tanning beds increases the risk of malignant melanoma formation, especially in women younger than 45 years (Ting *et al.* 2007).

Individuals with a low eumelanin/pheomelanin ratio have an increased risk to develop malignant melanoma because only eumelanin is able to absorb harmful UV radiation and transform the energy into harmless heat through a chemical process called internal conversion. This photoprotective property prevents UV radiation from reaching genomic DNA where it can cause damage (Garibyan *et al.* 2010). The generation of mutations via UV radiation-induced DNA damage in key tumor suppressor and proto-oncogenes involved in apoptosis, DNA repair, cell cycle regulation, and other essential homeostatic pathways, is believed to represent the driving factors in carcinogenesis. Several reports have implicated UV as a cause of mutations in important melanoma-associated genes such as *INK4A*, *PTEN*, *FGFR2*, *NRAS*, and *BRAF* (Garibyan *et al.* 2010).

Some melanomas arise at sites such as palms, soles, and mucosal surfaces, which do not have direct exposure to UV light. These melanomas are increasingly understood to harbor distinct oncogenic mutations, suggesting different mechanisms of carcinogenesis (Garibyan *et al.* 2010) (see also 1.2.2.1).

There are three main subtypes of skin cancer: basal cell carcinoma, squamous cell carcinoma and malignant melanoma. Malignant melanoma is the least common but most serious type of skin cancer. It comprises only 3% of all malignant tumors of the skin, but due to the increasing frequency and rapid growth and dissemination malignant melanoma accounts for 75% of deaths due to malignant skin tumors (Radovic-Kovacevic *et al.* 1997, Garibyan *et al.* 2010). About 80% of all melanoma cases are diagnosed in the white populations of Northern America, Australia, New Zealand and Europe. In Europe cutaneous melanoma is the 11th most frequent type of cancer with an estimated 84000 cases in 2008 (Ferlay *et al.* 2010a). The incidence for melanoma strongly increased during the last 3 decades; in Germany it increased more than 3-fold from about 4.5 per 100000 in 1980 up to about 15 per 100000 in 2005. In 2008 the melanoma incidence for Germany was 16230 (Ferlay *et al.* 2010b). In females melanoma prevalence is slightly higher compared to men and accounts for 3% of all cancer cases in Europe as well as for 1.2% cancer related deaths. Overall, the estimated number of melanoma related deaths in Europe in 2008 was 20040; in Germany it was 2510 (Ferlay *et al.* 2010a).

While the incidence of melanoma is further increasing, the mortality of melanomas remains more or less stable mainly due to greater awareness resulting in an earlier

diagnosis when compared to the past (Schubert 2011). About 90% of melanomas are diagnosed as primary tumors without metastasis. The tumor-specific 10-year survival for such tumors is around 75–80%. When distant metastases have developed the prognosis decreases dramatically to a median survival in untreated patients of only 6–9 months (Garbe *et al.* 2007).

Prognostic factors for the outcome of malignant melanoma are the age and sex of the patient as well as tumor thickness, histology, body site, ulceration and mitotic index of the tumor. In general the prognosis is most favorable in young, female patients with a thin superficial spreading melanoma (compare 1.2.3.1) which is not located on the trunk, hands or feet, has a low mitotic index and no ulceration (LeBoit *et al.* 2006). Further prognostic markers with clinical relevance especially for thin melanomas are MITF, C-KIT, C-MYC, P53, GP100, MMP-2 and ICAM-1 (LeBoit *et al.* 2006).

1.2.2 Pathophysiology

Tumor progression that originates from human epidermal melanocytes can be classified into six distinct lesional steps: 1) the common acquired melanocytic nevus; 2) a melanocytic nevus with lentiginous melanocytic hyperplasia; 3) a melanocytic nevus with aberrant differentiation and melanocytic nuclear atypia. Lesions of this stage are characterized by a relatively homogenous brown pigmentation with slightly irregular borders. The malignant melanocytes are still confined to the epidermis (melanoma *in situ*); 4) the radial growth phase of primary melanoma, showing more irregular contours and variegations of the pigmentation, and revealing histopathologically involvement of the papillary dermis. When the papillary dermis is filled by neoplastic melanocytes the lesions appear as irregular, unevenly pigmented plaques; 5) the vertical growth phase of primary melanoma; and 6) metastatic melanoma (Clark *et al.* 1984, LeBoit *et al.* 2006).

1.2.2.1 Genetic characteristics in melanoma

Recently, several oncogenic mutations in melanomas involving *NRAS* (15-30%), *BRAF* (50-70%), and *C-KIT* (2%) have been identified. Curtin *et al*. found that 81% of cutaneous melanomas without chronic sun-induced damage had mutations in *BRAF* or *NRAS* (Curtin *et al.* 2005). The *BRAF* gene encodes a serine/threonine kinase that plays a key role in the MAPK signaling pathway and has emerged as an important therapeutic target for melanoma. The most common *BRAF* mutation found in melanomas is a glutamic acid for valine substitution at position 600 (V600E). This mutation leads to constitutive activation of *BRAF*, and subsequently activation of the MAPK pathway (Garibyan *et al.* 2010). Cutaneous melanomas without sun damage with wild type *BRAF* or *NRAS* frequently had increases in the copy number of the genes for *CDK4* and *CCND1*, downstream components

of the RAS–BRAF pathway (Curtin *et al.* 2005). DNA copy gain involving the *AKT3* locus is found in 40-60% of melanomas and leads to overexpression of this oncogene. On the other hand, many tumor suppressors are genetically altered in melanoma. *CDKN2A* is deleted, mutated, or silenced in 30-70% of the melanoma patients. *PTEN* is deleted or mutated in 5–20%, *APAF1* silenced in 40% and *TP53* lost or mutated in 10% of the melanoma patients. Other common gene alterations concern *CCND1* (6-44% amplified) and *MITF* (amplified in 15- 20% of metastatic melanoma) (Palmieri *et al.* 2009, Romano *et al.* 2011). These genetic aberrations may lead to a prospective molecular classification of melanoma in which the biologically distinct subsets share a common oncogenic mechanism, behave clinically in a similar fashion and require similar clinical management (Scolyer *et al.* 2011).

1.2.3 Diagnosis, classification and staging of melanoma

The presence of an irregular pigment network, of black or brown dots irregularly distributed within the lesion, of irregular lines at the periphery of the lesion that are not clearly combined with the pigment network, of a blue-whitish veil below a thick epidermis with hypergranulosis, of an atypical vascular pattern, and of regression structures are of particular value in the diagnosis of melanoma. These criteria for dermatoscopic scoring of atypical melanocytic lesions allow diagnosis of melanoma with a sensitivity of 95% and a specificity of 75% (LeBoit *et al.* 2006). Examples are shown in **Figure 1.3**.

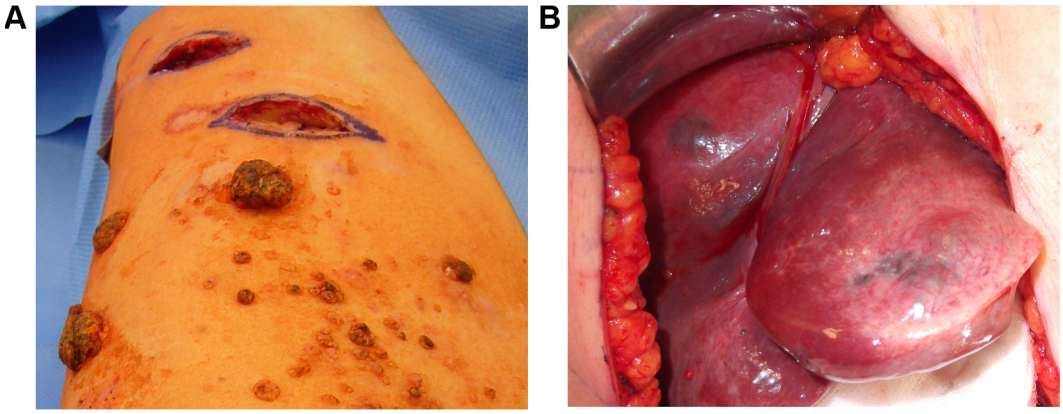

Figure 1.3: Skin and liver melanoma metastases.
Typical melanoma metastases on the skin (A) with irregular pigmentation and lesion borders. Two lesions were already surgically removed. In (B) pigmented liver metastases of a malignant melanoma are shown.

The most common signs of melanoma are considered in the ‘‘ABCD rule’’. This acronym stands for: (A) asymmetry (one half does not match the other), (B) irregular border (the edges are ragged, notched or blurred), (C) color (the pigmentation is not uniform) and (D) diameter (the width is > 6 mm) (Gola Isasi *et al.* 2011). In case of a differential diagnosis between poorly differentiated carcinoma, sarcoma, lymphoma and melanoma a panel of

various differentiation markers is applied. Melanoma is likely if the tumor stains positive for S100β and MART-1 (Ohsie *et al.* 2008).

1.2.3.1 Histological classification

The traditional classification scheme for melanoma according to the WHO is based on clinical and pathological features and includes four major subtypes which were already defined by Clark *et al*. in 1986: superficial spreading melanoma (SSM), nodular melanoma (NM), lentigo maligna melanoma (LMM) and acral lentiginous melanoma (ALM) (Clark *et al.* 1986, Scolyer *et al.* 2011, LeBoit *et al.* 2006). The main criteria for these most common subtypes of malignant melanoma are summarized in **Table 1.1**.

Table 1.1: Criteria for subtypes of malignant melanoma.
Main criteria for the four most common subtypes of malignant melanoma based on the World Health Organization classification of tumors (LeBoit *et al.* 2006).

Superficial spreading melanoma (SSM)				
Clinical features	**Epidemiology**	**Localization**	**Somatic genetics**	**Prognosis**
Radial growth phase comprised of large neoplastic melanocytes before vertical invasion develops	Most frequent type of melanoma ≈ 66% of all melanomas; Frequently present in young patients	On almost the entire body, on body sites with acute-intermittent sun exposure (legs, trunk)	High incidence of BRAF mutations	Relatively favourable prognosis
Nodular melanoma (NM)				
Rapidly growing pigmented papule, nodule or plaque with bleeds or ulcerates exclusively in vertical growth phase	Second most common subtype of melanoma ≈ 10-15% of all melanomas in Caucasian people; More frequently in older individuals than SSM	On body sites with intermittent sun exposure, common on the trunk, head and neck and lower legs	No unique genetic features that distinguish NM from other malignant melanoma	Most aggressive type of melanoma
Lentigo maligna melanoma (LMM)				
Invasive tumor along the dermal-epidermal junction and down the walls of hair follicles and sweat ducts which arises in a lentigo maligna	Most frequent in the head and neck region and in elderly people (Elwood *et al.* 1987)	On chronically sun-damaged skin of elderly people (face, neck, forearm) evi–denced by solar elastosis (Forman *et al.* 2008)	BRAF mutations rare; Accumulation of unrepaired DNA lesions	Relatively favourable prognosis; Melanoma *in situ* curative by excision
Acral lentiginous melanoma (ALM)				
Pigmented lesions arising on the palm of the hand, sole of the foot or under the nails	Most common type of melanoma in heavily pigmented people; ≈2% of cuteneous melanoma in Caucasian and 80% in dark-skinned patients; More frequent in older people	On the palm of the hand, sole of the foot or under the nails; Exposure to sun light is negligible	Gene amplifica–tions very common, especi–ally the chromo–some region 11q13; Low BRAF mutation rate	Poor prognosis of invasive ALM

Epidemiological studies have shown that SSM is the most common subtype of malignant melanoma in Caucasians (LeBoit *et al.* 2006) while LMM is particularly frequent in white Americans (Forman *et al.* 2008) and ALM the most prevalent form of malignant melanoma in Hispanics, Asians and Black patients (Bradford *et al.* 2009, Cress *et al.* 1997). Since this clinical classification has little prognostic value and diagnostic relevance it is of only marginal profit for clinical practice (LeBoit *et al.* 2006).

1.2.3.2 Staging

Staging of tumors is used to predict disease progression and overall survival of the patients and to choose the optimal treatment procedure. One of the first widely accepted staging systems for malignant melanoma was published in 1969 by Wallace Clark (Clark *et al.* 1969). He graded this tumor by five anatomic levels of invasion, which can be correlated with the median survival of the patients. These levels are described in **Table 1.2**. Accordant to Clark's findings, only invasion into deeper dermal layers with its lymph and blood vessels correlates with the dissemination of the tumor and congruously with the prognosis for the patient (Clark *et al.* 1969). However, today level of invasion is not used as sole predictor of prognosis but is complemented by other staging systems.

Table 1.2: Definition of the five Clark levels.

Clark Level	Levels of invasion
I	Melanoma *in situ*, all tumor cells are above the basement membrane
II	Tumor cells invaded the papillary dermis but not the reticular dermis
III	Invasion to the junction of the papillary and reticular dermis
IV	Tumor cells invaded into the reticular dermis
V	Invasion into the subcutaneous tissue

The staging of melanoma according to Breslow considers only the thickness of the tumor (Breslow 1975)(see **Table 1.3**). There is an inverse relationship between tumor thickness and prognosis with a significant decrease in survival with increasing tumor thickness (Patnana *et al.* 2011, Balch *et al.* 2000). Furthermore, the relationship between tumor thickness and relative risk of death caused by melanoma was found to be almost linear to a tumor thickness of 6 mm (Buttner *et al.* 1995).

Table 1.3: Melanoma classification according to Breslow´s depth.

Breslow index	Tumor thickness
I	< 0,75 mm
II	0.76-1.5 mm
III	1.51- 4.0 mm
IV	> 4 mm

The tumor-nodes-metastases (TNM) classification model involves the extent of the primary tumor (T) (combination of Breslow and Clark), regional nodal involvement (N), and the presence or absence of distant metastases (M) (Balch *et al.* 2004). Thereby, the T

classification combines the criteria of Breslow and Clark, which are thickness of the tumor and depth of penetration. Also ulceration, which is correlated with tumor thickness and poor prognosis of melanoma patients, is considered in the T classification (Balch *et al.* 1980, McGovern *et al.* 1982). Beyond these classical staging systems a variety of country-specific models like the American Joint Committee on Cancer (AJCC) model do exist. In addition to the TNM classification, AJCC staging comprises several important prognostic factors, including the mitotic rate per mm^2 and the presence of microtumor burden in lymph nodes (Gershenwald *et al.* 2010, Nading *et al.* 2010).

1.2.4 Therapy of malignant melanoma

Surgical excision of the primary malignant melanoma is still the most promising therapeutic intervention. Based on prospective trials lateral safety margins of 0.5-2 cm for excision depending on tumor thickness are recommended (Navysany *et al.* 2010). If the tumor thickness exceeds 1 mm according to Breslow criteria surgical removal and examination of the sentinel lymph node is also suggested. Adjuvant therapy with IFN-α is recommended for tumors of more than 2 mm depth according to the German guideline for malignant melanoma (Garbe *et al.* 2008). Clinical trials showed that IFN-α increases the overall survival remarkably and the relapse free survival of melanoma patients significantly (Kähler *et al.* 2011). In individual patients where surgical excision of the tumor is unfeasible, radiotherapy of primary malignant melanoma is indicated (Garbe *et al.* 2005). For metastasized melanoma chemotherapy, radiotherapy, and immunotherapy as well as combined chemo- and immunotherapy are applied after surgical removal of the metastases. Commonly used chemotherapeutics include dacarbazine (DTIC), temozolomide, vindesine, fotemustin and cisplatin. In general malignant melanoma is characterized by a poor response rate (5-12%) to chemotherapeutics (Eigentler *et al.* 2010). E.g. for dacarbazine, the most appropriated cytostatic drug for melanoma patients with distant metastases, the response rate is only 20% and the 5-year survival rate 2% (Keilholz *et al.* 2003). For patients with brain metastases temozolomide is the preferred chemotherapy since it penetrates the blood–brain barrier (Quirbt *et al.* 2007). Because of the very low success rate of chemotherapeutics the German guideline for malignant melanoma explicitly advises melanoma patients with distant metastases to join clinical trials since they are most promising.

The most promising targeted therapy for the 50-70% patients with malignant melanoma carrying the *BRAF* V600E gene mutation (compare 1.2.2.1) is the use of vemurafenib (PLX-4032). Response rates for vemurafenib of about 80% are remarkably higher compared to standard chemotherapeutics. Furthermore, studies showed that vemurafenib produced

improved rates of overall and progression-free survival in patients with previously untreated melanoma with the *BRAF* V600E mutation (Chapman *et al.* 2011). Unfortunately, other studies revealed that the tumor cells of these patients develop drug resistance frequently after initial responses. Mechanisms of this acquired resistance to BRAF inhibition include PDGFRβ upregulation, which activate alternative survival pathways or NRAS mutations, which reactivate the MAPK pathway (Nazarian *et al.* 2010).

1.3 Cancer stem cells

1.3.1 History of the CSC theory

Already 150 years ago, the German pathologist Rudolf Virchow postulated in his theory of the cellular pathology that cancer initiates from immature cells (Virchow 1858). But only 100 years later Sajiro Makino introduced the term "tumor stem cell" for a small subpopulation of cells that were insensitive to chemotherapy and had chromosomal features different from the bulk of cells (Makino 1959). In the 1970s *in vivo* transplantation experiments and *in vitro* colony-forming assays supported Makino's observation that tumors could arise from rare cells with self-renewal capacities. Experiments indicated that these cells are able to recapitulate all cell types within an individual tumor and establish immortal cell lines (Hamburger *et al.* 1977a, Hamburger *et al.* 1977b, Park *et al.* 1971).

These so called cancer stem cells (CSC) have been proposed to originate either from malignant transformation of a normal somatic stem cell or a progenitor cell (Reya *et al.* 2001, Jacob 1983, Krivtsov *et al.* 2006) (**Figure 1.4**). Since stem cells proliferate throughout life they are more susceptible to accumulate oncogenic mutations than differentiated cells with their comparatively short life span (Monzani *et al.* 2007, Morris 2000). The identification of melanocyte-producing stem cells in the dermis of the skin, led to the hypothesis that these cells might be the origin of CSCs in melanoma since UVA can penetrate through to these cells and can potentially target them for malignant transformation (Zabierowski *et al.* 2011). This would result in cells with combined tumor and stem cell characteristics. On the other hand, it could be that differentiated cells reacquire stem cell-like characteristics by the reactivation of signaling pathways like the Wnt/β-catenin and Bmi-1 pathway or certain *HOX* genes that facilitate self-renewal and are linked to malignant transformation of cells (Lessard *et al.* 2003, Regenbrecht *et al.* 2008, Reya *et al.* 2005).

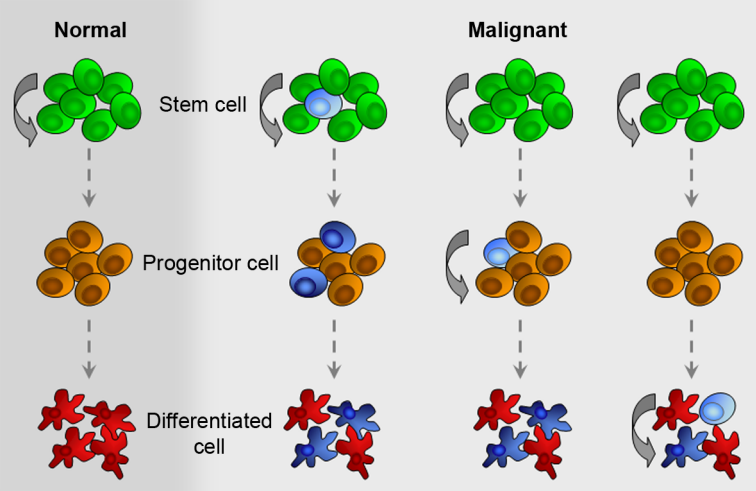

Figure 1.4: Origin of cancer stem cells.
In normal tissue, stem cells (green) divide asymmetrically into progenitor cells (orange) from which then terminally differentiated cells (red) are produced (left). In tumorigenesis mutations can transform stem cells into cancer stem cells (light blue), which then result in tumorigenic progenitor cells and differentiated tumor cells (dark blue). But also, by mutations in developmental pathways progenitor cells and differentiated cells can re-acquire stem cell-like properties and turn into cancer stem cells (right).

1.3.2 CSCs and the failure of conventional cancer therapies

One of the great advantages of the cancer stem cell hypothesis is that it also helps understanding other cancer concepts such as cancer as a minimal residual disease. Even a single cell that evades the surgeon's blade or adjuvant therapies by acquired resistance mechanisms recapitulates the whole tumorigenesis resulting in a relapse after what seems like a successful cancer treatment (**Figure 1.5**).

Existing therapies have been developed largely against the bulk population of tumor cells because they are often identified by their ability to shrink tumors. Because most cells within a cancer have limited proliferative potential, an ability to shrink a tumour mainly reflects an ability to kill these cells (Reya *et al.* 2001) but these therapy strategies may spare CSCs as indicated by recent studies.

For normal stem cells protection from damage or death is critical because these cells need to remain intact throughout the life of an organism. One principal mechanism of protection is through high expression of multifunctional efflux pumps - the ATP–binding cassette (ABC) transporters - that are the "guardians" of the stem cell population. ABC transporters are expressed in stem and progenitor cells derived from several types of normal tissue and also in hematopoietic cells. Ironically, it has been shown that high amounts of active ABC transporters also afford protection to CSCs, shielding them from the adverse effects of chemotherapeutic insult (Moitra *et al.* 2011).

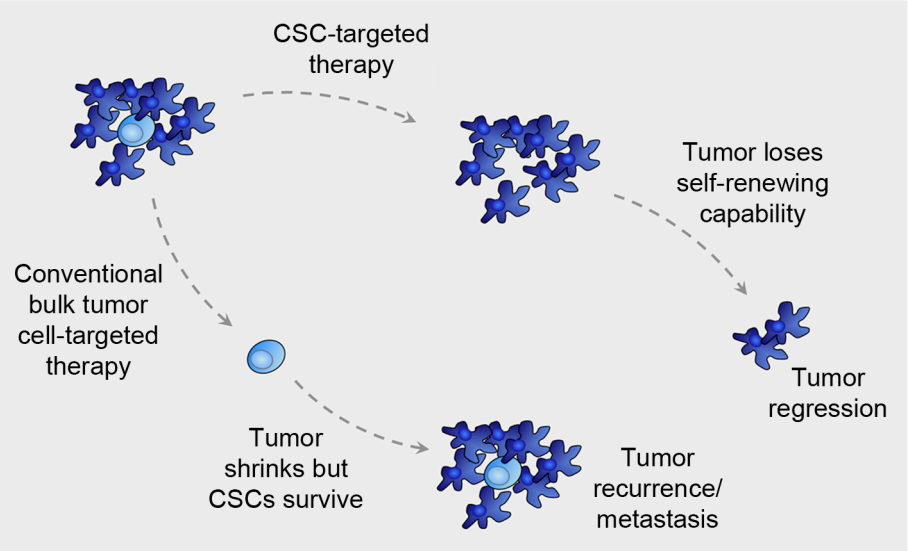

Figure 1.5: Hypothesis of CSC-related therapy failure.
Adapted from Reya *et al.* 2001. Conventional cancer treatment kills the majority of tumor cells (dark blue) but spares therapy resistant CSCs (light blue). This leads to tumor recurrence or metastasis after completion of cancer therapy due to the self-renewal capacities of CSCs. Persistently successful cancer therapies need to be CSC-directed so that the tumor loses ist self-renewing capacity and will finally degenerate completely.

Additionally CSCs comprise very efficient anti-apoptotic mechanisms and the same effective DNA repair mechanisms used by tissue-specific stem cells to mediate resistance to chemo- and radiotherapy (Hussein *et al.* 2011) as well as possess high radioresistance (Blanpain *et al.* 2011). Hittelman *et al*. suggested that radioresistance of CSCs might be owed to different intrinsic and extrinsic factors, including quiescence, activated radiation response mechanisms (e.g. enhanced DNA repair, upregulated cell cycle control mechanisms and increased free-radical scavengers) and a surrounding microenvironment that enhances cell survival mechanisms (e.g. hypoxia and interaction with stromal elements) (Hittelman *et al*. 2010). Human embryonic stem cells possess more efficient DNA mechanisms due to higher levels of several DNA repair genes and overregulation of multiple DNA repair pathways. At least for glioma CSCs the group of Frosina showed that DNA repair rates are normal but low proliferation and constitutive activation of the DNA damage checkpoint response confer increased time for lesion removal or bypass before arrival of the replication fork, which might contribute to glioma CSC radioresistance (Frosina 2010, Ropolo *et al.* 2009).

If CSCs from other tumor entities have similar characteristics as all normal stem cells do, they all should be slowly proliferating cells like the glioma CSCs investigated by Ropolo *et al*. (Ropolo *et al*. 2009). The anti-neoplastic effect of many cancer drugs e.g. dacarbazine - the most appropriated cytostatic drug for melanoma patients with distant metastases - is based on the cell cycle dependent inhibition of DNA synthesis and prevention of cell division. Thus, slowly cycling CSCs would also be more resistent to these therapeutics.

Due to these diverse resistance mechanisms of CSCs even therapies that lead to what seems like complete remission of the disease might spare enough CSCs to allow regrowth of the tumor. If the cancer stem cell hypothesis holds true at least for some tumor entities, this calls for new pharmacological approaches that are more specifically directed against these cells in order to prevent relapse and metastasis (see **Figure 1.5**).

While specific cell surface markers for CSCs in hematological malignancies are widely accepted and the concept of only a rare subpopulation of cancer cells that exhibit stem cell-like characteristics and promote growth of hematological tumors is far beyond any doubt, the situation looks totally different in solid tumors. Whereas some scientists still argue about the best method to identify and characterize CSCs, others put the CSC hypothesis in solid tumors into question (Quintana *et al.* 2008). So, in the past much effort has been made to identify novel key cancer stem cell markers for specific solid tumor entities, if not a universal marker or set of markers for CSCs in all cancers. But in reality the biology of a multicellular organism with all its feedback loops, branching, positive and negative modulators is much more complex. This makes it a challenge to identify the right components that uniquely define cancer stem cells.

1.3.3 Current standards of identification

For the identification of a putative cancer stem cell subpopulation, researchers so far take advantage of known stem cell characteristics like the ability to self-renew, expression of stem cell markers and their multipotency. The most widely accepted assays to validate a candidate cancer stem cell subpopulation are efflux analysis of the DNA-binding dye Hoechst (Grichnik *et al.* 2006), sphere formation assays (Roesch *et al.* 2010, Perego *et al.* 2010) as well as detection of known stem cell markers (Monzani *et al.* 2007) in cancer cells and verification by xenotransplantations (Quintana *et al.* 2008).

1.3.3.1 Cell surface markers

In the last decade several molecular properties have been utilized to identify and characterize CSCs from different hematopoietic and solid tumors. The first markers used were cell surface proteins already known to define stem and progenitor cells, e.g. CD133 and CD166. Furthermore, molecules, which facilitate drug resistance in cancer cells like ABCB1 and ABCG2 were added to the list of putative CSC markers, as well as proteins for which no involvement in stemness or cancerogenesis was known, e.g. CD20.

Hematopoietic stem cells, endothelial progenitor cells, neuronal and glial stem cells express CD133 (also known as Prominin 1), a member of pentaspan transmembrane glycoproteins (Kobari *et al.* 2001, Pfenninger *et al.* 2007, Quirici *et al.* 2001), which

specifically localizes to cellular protrusions (Corbeil *et al.* 2000). Expression of CD133 has previously also been shown in subpopulations of cancer cells from brain, colon, lung, melanoma and other solid tumors. This led to the assumption that CD133 expressing tumor cells have stem cell- or progenitor-like properties and CD133 was proposed as CSC marker (Bertolini *et al.* 2009, Gedye *et al.* 2009, Ieta *et al.* 2008, Monzani *et al.* 2007, Singh *et al.* 2004).

In 2007 Klein *et al.* observed an increased expression of CD133 in primary and metastatic melanoma compared to melanocytic nevi (Klein *et al.* 2007). Previously, disseminated tumor cells of melanoma patients with metastatic disease have been shown to express stem cell markers CD133 and NESTIN (Fusi *et al.* 2009: e22056). Those disseminated tumor cells are currently under debate of being involved in the formation of metastases and correlate with poor prognosis (Ossowski *et al.* 2009). However, beyond any doubt is the anchorage-independent growth of these disseminated tumor cells, which is also a characteristic of stem cells from various types of self-renewing tissue (Reynolds *et al.* 1992b, Toma *et al.* 2001).

In cell culture experiments, antibody reactivity against CD133 has been shown to correlate with the cell cycle DNA profile of colon cancer, melanoma, and human embryonic stem cells. Cells with highest ectopic expression of CD133 had a DNA content of 4N or even greater and reflect cycling cells (Jaksch *et al.* 2008). These findings are concordant with the results of Grskovic and Liu that $CD133^+$ cells have a higher mitotic index compared to $CD133^-$ cells in the first week of cultivation (Grskovic *et al.* 2004, Liu *et al.* 2006).

Moreover, Liu *et al.* showed that $CD133^+$ cells in three primary glioblastoma cell lines overexpress proteins associated with neural precursors, e.g. CD90, NESTIN and MSI-1 compared to autologous $CD133^-$ cells as well as ABCG2, the DNA repair protein MGMT and anti-apoptotic genes. For the first time ever, this study provided evidence that these properties contribute to the tumor's resistance to chemotherapy. $CD133^+$ CSCs were significantly more resistant to chemotherapeutic agents compared to autologous $CD133^-$ cells (Liu *et al.* 2006) and consequently, treatment of melanoma cells with dacarbazine selected for progressively resistant cells with increased expression of CD133 (Gedye *et al.* 2009). $CD133^+$ cells within human melanomas were also shown to have many CSC-like properties as enhanced clonogenicity and self-renewal *in vitro* (Gedye *et al.* 2009) for example formation of sphere-like colonies after cultivation under serum-free conditions (Monzani *et al.* 2007, Tirino *et al.* 2008).

Finally, $CD133^+$ cells of various tumor entities were shown to have an increased tumorigenic potential. For melanoma, Monzani and collegues demonstrated this for the first time. Magnetically sorted $CD133^+$ and $CD133^-$ cells were injected into NOD-SCID mice, respectively. After 40–50 days, mice injected with $CD133^+$ cells developed detectable tumors, whereas mice injected with $CD133^-$ melanoma cells did not develop neoplasia even four months after injection (Monzani *et al.* 2007).

Comparably results as for CD133 were obtained from the investigations of various ABC transporters. Schatton *et al.* described tumor-initiating cells capable of self-renewal and differentiation in human melanoma defined by expression of the chemoresistance mediator ABCB5. The expression of ABCB5 in tumor cells correlates with clinical melanoma progression. In serial xenotransplantation experiments $ABCB5^+$ melanoma cells were more tumorigenic than $ABCB5^-$ cells. Additionally, $ABCB5^-$ cells showed no differentiation capacity since they exclusively gave rise to $ABCB5^-$ cells whereas $ABCB5^+$ cells regenerated both subpopulations. Using a monoclonal anti-ABCB5 antibody in nude mice, initial tumor growth as well as growth of established tumors was inhibited by antibody-dependent cell-mediated cytotoxicity in $ABCB5^+$ cells (Schatton *et al.* 2008). Monzani *et al.* identified a subpopulation of human melanoma cells co-expressing ABCB1, ABCB5 and ABCC2 in addition to stem cell markers, which demonstrated higher clonogenicity, self-renewal capacity and anchorage-independent growth than the negative fraction (Keshet *et al.* 2008). Furthermore, they identified tumor-initiating cells in human melanoma by the expression of ABCG2, which is coexpressed with CD133 (Monzani *et al.* 2007). Concluding these results, it seems as if CSCs in solid tumors can be defined or at least enriched with certain markers or set of markers.

1.3.3.2 Dye exclusion assays

In contrast to preferably cell-type specific surface markers, the use of Hoechst dye to identify and isolate CSCs as a so called side population (SP) overcomes the barrier of phenotypical markers and replaces it with more direct functional markers (Hadnagy *et al.* 2006). The blue fluorescent Hoechst 33342 is a cell permeable bisbenzimidazole derivative that binds to the minor groove of the DNA. After excitation of Hoechst its emission can be measured simultaneously in the blue and red spectrum. But although Hoechst enters viable cells, ABC transporters of the cell membrane actively efflux the dye (Scharenberg *et al.* 2002, Zhou *et al.* 2002, Zhou *et al.* 2001). Goodell *et al.* were the first to identify that hematopoietic stem cells are particularly effective at pumping out Hoechst (Goodell *et al.* 1996) since they express high levels of ABC transporters resulting in a small side population of weakly stained cells which can be identified by flow cytometric analysis.

To determine the size of the side population, verapamil, an L-type calcium channel-blocking agent serves as a functional control. Blocking the calcium channels inhibits the efflux of Hoechst dye from these cells, so it is then possible to gate for the side population, which is suspected to consist of cancer stem cells. Subsequently, side populations were identified in various established cell lines from breast cancer, lung cancer and glioblastoma, suggesting that this phenotype defines a class of cancer stem cells with inherently high resistance to chemotherapeutic agents due to rapid efflux of those compounds (Hirschmann-Jax *et al.* 2004). Kondo *et al.* were the first to come up with the hypothesis that the side population resembles the source of CSCs in C6 glioma cells since only SP cells initiated tumors in multiple tissues in nude mice (Kondo *et al.* 2004).

ABC transporters that most notably account for the efflux of Hoechst are ABCG2 (BCRP1) and ABCB1 (also known as P-glycoprotein or MDR1) (Chaudhary *et al.* 1991, Goodell *et al.* 1996, Scharenberg *et al.* 2002, Schinkel *et al.* 1994, Zhou *et al.* 2001). This is concordant with the findings that these genes are highly expressed on SP cells but not on non-SP cells (Hirschmann-Jax *et al.* 2004, Patrawala *et al.* 2005). Accordingly, putative CSCs of the SP have higher capacity to expel cytotoxic drugs used in cancer therapy, therefore improve their survival and finally recapitulate the whole tumorigenesis resulting in a relapse after what seems like a successful cancer treatment (Hirschmann-Jax *et al.* 2005, Hirschmann-Jax *et al.* 2004).

The main criterion of CSCs in contrast to non-CSCs is their unique capability to differentiate and recapitulate all cell types within a tumor. The results of several groups demonstrated that only SP cells generate both SP and non-SP cells in cell culture while non-SP cells fail to do so (Hirschmann-Jax *et al.* 2004, Kondo *et al.* 2004, Wang *et al.* 2007, Wang *et al.* 2009b). Furthermore, they were able to initiate tumors in xenograft transplantation experiments with very low numbers of SP cells, whereas non-SP cells were either not at all tumorigenic or only upon injection of multifold more cells compared to the SP.

Grichnik *et al.* identified SP cells in metastatic melanoma cell lines which, compared to non-SP cells were small in size, less melanotic, had a decreased proliferation rate and gave rise to a heterogeneous cell population (Grichnik *et al.* 2006). All these findings support the isolation of side populations via Hoechst staining as an identification method for CSCs. Additionally, this method could help to identify more specific molecular CSC markers by comparing the expression profiles of SP and non-SP cells which is crucial for the establishment of targeted cancer therapies.

1.3.3.3 Sphere formation assays

Another method to identify and enrich CSCs is the "sphere formation assay". This assay has its origin in the stem cell research of the 1990s, where stem cells have been described in embryonic and postnatal mouse brain in the form of proliferative clusters, called ''neurospheres'', that can be harvested and cultured from different brain areas (Kukekov *et al.* 1997). Reynolds *et al*. reported that via induction with EGF single cells from the embryonic striatum gave rise to a cluster of undifferentiated cells with properties of neuroepithelial stem cells, which in turn can generate neurons and glia (Reynolds *et al.* 1992a, Reynolds *et al.* 1992b). Over the time an *in vitro* system has been developed that uses serum and anchorage withdrawal, and a medium supplemented with methyl cellulose and growth factors [epidermal growth factor (EGF), basic fibroblast growth factor (FGF2), and insulin] to generate clonal neurospheres from normal and tumor tissue (Singh *et al.* 2003) and it was suggested that sphere formation may be a common growth characteristic of stem cells (Fang *et al.* 2005).

Primarily, in cancer research sphere formation assays were used to identify cancer stem cells from brain tumors. Singh *et al*. demonstrated that 0.3%-25.1% of cells from brain tumors grow as neurosphere-like clusters, termed tumor spheres. Whereas tumor spheres remained nonadherent and continued to proliferate, the remaining majority of tumor cells exhibited adherence, loss of proliferation, and subsequent differentiation (Singh *et al.* 2003). To build on the analogy between neurosphere and tumor sphere, Singh *et al*. subjected tumor spheres to stem cell assays designed to test the self-renewal, proliferation, and differentiation capacities. They found that cells of tumor spheres expressed neural stem cell markers but no markers for differentiated neurons, astrocytes, or oligodendrocytes. Furthermore, they showed increased chemoresistance due to a high activity of ABC transporters and enhanced rates of DNA repair and had the ability to self-renew and to differentiate to recapitulate the phenotype of the tumor from which they were derived (Hussein *et al.* 2011, Singh *et al.* 2003). Later on, sphere-forming cells were also found in malignant melanoma. Several studies indicated that these sphere-forming cells compared to adherent melanoma cells display higher tumorigenic capacity, express stem cell markers like the transcription factors SOX2, OCT4 and NANOG, have higher migratory and invasive capacities, self-renew and can differentiate under appropriate conditions into multiple cell lineages, such as melanocytic, adipocytic, osteocytic, and chondrocytic lineages (Monzani *et al.* 2007, Roesch *et al.* 2010, Fang *et al.* 2005, Perego *et al.* 2010). Furthermore, sphere-forming melanoma cells were shown to have immune-modulator functions since they elicit a poorer allogenic response from immune cells and

inhibit mitogen-dependent T cells activation and proliferation more efficiently than their adherent counterparts (Ramgolam *et al.* 2011).

Taken together, sphere formation assays can provide an indication of the existence of CSCs but Clarke *et al*. insisted to confirm this indication by *in vivo* transplantation experiments (Clarke *et al.* 2006).

1.3.3.4 *In vivo* transplantation experiments

Until today, the gold standard in validating the tumorigenic potential of a putative human CSC population is xenotransplanting the cells into immunodeficient mice. If CSCs are really enriched in this population, these cells should have a several-fold higher capacity to form tumors compared to the control fraction where the cells lack this CSC marker or the typical characteristics as rapid efflux of Hoechst due to high expression of ABC transporters.

Using mouse models, the Hoechst SP was proved to be enriched of tumor-initiating cells in thyroid (Mitsutake *et al.* 2007), ovarian (Szotek *et al.* 2006) and breast cancer (Patrawala *et al.* 2005), glioma (Kondo *et al.* 2004, Patrawala *et al.* 2005), melanoma (Dou *et al.* 2009) and hepatocellular carcinoma (Chiba *et al.* 2006). Furtheron, xenotransplantation experiments validated certain CSC markers like ABCB5, CD20 and CD133 for melanoma (Schatton *et al.* 2008, Monzani *et al.* 2007, Fang *et al.* 2005).

1.4 Human embryonic and tissue stem cells

1.4.1 Characteristics

In skin, as in all other adult tissues a highly regulated process of stem cell self-renewal, transient-amplifying cells, differentiation and death sustains homeostasis. The essential characteristics of all stem cells are prolonged self-renewal and the long-term potential to form one or more differentiated cell types. Whereas stem cells present in adult tissues form only a limited number of cell types, human embryonic stem cells (hESC) are pluripotent cells, which differentiate into derivatives of all three germ layers and have the potential to form practically any cell type *in vivo* and *in vitro*. (Thomson *et al.* 2000, Dvash *et al.* 2006).

Human ESCs are derived from the inner cell mass of human blastocyst-stage embryos and are characterized by their unlimited capacity to self-renew in culture with maintenance of a normal euploid karyotype (Dvash *et al.* 2006). To analyze pluripotency of hESCs, embryoid body formation *in vitro* and teratoma formation after injection into immunocompromised mice with differentiation into ectoderm, endoderm and mesoderm

are currently used (Hoffman *et al.* 2005, O'Connor *et al.* 2008). Besides pluripotency and self-renewal capacity hESCs are characterized by the expression of a specific set of cell surface molecules and activity of several enzymes e.g. telomerase and alkaline phosphatase (Dvash *et al.* 2006). In 2007 the International Stem Cell Initiative identified several markers, which characterize hESCs in a comparative study of a large and diverse set of 59 independently derived hES cell lines derived and maintained in different laboratories worldwide. Among these markers are the glycolipid antigens SSEA3 and SSEA4, the keratan sulfate antigens TRA-1-60, TRA-1-81, GCTM2 and GCT343, and the protein antigens CD9, CD90, tissue-nonspecific alkaline phosphatase and class 1 HLA, as well as the strongly developmentally regulated genes NANOG, OCT4, TDGF1, DNMT3B, GABRB3 and GDF3 (Adewumi *et al.* 2007).

State of the art culture media formulations contain serum replacement and basic fibroblast growth factor (bFGF or FGF2) to maintain undifferentiated and self-renewing hESCs (Hoffman *et al.* 2005, Amit *et al.* 2000) because it is known that representatives from the FGF, TGF-β, Notch, Hedgehog and Wnt signaling pathways consistently mark and maintain the undifferentiated state (Noggle *et al.* 2005).

1.4.2 Importance of TGF-β signaling for hESC self-renewal

TGF-β1, which is a member of the TGF-β superfamily is found in the matrigel matrix, which supports hESC growth in feeder layer-free conditions (Amit *et al.* 2004). *In vitro* the importance of the TGF-β pathway for maintaining self-renewal and pluripotency was demonstrated by cellular differentiation in short-term cultures as a result of TGF-β1 signaling inhibition (Hoffman *et al.* 2005). Greber *et al.* showed that FGF2 promotes self-renewal of hESCs by modulating the expression of TGF-β ligands (Greber *et al.* 2007a).

TGF-β ligands can be classified into two subfamilies: the TGF-β/Activin/Nodal subfamily (SMAD 2/3 branch), and the BMP/growth and differentiation factor (GDF) subfamily (SMAD 1/5/8 branch) (Rao *et al.* 2005). To prevent differentiation the TGF-β/Activin/Nodal branch of the pathway needs to be activated. Data suggest a regulatory circuit essential for maintaining self-renewal in hESCs, which is characterized by exogenous and autocrine FGF2 signaling being upstream of key TGF-β ligands that sustain OCT4, NANOG, and SOX2 expression, whereas these, in turn, activate endogenous expression of FGF2 (Greber *et al.* 2007a, Vallier *et al.* 2005, Greber *et al.* 2008). In this process FGF2 contributes to maintenance of hESCs through activation of the MEK1/ERK pathway by phosphorylating ERK and inducing the early response gene C-FOS. C-FOS, in turn, is linked to increased activity of the transcription factor complex AP-1, and AP-1 contributes, at least in part, to the expression of genes essential for stem cell proliferation

and self-renewal (Kang *et al.* 2005). **Figure 1.6** illustrates the correlation of TGF-β, FGF2 and MAPK pathways.

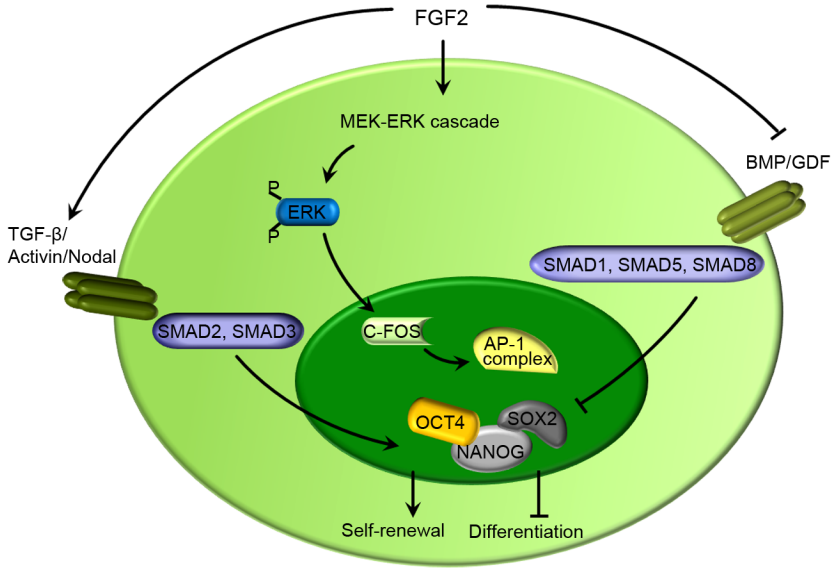

Figure 1.6: TGF-β, FGF2 and MAPK pathway cross-signaling for maintaining hESC self-renewal.
In hES cells activation of the TGF-β/Activin/Nodal branch of the TGF-β pathway or FGF2 mediated activation of the MEK-ERK cascade and subsequent activation of the AP-1 complex prevent differentiation. FGF2-mediated modulation of TGF-β ligand expression towards the expression of the TGF-β/Activin/Nodal subfamily regulates cross-signaling of these pathways.

1.4.3 Pluripotency factor OCT4

Several studies have highlighted the existence of a transcriptional network that controls ES cell identity. This network comprising of OCT4, SOX2 and NANOG has an essential role in early development and is required for the propagation of undifferentiated embryonic stem (ES) cells in culture. In hESCs OCT4, SOX2 and NANOG co-occupy at least 353 genes and regulate them significantly (Boyer *et al.* 2005). Target genes frequently encode transcription factors, many of which are developmentally important homeodomain proteins. Examples are components of the TGF-β (e.g., TDGF1, LEFTY2/EBAF) and Wnt (e.g., DKK1, FRAT2) signaling pathways, FGF4 (fibroblast growth factor 4), PDGFAR (platelet-derived growth factor receptor alpha) (Boyer *et al.* 2005, Lee *et al.* 2006). Furthermore, studies indicate that only OCT4 might be the master regulator of the pluripotent state in mammalian cells (Buitrago *et al.* 2007, Nichols *et al.* 1998).

OCT4, sometimes termed OCT3, belongs to the POU family of transcription factors. They are composed of an N-terminal subunit known as the POU-specific domain, and a C-terminal subunit called the homeobox domain. Both subdomains are required for high affinity sequence-specific DNA-binding. OCT4 activates transcription via the binding of the POU domain to the octamer DNA motif 5´-ATGCAAAT-3´ at promoter and enhancer

regions of its target genes (Lee *et al.* 2006, Rosner *et al.* 1990). In humans, OCT4 is present throughout all stages from the unfertilized oocyte to blastocysts. It is also present in hESCs (Hansis *et al.* 2000, Lee *et al.* 2006). Loss of OCT4 expression allows ES cells to differentiate into different cell fates. In addition, previous reports have detected OCT4 expression in human embryonal carcinoma cells as well as in somatic-cell tumors (Buitrago *et al.* 2007).

1.4.3.1 Splice variants and pseudogenes of *OCT4*

Alternative splicing, as well as usage of alternative translation initiation codons, results in multiple *OCT4* isoforms. To date there are at least six pseudogenes and several alternatively spliced transcripts known (Takeda *et al.* 1992). Some are expressed in cancers, both at the mRNA as well as protein level (Zhao *et al.* 2011). *OCT4* pseudogenes have been identified on chromosomes 1, 3, 8, 10, and 12 whereas the two main protein coding isoforms *OCT4A* and *OCT4B* are located on chromosome 6.

All human *OCT4* isoform mRNAs encode proteins with identical POU DNA binding domains and C-terminal domains. The proteins differ only in their N-terminal domains. The longer isoform *OCT4A* consists of five exons with 1406 bp, which are translated into a 360-amino acid protein. *OCT4B* differs in the 5' UTR, lacks a portion of the 5' coding region, and uses a downstream non-*AUG* (*CUG*) start codon, compared to *OCT4A*. The resulting isoform is shorter at the N-terminus, compared to OCT4A. It consists of 265 amino acids encoded by 1732 bp. If this sequence is organized in four or five exons, is still under debate. Recently, a novel *OCT4* alternative spliced variant, termed *OCT4B1* was detected. Compared with the *OCT4B* mRNA, *OCT4B1* mRNA is generated by retaining intron 2 as a putative novel cryptic exon termed exon 2b. Amino acids 1–80 of OCT4B and OCT4B1 proteins are identical, including a similar N-terminal domain and a part of the POU-specific domain. However, OCT4B1 lacks the rest of the POU-specific domain, as well as the homeodomain and the C-terminal transactivation domain (Atlasi et al., 2008).

Previous data suggest that the DNA binding, transactivation, and abilities to confer self-renewal differ tremendously between the human OCT4 isoforms. Unlike human OCT4A, OCT4B cannot sustain stem cell properties. It was shown that, OCT4B does not bind to a probe carrying the OCT4 consensus binding sequence due to two separate regions of its N-terminal domain that inhibit DNA binding (Lee *et al.* 2006).

The function of OCT4B remains elusive. Due to alternative translation initiation a single *OCT4B* mRNA, can encode at least three protein isoforms of which one isoform has been demonstrated to respond to cell stress (Wang *et al.* 2009a). *OCT4B1* mRNA is highly

expressed in human ESCs and embryonal carcinoma cells and downregulated following differentiation. Therefore, a potential correlation between *OCT4B1* and pluripotency has been considered (Gao *et al.* 2010, Atlasi et al., 2008). In accordance with the functional properties, the subcellular localization of OCT4 isoforms differs. Whereas, the human OCT4A isoform is clearly localized to the nucleus, OCT4B is mainly present in the cytoplasm of the cell (Liedtke *et al.* 2008).

1.5 Aims of this work

The focus of this work was on the identification and characterization of so called cancer stem cells (CSCs), tumor cells with stem cell characteristics, in cutaneous malignant melanoma. In order to accomplish this I used a multi-layered approach as follows:

The primary goals comprised:

- Establishment of patient-derived melanoma cell lines
- Establishing approaches which allow the identification and enrichment of CSCs

Secondary aims were:

- Characterization of the established panel of melanoma cell lines
- Application of the current standard methods to identify CSCs which comprise sphere formation assays, dye exclusion assays and expression analysis of known CSC markers

Tertiary aims involved:

- Verification of the usefulness of these standard identification methods
- Enrichment of a putative CSC fraction from melanoma cell lines using magnetic-activated cell sorting (MACS) for cell surface proteins and fluorescence-activated cell sorting (FACS) for intracellular proteins
- A detailed characterization and functional analysis of melanoma CSCs by means of gene expression and sequencing analyses, *in vitro* analyses of drug resistance, growth and mobility as well as *in vivo* xenotransplantation experiments.

I was particularly interested in identifying a useful CSC marker or a combination of markers to characterize melanoma CSCs. Therefore, human embryonic stem cells (hESC) and human embryonic carcinoma cells were used as control and comparative cells to find common features between stem and cancer stem cells. Consequently, I focused on the key stem cell properties like the ability to self-renew and the master regulator of pluripotency OCT4.

Furthermore, the study was aimed at investigating the robustness of putative CSC markers *in vitro* (dynamic equilibrium vs. static state). Finally, the main criterion of CSCs, their tumor-initiating capacity, was proved for enriched putative melanoma CSCs and compared to bulk tumor cells.

2 Materials and Methods

Trademarks appear throughout this thesis without any trademark symbol; they are the property of their respective trademark owner. There is no intention of infringement; the usage is to the benefit of the trademark owner.

2.1 Materials

Table 2.1: Chemicals and reagents

Product	Company
(±)-Verapamil hydrochloride ≥99.0% (TLC)	Sigma-Aldrich, Inc., USA
2-Mercaptoethanol	Sigma-Aldrich, Inc., USA
30% Acrylamide/Bis Solution	Bio-Rad Laboratories, Inc., USA
5-aza-2'-deoxycytidine	Sigma-Aldrich, Inc., USA
Accutase	PAA Laboratories GmbH, Germany
Acidic acid (100 %)	Merck KGaA, Germany
Agarose NEEO Ultra-Qualität	Carl Roth GmbH & Co. KG, Germany
alamarBlue	Invitrogen GmbH, Germany
Ammonium acetate (5 M)	Invitrogen GmbH, Germany
Ammonium persulfate for electrophoresis, ≥98%	Sigma-Aldrich, Inc., USA
Bacto Agar	BD Biosciences, USA
Bacto Trypton	BD Biosciences, USA
Bacto yeast extract	BD Biosciences, USA
Basic Fibroblast Growth Factor (bFGF)	PeproTech, UK
Betaine hydrochloride	Sigma-Aldrich, Inc., USA
bisBenzimide H 33342 trihydrochloride (Hoechst)	Sigma-Aldrich, Inc., USA
Blotting-Grade Blocker, nonfat dry milk	Bio-Rad Laboratories, Inc., USA
Boric acid	Merck KGaA, Germany
Bromophenol Blue	Sigma-Aldrich, Inc., USA
Bovine serum albumin (BSA)	Serva GmbH, Germany
Calciumchlorid	Merck KGaA, Germany
4´,6-Diamidino-2-phenylindole dihydrochloride (DAPI)	Sigma-Aldrich, Inc., USA
DEPC-treated water	Applied Biosystems, USA
Difco Agar, Noble	BD Biosciences, USA
Dimethyl sulfoxide (DMSO) (99.9 %)	Sigma-Aldrich, Inc., USA
DNA Marker 100 bp	Invitrogen GmbH, Germany
D-PBS without Ca, Mg	PAA Laboratories GmbH, Germany
ECL Plus Western Blotting Detection Reagents	GE Healthcare, Germany
Ethylenediaminetetraacetic acid disodium salt dehydrate (EDTA)	Sigma-Aldrich, Inc., USA
Endothelin 3 (ET3) Lyophilized	Lonza Walkersville, Inc., USA
Ethanol	Mallinckrodt Baker, Germany
FACS Clean Solution	BD Biosciences, USA
FACS Flow	BD Biosciences, USA
FACS Rinse Solution	BD Biosciences, USA
Fetal bovine serum (FBS) Superior	Biochrom, Germany
Ficoll-Paque Plus	GE Healthcare, Germany
G-418-Sulphate Solution (50 mg/ml)	PAA Laboratories GmbH, Germany
GelRed Nucleic Acid Stain 10000x in Water	Biotrend Chemikalien, Germany
Glycerol	Merck KGaA, Germany
Glycine	Merck KGaA, Germany
GoTaq DNA Polymerase	Promega Corporation, USA
Hanks' balanced salt solution	Invitrogen GmbH, Germany

HEPES, free acid, ULTROL grade	Merck KGaA, Germany
Hi-Di Formamide	Applied Biosystems, USA
Isopropanol (2-Propanol)	Mallinckrodt Baker, Germany
Kaliumchloride	Sigma-Aldrich, Inc., USA
KnockOut DMEM	Invitrogen GmbH, Germany
KnockOut Serum Replacement	Invitrogen GmbH, Germany
Lipofectamine 2000 Reagent	Invitrogen GmbH, Germany
L-Glutamine (200 mM)	Invitrogen GmbH, Germany
MagicMark XP Western Protein Standard	Invitrogen GmbH, Germany
Matrigel Basement Membrane Matrix	BD Biosciences, USA
Methanol	Merck KGaA, Germany
MEM Non-Essential Amino Acids Solution (100X) (NEAA)	Invitrogen GmbH, Germany
MGM-4 BulletKit	Lonza Walkersville, Inc., USA
Mitomycin C from Streptomyces caespitosus	Sigma-Aldrich, Inc., USA
Natriumchloride	Merck KGaA, Germany
Natriumdihydrogenphosphat	Merck KGaA, Germany
di-Natriumhydrogenphosphat	Merck KGaA, Germany
Natriumhydroxid	Merck KGaA, Germany
Nonfat dry milk	Bio-Rad Laboratories, Inc., USA
Odyssey Blocking Buffer	LI-COR Biosciences, USA
Orange G	Carl Roth GmbH & Co. KG, Germany
PageBlue Protein Staining Solution	Fermentas, Canada
PageRuler Prestained Protein Ladder	Fermentas, Canada
Paraformaldehyde (PFA)	Merck KGaA, Germany
Penicillin-Streptomycin, liquid (100x)	Invitrogen GmbH, Germany
PolyAcryl Carrier	MRC, Inc., USA
Ponceau S practical grade	Sigma-Aldrich, Inc., USA
Potassium phosphate monobasic ReagentPlus	Sigma-Aldrich, Inc., USA
Propidium iodide ≥94%, suitable for fluorescence	Sigma-Aldrich, Inc., USA
Protease Inhibitor Cocktail for mammalian cell and tissue extracts	Sigma-Aldrich, Inc., USA
Quantum 263	PAA Laboratories GmbH, Germany
Random primers	Promega Corporation, USA
Red Blood Cell Lysis Solution	Miltenyi Biotec GmbH, Germany
Ribonuclease A from bovine pancreas - Type III-A	Sigma-Aldrich, Inc., USA
RiboRuler High Range RNA Ladder	Thermo Fisher Scientific, Inc., USA
RNaseOUT Recombinant Ribonuclease Inhibitor	Invitrogen GmbH, Germany
Roti-Block	Carl Roth GmbH & Co. KG, Germany
Set of dATP, dCTP, dGTP, dTTP	Promega Corporation, USA
Sodium Hydroxide, Pellets	Merck KGaA, Germany
Sodium n-Dodecyl Sulfate, 20% Solution (w/v)	Merck KGaA, Germany
SYBR-Green PCR master mix	Applied Biosystems, USA
Tetramethylethylenediamine (TEMED)	Sigma-Aldrich, Inc., USA
Tris(hydroxymethyl)-aminomethan (Tris Base)	Merck KGaA, Germany
Triton X-100	Roche Holding GmbH, Germany
Trypsin-EDTA (1x) 0,05%/0,02% in DPBS	PAA Laboratories GmbH, Germany
Trypsin Neutralizing Solution	Lonza Walkersville, Inc., USA
Trypsin-Versene (EDTA) Mixture (1x)	Lonza Walkersville, Inc., USA
Tween 20 Detergent	Merck KGaA, Germany
UltraPure Phenol:Chloroform:Isoamyl Alcohol (25:24:1)	Invitrogen GmbH, Germany

Table 2.2: Kits

Product	Company
BCA Protein Assay Kit	Thermo Fisher Scientific, Inc., USA
BigDye Terminator v3.1 Cycle Sequencing Kit	Applied Biosystems, USA
Cell Death Detection ELISA Plus	Roche Holding GmbH, Germany
EndoFree Plasmid Maxi Kit	Qiagen GmbH, Germany
Indirect CD133 Microbead Kit human	Miltenyi Biotec GmbH, Germany
Illumina TotalPrep RNA Amplification Kit	Applied Bioscience, USA
NE-PER Nuclear and Cytoplasmic Extraction Reagents	Thermo Fisher Scientific, Inc., USA
PlatinumR SYBRR Green qPCR SuperMix UDG	Invitrogen GmbH, Germany
QIAamp DNA Mini Kit	Qiagen GmbH, Germany
QIAquick PCR Purification Kit	Qiagen GmbH, Germany
Quant-iT dsDNA BR Assay Kit	Invitrogen GmbH, Germany
Quant-iT RNA Assay Kit	Invitrogen GmbH, Germany
RiboMinus Transcriptome Isolation Kit	Invitrogen GmbH, Germany
RNeasy Mini Kit	Qiagen GmbH, Germany
SuperScript VILO cDNA Synthesis Kit	Invitrogen GmbH, Germany
SuperScript Double Stranded cDNA Synthesis Kit	Invitrogen GmbH, Germany
Stemgent Alkaline Phosphatase Staining Kit II	Miltenyi Biotec GmbH, Germany

Table 2.3: Primary and secondary antibodies

Product	Dilution/Buffer	Company
Alexa Fluor 488 goat anti-rabbit IgG (H+L)	1:800 in 2nd antibody buffer	Invitrogen GmbH, Germany
Anti-mouse IgG, HRP-linked Ab	1:2000 in milk blocking solution	Cell Signaling Technology, Germany
Anti-rabbit IgG, HRP-linked Ab	1:2000 in milk blocking solution	Cell Signaling Technology, Germany
CD133 (C24B9) Rabbit mAb	1:1000 in PBST/LI-COR blocking Buffer (1:1)	Cell Signaling Technology, Germany
anti-GAPDH (6C5) mouse mAb	1:8000 in milk blocking solution	Applied Biosystems, USA
GFP antibody rabbit polyclonal Ab	1:2000 in PBST/LI-COR blocking Buffer (1:1)	Abcam plc, UK
IRDye680CW goat anti-mouse	1:10000 in PBST/LI-COR blocking Buffer (1:1)	LI-COR Biosciences, USA
IRDye800CW goat anti-rabbit	1:10000 in PBST/LI-COR blocking Buffer (1:1)	LI-COR Biosciences, USA
ß-Tubulin antibody rabbit polyclonal Ab	1:1000 in PBST/LI-COR blocking Buffer (1:1)	Cell Signaling Technology, Germany
Oct-4 (C52G3) rabbit monoclonal Ab	1:1000 in BSA buffer	Cell Signaling Technology, Germany
p44/42 MAP Kinase rabbit polyclonal Ab	1:1000 in milk blocking solution	Cell Signaling Technology, Germany
Phosphor-p44/42 MAPK (Thr202/Tyr204) (E10) mouse monoclonal Ab	1:1000 in milk blocking solution	Cell Signaling Technology, Germany
Stemgent DyLight 488 rabbit anti-human/mouse OCT4 Ab	1:100 in PBST/LI-COR blocking Buffer (1:1)	Miltenyi Biotec GmbH, Germany

Table 2.4: Enzymes

Product	Company
*Apa*I restriction enzyme	New England Biolabs, Inc., USA
Collagenase IV	Sigma-Aldrich, Inc., USA
DNase I	Applichem GmbH, Germany
RNase-Free DNase Set (50)	Qiagen GmbH, Germany
*Tsp*45I restriction enzyme	New England Biolabs, Inc., USA

Table 2.5: Drugs/ Kinase inhibitors

Product	Target	Company
ABT-869	VEGFR, PDGFR	Selleck Chemicals LLC, USA
Bosutinib	SRC, ABL	Axon Medchem BV, Netherlands
Dasatinib	ABL, SRC	Axon Medchem BV, Netherlands
GDC-0941	PI3K	Axon Medchem BV, Netherlands
Gefitinib	EGFR	Axon Medchem BV, Netherlands
Imatinib	ABL, KIT, PDGF	Axon Medchem BV, Netherlands
Lapatinib	EGFR, HER2	Axon Medchem BV, Netherlands
Nilotinib	ABL	Axon Medchem BV, Netherlands
PD184352	MEK	Axon Medchem BV, Netherlands
PD98059	p38 MAPK	Merck KGaA, Germany
PI-103	PI3K, DNA-PK, mTOR1/2	Cayman Chemical Company, USA
PLX-4032	BRAF	Selleck Chemicals LLC, USA
Rapamycin	MTOR	Sigma-Aldrich, Inc., USA
Sorafenib	PDGFR, VEGFR, RAF	Axon Medchem BV, Netherlands
Staurosporin	Broad Spectrum	Selleck Chemicals LLC, USA
SU5402	FGFR1	Merck KGaA, Germany
Sunitinib	PDGFR, VEGFR	Axon Medchem BV, Netherlands
U0126	MEK1	Promega Corporation, USA
Vandetanib	VEGFR, EGFR	Axon Medchem BV, Netherlands

Table 2.6: Human cell ines and primary cells

Cell line	Cell type	Melanoma subtype	Sex	Breslow Index	Clark Level	Source
A375	malignant melanoma	NA	female	NA	NA	DKFZ, Heidelberg
ChaMel19	melanoma metastasis	NM	male	3.81 mm	IV	Clinical Research Group Tumor Immunology, Department of Dermatology, Charité Berlin
ChaMel21		SSM	female	1.00 mm	III	
ChaMel39		SSM	female	1.10 mm	NA	
ChaMel41		SSM	female	2.20 mm	IV	
ChaMel47		NA	male	NA	NA	
ChaMel68		NA	male	NA	NA	
ChaMel73		SSM	female	3.70 mm	NA	
ChaMel81		SSM	female	1.30 mm	NA	
ChaMel84		NM	male	4.00 mm	IV	
ChaMel91		SSM	male	1.83 mm	III	
ChaMel100		NA	male	NA	NA	
ChaMel114		NA	female	NA	NA	
ChaMel115		NA	male	NA	NA	
NHEM-melanocytes	neonatal melanocytes from foreskin	---	male	---	---	Lonza Walkersville, Inc., USA

NHEM-Ad-melanocytes	adult melanocytes from breast tissue	---	female	---	---	Lonza Walkersville, Inc., USA
NCCIT	embryonal carcinoma; teratocarcinoma	---	male	---	---	LGC Standards GmbH, Germany
Pat1T1k	melanoma metastasis	NM	male	2.50 mm	IV	AG Regenbrecht, Charité Berlin

Table 2.7: Primer sequences for standard PCR and cycle sequencing

Gene		Sequence (5´ - 3´)
ABCB1	se	CATTGGTGTGGTGAGTCAGG
	as	GACCACTGCTTCGCTTTCTGT
ABCB5	se	CAATGGCCTTTTGTGGTTCTG
	as	CCCTGCTCTGCCGTAAAATA
ABCC2	se	CTTAGTGGGGGTCAGAAGCA
	as	CCAGGAGAGCACTGTAGGA
ABCG2	se	CGTGGTGTGTCTGGAGGAGA
	as	CGAGGCTGATGAATGGAGAAG
BMI-1	se	CGATACTTACGATGCCCAGCA
	as	TGGATGAGGAGACTGCACTG
BRAF	se	TCATAATGCTTGCTCTGATAGGA
	as	GGCCAAAAATTTAATCAGTGG
C-KIT	se	CCGTTTGGAAAGCTAGTGGT
	as	AAGGAGTGAACAGGGTGTGG
C-MYC	se	CCTACCCTCTCAACGACAGC
	as	CTCTGACCTTTTGCCAGGAG
CD133	se	CCTGGGGCTGCTGTTTATTA
	as	TTGATCCGGGTTCTTACCTG
CD166	se	CGATCTAGCCCGTCATTTTC
	as	ACGCTTCCACTGCCAGTAAT
CD20	se	GCTGCCATTTCTGGAATGAT
	as	TTCCTGGAAGAAGGCAAAGA
CD90	se	TAGTGGACCAGAGCCTTCGT
	as	GCCCTCACACTTGACCAGTT
CSPG4	se	TCTGGGTCTGAGGATCTGGT
	as	CTTCAGCGAGAGGAGCACTT
DNMT3B	se	TACCATCGACCTCACAGACG
	as	GGTCCCCTATTCCAAACTCC
EDNRB	se	TTGTGTCCTGCCTTGTGTTC
	as	TGATTCCCACAGAGGCTTTC
EGFP	se	GTAAACGGCCACAAGTTCAGC
	as	GGCGGATCTTGAAGTTCA
FGF2	se	ACCGTTACCTGGCTATGAAGG
	as	GACTGCCCAGTTCGTTTCAGT
FGFR1	se	GTGGGAGATCTTCACTCTGG
	as	GCTTGAAGGTGGGTCTCTGT
GABRB3	se	AGTGTCACTGAGCTTTCGGTTG
	as	GGTTGCCTTGGCTGTCTTTTCT
GDF3	se	CTTCACCCCAGAAGTTCCAA
	as	GCAGGTTGAAGTGAACAGCA
HPRT	se	GTTGTAGGATATGCCCTTGAC
	as	GCCCAAAGGGAACTGATAGT
JARID1B	se	AACAACATGCCAGTGATGGA
	as	TACCAGGTTTTTGGCTCACC
KLF4	se	TCCCATCTTTCTCCACGTTC
	as	GGTCTCTCTCCGAGGTAGGG

LIN28	se as	CTTCTCCGAACCAACCCTTT CGCACGTTGAACCACTTACA
MITF	se as	CTTGGGCTTGATGGATCCTG GGTTGGCTGGACAGGAGTTG
MSI-1	se as	GTTCGGGTTTGTCACGTTTG ATGAAGGCGTCCATTCCGTA
NANOG	se as	CAACTGGCCGAAGAATAGCAA CGAATTTGGCTGGAACTGCAT
NESTIN	se as	TCCAAGACTTCCCTCAGCTT TGCTTACCACTTTGCCCTCT
OCT4A	se as	CCTTCGCAAGCCCTCAT TGATGTCCTGGGACTCCTC
OCT4A nested	se as	CGCCGTATGAGTTCTGTGG TGCTCCAGCTTCTCCTTCTC
SOX2	se as	CAGCTCGCAGACCTACATGA TGGAGTGGGAGGAAGAGGTA
TDGF1	se as	CGGAATTTGCTCGTCCATCTC CACATCGTGCTCACAGTTCC
TNC	se as	ACAGTAGAGGCAGCCCAGAA TCTACAGCAAGGGGTCGAGT
TYR	se as	ACCGGGAATCCTACATGGTT TGAGGAGTGGCTGCTTTTCT
se = sense primer; as = antisense primer. Green nucleotides are unspecific primer extensions to adjust the GC-contents to 50% and approximate the length of sense and antisense primer. All primers were obtained from Eurofins MWG GmbH, Germany.		

Table 2.8: Primer sequences for real-time PCR

Gene		Sequence (5´ - 3´)
ABCB1	se as	GCTGTCAAGGAAGCCAATGC GCTTCTGCCCACCACTCAAC
ABCB5	se as	GAGAGCAGCAAGGGAAGCAA CAGGGCAGACGTAGCCTCAT
ABCC2	se as	CTGGTTCCTGTCCCTATTCTGG CTGGAATCCGTAGGAGATGAAGA
ABCG2	se as	CGTGGTGTGTCTGGAGGAGA CGAGGCTGATGAATGGAGAAG
ACTB	se as	TCAAGATCATTGCTCCTCCTGAG ACATCTGCTGGAAGGTGGACA
BMI-1	se as	GATGCCCAGCAGCAATGACT GGCTGTTGGCCTTGTCACTC
CD166	se as	ACTGGCAGTGGAAGCGTCAT GTCTGCCTCATCGTGTTCTGG
CSPG4	se as	TCGTGCTGTTCTCACACAGA CTTCAGCGAGAGGAGCACTT
FGFR1	se as	TACGGCAGCATCAACCACAC TTGTCTGGGCCAATCTTGCT
GAPDH	Se as	CTGGTAAAGTGGATATTGTTGCCAT TGGAATCATATTGGAACATGTAAACC
MITF	se as	CTTGGGCTTGATGGATCCTG GGTTGGCTGGACAGGAGTTG
MSI-1	se as	GACGCCATGCTGATGTTTGA ATGAAGGCGTCCATTCCGTA
se = sense Primer; as = antisense Primer. All primers were obtained from Eurofins MWG GmbH, Germany.		

Table 2.9: Buffers, solutions and media

Agarose gels	
Agarose gels	1-2% Agarose (w/v) in 1x TAE, 2 µl/50 ml GelRed
50x TAE	242 g Tris Base (MW 121.13), 18,6 g EDTA (MW 372.24) ad 1 l dH_2O, pH 8.0
DNA-Loading Buffer	1 ml 1 M Tris/HCl pH 7.5, 0.1 g Orange G, 20 ml Ficoll Plus ad 100 ml dH_2O
DNA Ladder (50 ng/µl)	25 µl 100 bp DNA Ladder, 125 µl DNA-Loading Buffer, ad 500 µl dH_2O
Cell culture	
Dissociation mix	1% Penicillin-Streptomycin, 1 mg/ml Collagenase IV and 0.1 mg/ml DNase I in RPMI
2x RPMI medium for soft agar assays	20 ml 10x RPMI, 20 ml FCS, 2 ml Penicillin-Streptomycin, 2 ml L-Glutamine, 10 ml $NaHCO_3$ ad 100 ml dH_2O
Q263	Quantum 263 and 1% Penicillin-Streptomycin
RPMI	RPMI, 1% Penicillin-Streptomycin and 10% FCS
bFGF solution	10 µg bFGF in 1 ml bFGF-buffer (2 mM EDTA, 0.5% BSA, ad 50 ml D-PBS), aliquots stored at -20°C
hESC medium	20 ml KnockOut DMEM, 5 ml KnockOut Serum Replacement, 0.25 ml L-Glutamine, 0.25 ml Penicillin-Streptomycin, 0.25 ml NEAA, 1.75 µl 2-Mercaptoethanol, mixed and sterile-filtered, addition of 10 µl bFGF solution (10 µg/ml)
PCR	
dNTPs-Mix (10 mM)	10 µl 100 mM ATP, GTP, CTP, TTP ad 100 µl H_2O
Primermix (25 µM)	25 µl 100 µM sense Primer and 25 µl 100 µM antisense Primer ad 100 µl dH_2O
Standard PCR-Mix	5 µl 5x Green GoTaq Reaction buffer, 0.5 µl dNTP-Mix, 1 µl Primermix, 0.125 µl GoTaq Polymerase, 1 µl template ad 25 µl dH_2O
Real-time PCR-Mix	3.5 µl cDNA, 1.5 µl primermix (each primer 2.5 µM), 5 µl SYBR-Green PCR master mix
Transformation and *E. coli* culture	
LB medium	10 g Bacto Trypton, 5 g Bacto yeast extract, 10 g NaCl ad 1 l dH_2O (pH 7.0)
LB agar	15 g Bacto Agar, 10 g Bacto Trypton, 5 g Bacto yeast extract, 10 g NaCl ad 1 l dH_2O (pH 7.0)
Immunofluorescence	
10x PBS	80 g NaCl, 2 g KCl, 14.4 g Na_2HPO_4, 2.4 g KH_2PO_4 ad 1 l dH_2O, pH 7.4
DAPI solution	2 µg DAPI ad 10 ml with PBS
2nd antibody buffer	0.05% Tween-20, 1% BSA in 1x PBS
SDS-PAGE	
Lysis buffer	2,5 ml 20% SDS solution, 0.5 ml 1 M Tris-HCl (pH 7.5), 0.2 ml 0.5 M EDTA (pH 8.0) ad 50 ml dH_2O
4x Loading buffer	8% SDS, 40% Glycerol, 0.25 M Tris-HCl (pH 6.8), 0.1% Bromophenol Blue, 20% 2-Mercaptoethanol
Running buffer	0.192 M Glycine, 0.1% SDS, 0.025 M Tris Base pH 8.3 in dH_2O
Resolving gel buffer	0.8% SDS, 1.5 M Tris Base pH 8.8 in dH_2O
Stacking gel buffer	0.4% SDS, 0.25 M Tris Base pH 6.8 in dH_2O
Resolving gel (10%)	3.3 ml 30% Acrylamide / Bis solution, 2.5 ml resolving gel buffer, 4.2 ml dH_2O, 10 µl TEMED and 60 µl 10% APS
Stacking gel	0.49 ml 30% Acrylamide / Bis solution, 1.88 ml stacking gel buffer, 1.39 ml dH_2O, 3.75 µl TEMED and 22.5 µl 10% APS
Western Blot	
BSA buffer	0.1% Tween-20, 5% BSA in 1x TBS
Milk blocking buffer	0.1% Tween-20, 5% Nonfat dry milk in 1x TBS
LI-COR blocking buffer	PBS and Odyssey Blocking Buffer mixed 1:1
PBST	0.1% Tween-20 in 1x PBS
10x TBS	100 ml 1 M Tris-HCl (pH 8.0), 300 ml 5 M NaCl ad 1 l dH_2O
TBST	0.1% Tween-20 in 1x TBS

MACS	
MACS buffer	2 mM EDTA, 5% FCS in PBS
FACS	
HBSS+ buffer	2% FCS, 10 mM HEPES in HBSS
MTT assay	
MTT solution	2.5 mg MTT in 1 ml PBS
Sequencing	
Sequencing reaction mix	0.25 µl Ready Reaction Mix (BigDye Terminator v3.1 Cycle Sequencing Kit), 2 µM sense and antisense primer, 2 µl BigDye Terminator v3.1 Sequencing Buffer (5X), 1 µl 5 M Betaine, 100 ng template ad 10 µl dH_2O

Table 2.10: Instruments and materials

Product	Company
6 tube magnetic stand	Applied Biosystems, USA
19G x 1.5“, 1.1 mm x 40 mm BD Microlance 3 needles	BD Biosciences, USA
3730*xl* DNA Analyzer	Applied Biosystems, USA
BD BioCoat BD Matrigel Invasion Chamber, 8.0 µm Pore, PET Membrane, 24 well	BD Biosciences, USA
BD BioCoat Control Chamber, 8.0 µm PET Membrane, 24 well	BD Biosciences, USA
Biological Safety Cabinets	NuAire, Inc., USA
Biopur Combitips plus 0.2ml, 1 ml and 5 ml	Eppendorf AG, Germany
Cell culture flasks; 25, 75 and 175 cm^2	BD Biosciences, USA
Cell scraper	TPP AG, Switzerland
Cell Strainer (70 µm mesh size)	Miltenyi Biotec GmbH, Germany
Centrifuge Avanti J-25	Beckman Coulter GmbH, Germany
Centrifuge 5424	Eppendorf AG, Germany
Centrifuge 5810R	Eppendorf AG, Germany
Centrifuge MiniSpin Plus	Eppendorf AG, Germany
Combitips 0.1, 0.2, 1 and 5 ml	Eppendorf AG, Germany
EPICS XL-MCL flow cytometer with MPLUS cell cycle software	Beckman Coulter GmbH, Germany
FACSCalibur System with CellQuest Pro Software 4.0.1	BD Biosciences, USA
FACSDiva Flow Cytometer & Cell Sorter with BD FACSDiva Software 6.0	BD Biosciences, USA
Gel documentation system Syngene G:Box Chemi HR16 with Gene Snap 7.04.05 software	New England BioGroup, USA
gentleMACS dissociator	Miltenyi Biotec GmbH, Germany
gentleMACS C Tubes	Miltenyi Biotec GmbH, Germany
Glass coverslips	Carl Roth GmbH & Co. KG, Germany
Heraeus Cytoperm 2 CO_2 incubator	Thermo Fisher Scientific, Inc., USA
iBlot Dry Blotting System	Invitrogen GmbH, Germany
iBlot Transfer Stack, Mini (Nitrocellulose)	Invitrogen GmbH, Germany
iBlot Transfer Stack, Mini (PVDF)	Invitrogen GmbH, Germany
Illumina HumanWG-6_V3 Expression BeadChips	Illumina, Inc., USA
Illumina HumanRef-8_V3 Expression BeadChips	Illumina, Inc., USA
Illumina HumanWG-12_V4 Expression BeadChips	Illumina, Inc., USA
Illumina BeadStation 500 platform	Illumina, Inc., USA
Laminar flow hood Antair BSK	Heraeus Holding GmbH, Germany
LSR II Flow Cytometer System with FlowJo Software 6.4.7	BD Biosciences, USA
Luminescent Image Analyzer LAS-1000 with Image Reader LAS-1000 Pro V2.61 software	FujiFilm, USA
MACS Seperation Columns 25 LS Columns	Miltenyi Biotec GmbH, Germany
MicroAmp optical 384 well reaction plates	Applied Biosystems, USA
MicroAmp 8-Tube Strip (0.2 ml)	Applied Biosystems, USA

MicroAmp 8-Cap Strip	Applied Biosystems, USA
Microplate Spectrophotometer Benchmark Plus	Bio-Rad Laboratories, Inc., USA
Microscope slides, cut edges	Carl Roth GmbH & Co. KG, Germany
Mini-Protean Tetra System	Bio-Rad Laboratories, Inc., USA
NanoDrop spectrophotometer	NanoDrop Technologies, USA
Neubauer improved counting chamber	Carl Roth GmbH & Co. KG, Germany
Odyssey (Infrared Imaging Systems)	LI-COR Biosciences, USA
One Shot TOP10F´ chemically competent *E. coli*	Invitrogen GmbH, Germany
Optical adhesive covers	Applied Biosystems, USA
Orbital shaking incubator GFL 3031	GFL, Germany
pH-Meter Φ 340	BD Biosciences, USA
Pipet Safe-Seal-Tips Premium Line; 10, 20, 200, 1000 µl	Biozym Scientific GmbH, Germany
Power supply PowerPac Basic	Bio-Rad Laboratories, Inc., USA
Pre-Separation Filters	Miltenyi Biotec GmbH, Germany
QuadroMACS Separator	Miltenyi Biotec GmbH, Germany
Qubit assay tubes *set of 500*	Invitrogen GmbH, Germany
Reaction tubes 0.5 ml, 1.5 ml and 2 ml	Eppendorf AG, Germany
Round-bottom tubes, 5 ml, polystyrene	BD Biosciences, USA
Round-bottom tube with cell strainer	BD Biosciences, USA
RPMI-1640, 1x	Invitrogen GmbH, Germany
Savant Speed Vac SC100 with refrigerated Vapor Trap RVT100	Savant, Inc. Laboratory, USA
Serological pipets, steril; 2, 5, 10 and 25 ml	BD Biosciences, USA
S.O.C. Medium (10x 10 ml)	Invitrogen GmbH, Germany
Steritop-GP Filter Unit 250 and 500 ml	Millipore, USA
Syringes 1ml	BD Biosciences, USA
Thermal cycler PTC-100	MJ Research, Inc., USA
Thermal cycler PeqStar 96 HPL	PEQLAB Biotechnologie GmbH, Germany
Thermomixer	Eppendorf AG, Germany
Tissue culture plates; 6, 12, 24 and 96 well	BD Biosciences, USA
Vacofuge Concentrator 5301	Eppendorf AG, Germany
VECTASHIELD Mounting Medium for fluorescence	Biomol GmbH, Germany
Water Purification System	Millipore, USA
Zeiss Axiovert 40 CFL microscope with illuminator HPX 120C and AxioVision Rel.4.8 software	Carl Zeiss AG, Germany

2.2 Cell culture

2.2.1 Establishment of primary cell cultures

Surgically obtained tumor samples were cut into small pieces of 2-4 mm with sterile scalpels and transferred into gentleMACS C Tubes containing 10 ml dissociation mix. C Tubes were placed into the gentleMACS dissociator and program “h_tumor_01” was used to mince the tumor followed by 30 min incubation at 37°C with continuous rotation. After a subsequent run in the gentleMACS dissociator with program “h_tumor_02” this incubation step was repeated and a final run with the gentleMACS program “h_tumor_03” was performed. The resulting cell suspension was dissociated by applying it onto a 70 µm cell strainer placed on a 50 ml tube followed by a washing step with 5 ml Q263. After

5 min centrifugation at 1000 rpm, the supernatant was discarded and the cell pellets were resuspended in 500 µl PBS.

To remove erythrocytes from the cell suspension, 5 ml of the 1x Red Blood Cell Lysis Solution was added, vortexed and incubated at room temperature for 10 min. Cells were spun down for 5 min at 1000 rpm, resuspended in Quantum 263 medium (Q263) and seeded into an appropriate cell culture flask. Q263 is a basal medium optimized for tumor cells and based on RPMI 1640 medium. Q263 contains an optimized mixture of trace elements, growth factors and selected serum components and a synthetic iron-binding molecule which facilitates the transport of iron ions into the cells. All cells were routinely cultivated at 37°C and 5% CO_2.

2.2.2 Maintenance of primary cell cultures

According to the requirements of the cells medium was replaced every 2 to 5 days until confluence had reached 80-100%. Then, cells were washed with PBS and incubated with a thin layer of Trypsin-EDTA until cells detached from the surface. Trypsination was stopped by adding medium. For further cultivation cells were splitted into new culture dishes. For RNA, DNA or protein isolation cell numbers were determined using a Neubauer counting chamber. Required amounts of cells (usually 2x 10^6 cells) were centrifuged, washed once with PBS and pelleted into 1.5 ml tubes. Supernatant was discarded and cell pellets were shock frozen in liquid nitrogen. Finally, pellets were stored at -80°C for further use.

2.2.3 Melanocyte culture

Melanocytes obtained from Lonza were thawed and subcultured according to the manufacturer´s instructions for the Clonetics Normal Human Melanocyte Cell System. Neonatal melanocytes were acquired from a newborn, male Caucasian and adult melanocytes from a 29 years old female Caucasian individual.

2.2.4 Cell culture with hESC medium

Tumor cells grown to 80% confluence in Q263 medium in 75 cm^2 flasks were harvested as described above (see section 2.2.2), splitted 1 to 10, resuspended in 2 ml hESC medium and seeded in 6 well culture plates. Every other day medium was exchanged without disrupting the colonies and replaced by freshly prepared hESC medium.

2.3 Cell sorting

2.3.1 MACS

In order to sort tumor cells into $CD133^+$ and $CD133^-$ fractions the Indirect CD133 MicroBead kit was used on LS columns and the QuadroMACS from Miltenyi. 80% confluent cells were washed with PBS and detached from the flasks by 3 min incubation with accutase. Enzyme activity was stopped by adding medium and cell numbers were determined using a Neubauer counting chamber. A maximum amount of $4x\ 10^7$ cells was centrifuged and resuspended with 350 µl MACS buffer, 100 µl FcR blocking reagent and 50 µl CD133/1 (AC133)-Biotin-conjugated antibody from the Indirect CD133 MicroBead kit. Subsequently, cells were incubated at 4°C for 10 min and washed twice with 10 ml MACS buffer. A 15 min incubation at 4°C with anti-Biotin microbeads and a final washing step with 10 ml MACS buffer followed. Labeled cells were resuspended in 500 ml MACS buffer and loaded onto an equilibrated LS column placed in a QuadroMACS separator. Columns were washed and $CD133^+$ cells were eluted following the company's protocol. To achieve a higher purity of $CD133^-$ cells, cells were applied again onto a new, equilibrated LS column. $CD133^+$ and $CD133^-$ cells were counted and seeded for 24 h in an appropriate culture dish before harvesting them for further analysis.

2.3.2 FACS

Fluorescence-activated cell sorting (FACS) was performed in order to fractionate melanoma cells on the basis of intracellular markers into OCT4-$EGFP^+$ and OCT4-$EGFP^-$ cells. Cells were harvested as described earlier (section 2.2.2), spun down for 5 min at 1000 rpm and the cell pellet resuspended in an appropriate volume of MACS buffer. The cells were sorted and analyzed by the Flow Cytometry and Cellsorting Core Facility (DRFZ, Berlin) using the FACS DiVa Flow Cytometer & Cell Sorter with BD FACSDiva Software 6.0. To recover from stress OCT4-$EGFP^+$ and OCT4-$EGFP^-$ cells were spun down and seeded again in an appropriate culture dish before harvesting them five days later for further analysis.

2.4 RNA and DNA analyses

2.4.1 Isolation and quantification of genomic DNA

QIAamp DNA Mini Kit was used for isolation of genomic DNA from frozen cells according to the manufacturer's instructions. Isolated DNA was quantified using the Quant-iT dsDNA BR Assay Kit according to the manufacturer´s instruction.

2.4.2 RNA isolation and quantification

RNA isolation from frozen cells was performed with the RNeasy Mini Kit following the manufacturer's protocol. Additionally at each time, 2x 10^6 cells were homogenized in 350 µl RLT buffer by passing the lysate five times through a 19G needle and a DNase I on column digestion was performed to remove trace amounts of genomic DNA. Total RNA was eluted in 30 µl RNase-free water. To ensure RNA integrity, all RNA samples were directly frozen in liquid nitrogen after RNA quantification and stored at -80°C until further use. Isolated RNA was quantified using the Quant-iT RNA Assay Kit according to the manufacturer´s instruction.

2.4.3 Reverse transcription

First-strand cDNA was generated from 2 µg RNA using the SuperScript VILO cDNA synthesis kit in 20 µl reaction volume. Generated cDNA was diluted with DEPC-treated water to a final volume of 50 µl for standard PCR and of 100 µl for real-time PCR.

2.4.4 Primer design

Starting point for the primer design were transcript sequences described by Ensembl Genome Browser, assembly GRCh37.p5, February 2009 (Retrieved 10 May 2011 <http://www.ensembl.org/index.html>). This database was chosen because here, the positions of exon-exon boundaries are marked for each multi-exon transcript. This facilitates the design of primers where sense and antisense primer are located in different exons. Consequentially, only mRNA is amplified during PCR and no genomic DNA that could be present in trace amounts after RNA isolation and reverse transcription.

Primer design was performed with Primer3 0.4.0 software (Rozen *et al.* 2000) (Retrieved 10 May 2011 <http://frodo.wi.mit.edu/primer3/>). Thereby, primer size was restricted to 18-22 bp and 3'self complementarity of each primer as well as complementarity of sense and antisense primer were supposed to be very low.

To adjust the GC-contents to 50% and approximate the length of sense and antisense primer recommended primers of Primer3 were unspecifically extended by single nucleotides at the 5´end. The size of the resulting PCR products was chosen according to the method applied. For real-time PCRs ideal product size should be 80-200 bp and for standard PCR it should range from 200-500 bp

2.4.5 Standard polymerase chain reaction (PCR)

Standard PCRs were performed in 96 well PCR Plates or MicroAmp 8-tube strips with 10 ng cDNA as template (adjusted to 1 µl). The standard PCR-mix for one reaction is listed

in **Table 2.9** and all primers used in **Table 2.7**. Standard PCR was carried out on thermal cycler PeqStar 96 HPL with the program specified in **Table 2.11**. Sole exception was the PCR with the OCT4A primers. This was performed on thermal cycler PTC-100 with the same PCR program but an annealing temperature of 58.5°C and a total of 35 cycles. For the sequencing and restriction digest 1 µl of the OCT4A PCR product was used again as template in a Re-PCR with OCT4A nested primers to increase the yield of the OCT4A sequence in melanoma samples.

Table 2.11: Program for standard PCR.

Step	Process	Time	Temperature
1	Denaturation	2 min	95°C
2	Denaturation	30 sec	95°C
3	Primer annealing	45 sec	55°C
4	Amplification	50 sec	72°C
5	Repeat of step 2-4 for an additional 29 times		
6	Final extension	10 min	72°C
7	Cool down	∞	4°C

2.4.6 Real-time polymerase chain reaction (real-time PCR)

Quantitative real-time PCR for analysis of differential gene expression was performed in optical 384 well reaction plates in a total volume of 10 µl real-time PCR-mix (see **Table 2.9**) and in duplicates for each gene (Primer sequences are listed in **Table 2.8**). Used PCR instrument was the ABI PRISM 7900HT Sequence Detection System with the program shown in Table 2.12. The last heating step in stage 4 was performed with an increment of 2% in order to allow the generation of a dissociation curve from the product.

Table 2.12: Program for quantitative real-time PCR.

Step	Process	Time	Temperature
1		2 min	50°C
2	Denaturation	10 min	95°C
3	Amplification	15 sec	95°C
		1 min	60°C
	Repeat of step 3 for an additional 39 times		
4	Dissociation curve	15 sec	95°C
		15 sec	60°C
		15 sec	95°C

The output data generated by the Sequence Detection System 2.2.1 software were analyzed with Excel 2007 (Microsoft, USA). Calculation of the differential gene expression was done with the comparative Ct (threshold cycle) method recommended by the manufacturer. Housekeeping genes GAPDH and ACTB served as endogenous controls for normalization.

2.4.7 Gel electrophoresis

PCR products and RNA samples for Illumina Bead Chip hybridization were separated via agarose gel electrophoresis.

2.4.7.1 Electrophoresis of DNA samples

According to the PCR product size 2% agarose gels were prepared (**Table 2.9**). 10 µl of each product were loaded on the gel and were run in 1x TAE at 80 V. As marker 5 µl of the DNA ladder (**Table 2.9**) were used. The results were documented with the gel documentation system Syngene G:Box Chemi HR16 with Gene Snap 7.04.05 software.

2.4.7.2 Electrophoresis of RNA samples

Isolated total RNA (see section 2.4.2) was quality checked by agarose gel electrophoresis. 1 µg RNA was diluted with 7 µl dH_2O and 8 µl 2x RNA Loading Dye (supplemented with RiboRuler High Range RNA Ladder) heated to 70°C for 10 min, chilled on ice and loaded on a 1% agarose gel (**Table 2.9**). 4 µl of the RNA Ladder were also denaturated and loaded on the gel as control. RNA integrity was evaluated by the sharpness and ratio of the 28S and 18S rRNA signals. For running conditions and documentation see section 2.4.7.1.

2.4.8 Restriction digest

For the restriction digest the *OCT4* PCR product (using *OCT4* nested primers) was purified with the QIAquick PCR Purification Kit according to the manufacturer´s instructions and eluted in 50 µl EB buffer. DNA concentration was determined again using the Quant-iT dsDNA HS Assay Kit and 500 ng purified DNA was digested with 5 U of the restriction enzymes *Apa*I and *Tsp*45I in a total volume of 20 µl, respectively applying the protocol and buffers from New England Biolabs.

2.4.9 Synthesis of biotin-labelled cRNA and Illumina Bead Chip hybridization

cRNA was Biotin-labelled using Illumina TotalPrep RNA Amplification Kit according to the manufacturer´s instructions with 500 ng of quality-checked total RNA in 11 µl RNase-free water as input. The quantity and quality of labeled cRNA was determined using a NanoDrop spectrophotometer. 750 ng cRNA in 5 µl RNase-free water and 1500 ng cRNA in 10 µl RNase-free water were hybridized on Illumina HumanWG-6, HumanRef-8 Expression and HumanHT-12 v4 Expression BeadChips, respectively. If the concentrations were below appropriate values the samples were concentrated by speed vac centrifugation. Chip hybridization, washing, Cy3-streptavidin staining, and scanning were

performed on an Illumina BeadStation 500 platform using reagents and protocols supplied by the manufacturer.

2.4.10 Gene expression and cluster analyses

Illumina bead-level data were summarized with the Illumina BeadStudio software and were quantile-normalized in R/Bioconductor (Gentleman *et al.* 2004) via the *lumi* package (Du *et al.* 2008). Gene expression was determined via a threshold of 0.05 for the Illumina detection p-value. Differential expression with respect to the control group was tested using Student's *t*-test, the Welch test and the Wilcoxon test in parallel. The Bioconductor package *q-value* (Storey 2002) was employed to control the false discovery rate. Genes were considered differentially expressed when the Illumina detection p-value of at least one of the control or treatment group and at least one of the p-values of the above tests was less than 0.05 and the ratio laid outside predefined thresholds (<0.75, >1.5).

Pathways and Gene Ontologies (GOs) were analyzed using the GOstats package and annotations packages from the R/Bioconductor environment (Ihaka *et al.* 1996, R Development Core Team 2008). Significant genes that have been determined in the preceding analyses were used as input. The signifcant genes' IDs were mapped to Entrez IDs. All IDs on the dedicated microarray mappable to Entrez IDs were used as background. The enriched KEGG (Kyoto Encyclopedia of Genes and Genomes) pathways (Kanehisa *et al.* 2010) were determined analogously. Enriched KEGG pathways and GO categories were calculated via the hypergeometric test.

Cluster analysis was performed via the methods "hclust" and "heatmap" from the statistical software package R (R Development Core Team 2008). Genes found to be differentially expressed were filtered from the quantile normalized Illumina bead summary data. The resulting genes were read into a data matrix with rows corresponding to different genes and columns corresponding to different experiments. Spearman's correlation was used as distance measure for the method "hclust" and "complete linkage" as agglomeration method. Cluster analysis following RT-PCR experiments was performed analogously. The values to be analyzed were read into a data matrix with rows corresponding to different experiments, here different cell lines and columns corresponding to different genes.

2.4.11 Cell cycle analysis

Cell cycle analysis was performed by our collaboration partners at the Elbeklinikum Buxtehude in the department of Molecular Cell Biology. Cells were harvested, fixed in 70% ice-cold ethanol and stored at -20°C for further use. For propidium iodide (PI) staining

cells were mixed with 500 µl TBS and pelleted at 3550 rpm for 10 min. The supernatant was discarded and the cells were resuspended in 1000 µl Roti-Block. Following 10 min blocking and a second centrifugation step, cells were incubated with 1000 µl PBS for 10 min at room temperature. Subsequently, cells were pelleted and resuspended in 497 µl 0.01% RNase supplemented with 6 µg/ml PI. Cells were incubated in the dark for 5 min before cell cycle distribution was determined on an EPICS XL-MCL flow cytometer with excitation wavelength of 488 nm and analyzed with MPLUS cell cycle software.

2.5 Cycle Sequencing

Cycle sequencing was performed in 96 well reaction plates on a thermal cycler PTC-100 using the BigDye Terminator v3.1 Cycle Sequencing Kit and isolated genomic DNA (see 2.4.1) or purified PCR products (using the QIAquick PCR Purification Kit) as template. Ingredients of the sequencing reaction mix are listed in **Table 2.9** and the program for cycle sequencing in **Table 2.13**.

Table 2.13: Program for cycle sequencing.

Step	Process	Time	Temperature
1	Denaturation	1 min	96°C
2	Denaturation	30 sec	96°C
3	Primer annealing	15 sec	50°C
4	Amplification	4 min	60°C
5	Repeat of step 2-4 for an additional 24 times		
7	Cool down	∞	4°C

To obtain best sequencing results excess dye terminators had to be completely removed after cycle sequencing since they can interfere with basecalling in the early part of the sequence. For this the ethanol/EDTA precipitation method was used. The 96 well reaction plate was removed from the thermal cycler and spun briefly. 1 µl 3 M sodium acetate (pH 5.5), 1 µl 125 mM EDTA and 25 µl 100% ethanol were added to each well. Subsequently, the plate was sealed and the samples mixed by extensive shaking. After an incubation period of 15 min at room temperature and a 60 min centrifugation step at 3200 rpm and 4°C the supernatant was discarded and the DNA pellet washed with 70 µl of 70% ethanol. Samples were again mixed by extensive shaking and centrifuged at 3200 rpm and 4°C for 30 min. The supernatant was discarded and the last washing step repeated. Finally, purified DNA pellets were dried by inverting the reaction plate and spun up to 800 rpm for 1 min and resuspended in 10 µl Hi-Di Formamide. Sample electrophoresis was performed on a 3730*xl* DNA Analyzer.

2.6 Whole transcriptome mRNA sequencing

For whole transcriptome mRNA sequencing total RNA was isolated as described in section 2.4.2. The quantity and quality of RNA was determined using the NanoDrop spectrophotometer and the Quant-iT RNA Assay Kit according to the manufacturer´s instruction.

2.6.1 rRNA removal

The selective removal of 18S and 28S rRNA molecules from total RNA using the RiboMinus Transcriptome Isolation Kit enabled the analysis of the whole transcriptome without any interference from rRNA molecules. This was performed with 10 µg total RNA following the manufacturer's instructions. Resulting rRNA depleted RNA fraction was concentrated using ethanol precipitation.

2.6.2 Ethanol precipitation

Samples were transferred to clean RNase-free 2 ml microcentrifuge tubes. 1 µl PolyAcryl Carrier (acryl polymer for precipitation of RNA and DNA), one-tenth RNA volume of 3 M sodium acetate (~ 50 µl) and 2.5x RNA volume of 100% ethanol were added, mixed well and incubated at -80°C for 30 min. Subsequently, tubes were centrifuged for 15 min at 12000 g at 4°C and the supernatant was discarded without disturbing the pellet. After adding 500 µl 70% cold ethanol tubes were centrifuged again for 5 min at 12000 g at 4°C and supernatant discarded. The washing step with 70% ethanol was repeated and the pellet air-dried for ~5 min. Finally, RNA pellets were resuspended in 10 µl RNase-free water.

2.6.3 Double-stranded cDNA synthesis

Double-stranded cDNA was synthesized using the SuperScript Double Stranded cDNA Synthesis Kit with 1 µl random hexamers (500 µg/ml) and eluted with 11 µl RNase-free water. Further processing for the transcriptome mRNA sequencing was performed by Bernd Timmermann at the MPI for Molecular Genetics, Berlin.

2.6.4 Sequencing data analysis

Detection analysis of differential single nucleotide polymorphisms (SNPs) in paired-end $CD133^+$ and $CD133^-$ samples was performed by Wasco Wruck as follows. First the reads were aligned versus a reference sequence (human hg19 from UCSC, provided as pre-built bowtie index) via the alignment software bowtie (Langmead *et al.* 2009) using default parameters, except parameters for paired-end alignment, multi-processor parallel thread launching and output in SAM (Sequence Alignment/Map) file format (Li *et al.* 2009). The

SAM file format was used for follow-up processing via the SAMtools. Here the software environment picard (Retrieved 10 March 2011 <http://picard.sourceforge.net>) was applied to remove duplicate reads. The SAMtools mpileup routine detected SNPs and short insertions and deletions of less than 50 nucleotides filtering out high maximum read depths (greater than twice the average read depth). Differing genotypes in the $CD133^+$ and $CD133^-$ samples were found applying the following criteria: both samples have differing genotypes; one of both samples' genotypes differs in both alleles from the reference base; the Phred score of the differing genotype is greater than 20 (corresponds to a p-value of 0.01). Finally, chromosomal positions found to differ between $CD133^+$ and $CD133^-$ samples were annotated with ENSEMBL gene and gene symbol via Biomart. Prediction method SIFT (Sorting Intolerant From Tolerant) was used to predict whether an amino acid substitution affects protein function (Ng *et al.* 2006).

2.7 Plasmid works

2.7.1 phOCT4-EGFP-1 construct

The phOCT4-EGFP-1 construct was kindly provided by Dr. Wei Cui. It was generated in 2004 by amplifying the human *OCT4* promoter with the following primers: hOCT4pr-F (5'-TT CCC ATG TCA AGT AAG TGG GGT GG-3') and hOCT4pr-R (5'-CGA GAA GGC AAA ATC TGA AGC CAG G-3') using human genomic DNA as a template. The fragment was cloned into TOPO vectors (Invitrogen) and the fidelity of the DNA sequence was confirmed by bi-directional sequencing. Subsequently, the correct hOCT4 promoter was cloned into the multiple cloning site (MCS) of the pEGFP-1 vector (BD Biosciences) upstream of the EGFP coding sequence (Gerrard *et al.* 2005).

EGFP is a derivative of wild type GFP, which has been optimized for brighter fluorescence and higher expression in mammalian cells. Proper processing of the 3' end of the EGFP mRNA is assured by the SV40 polyadenylation signals downstream of the EGFP gene. The vector also contains an SV40 origin for replication in mammalian cells expressing the SV40 T antigen. A neomycin-resistance cassette allows stably transfected eukaryotic cells to be selected using G-418. It consists of the SV40 early promoter, the neomycin/kanamycin resistance gene of Tn5, and polyadenylation signals from the Herpes simplex virus thymidine kinase (HSV TK) gene. A bacterial promoter upstream of this cassette confers kanamycin resistance in *E. coli*. The pEGFP-1 backbone also provides a pUC origin of replication for propagation in *E. coli* and an f1 origin for single-stranded DNA production. A map of the phOCT4-EGFP-1 construct is shown in **Figure 2.1**.

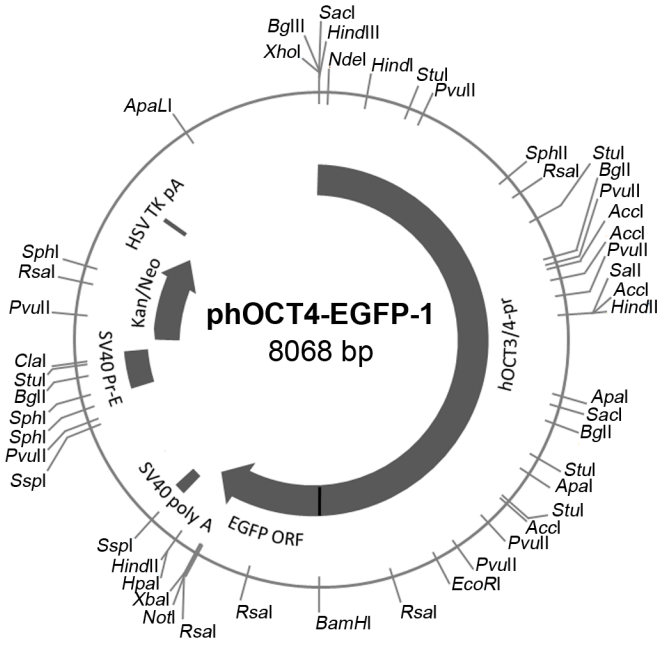

Figure 2.1: Map of the phOCT4-EGFP-1 construct.
The phOCT4-EGFP-1 plasmid was kindly provided by Dr. Wei Cui. It contains the EGFP reporter under control of the OCT4 promoter and a neomycin-resistance cassette as well as the SV40 origin for replication in mammalian cells expressing the SV40 T antigen.

2.7.2 Transformation and *E. coli* culture

50 µl aliquots of One Shot TOP10F´ chemically competent *E. coli* were thawed on ice and divided into two tubes. 25 µl were mixed with 10 ng phOCT4-EGFP-1 plasmid vector, the other half with equal volume dH_2O as negative control. Following 30 min incubation on ice cell suspensions were heated for 30 sec at 42°C and again cooled down on ice for 2 min. Thereafter, 250 µl S.O.C. medium were added, respectively and incubated in a water bath at 37°C for 1.5 h. Cells were centrifuged at 5000 rpm for 5 min and supernatant discarded except for 50 – 100 µl. Subsequently, cells were resuspended in the remaining supernatant and spread on lysogeny broth (LB) plates supplemented with 30 µg/ml kanamycin. After 16-18 h incubation at 37°C single colonies were picked with sterile tips and grown in 4 ml LB medium supplemented with 30 µg/ml kanamycin for 8 h shaking at 37°C. 500 µl starter culture were diluted with 100 ml LB medium supplemented with 30 µg/ml kanamycin and incubated overnight at 37°C shaking.

2.7.3 Isolation of plasmid DNA

Bacteria from the main 100 ml culture were pelleted via centrifugation at 3000 g and 4°C for 10 min. Isolation of plasmid DNA was then perfomed with the EndoFree Plasmid Maxi Kit according to the manufacturer's instructions. Plasmid DNA of one maxi preparation was finally eluted in 150 µl endotoxin-free TE buffer provided with the kit. DNA concentration was determined using the Quant-iT dsDNA BR assay kit.

2.7.4 Plasmid transfection

One day prior to transfection 3.5x 10^5 ChaMel91 cells or 4x 10^5 $CD133^+$ and $CD133^-$ ChaMel91 cells were seeded in 2 ml RMPI/10% FCS without PS into 6 well plates. For plasmid transfection 6 µg plasmid DNA were diluted ad 250 µl with RPMI and mixed gently. In a second reaction tube 15 µl Lipofectamine 2000 were diluted with 235 µl RPMI and incubated for 5 min at room temperature. Prepared DNA and Lipofectamine 2000 were combined and incubated for 20 min at room temperature. Subsequently, 500 µl of complexes were added to each well with cells and 2 ml medium and mixed gently. Cells were incubated at 37°C and 5% CO_2 with one medium change 5 h post transfection and tested for transgene expression after 24 h.

2.7.5 Cultivation of stable clones

For cultivating stably transfected clones of ChaMel91 cells they were treated with 500 µg/ml G-418-Sulphate (G-418). G-418 blocks polypeptide synthesis by inhibiting the elongation steps in cells. Only tumor cells that contain the phOCT4-EGFP-1 plasmid are resistant to this concentration of G-418 due to the neomycin-resistance cassette of the plasmid (see 2.7.1).

2.8 Protein analyses

2.8.1 Protein isolation and quantification

For isolating proteins from frozen cells, pellets were thawed on ice, loosened by flicking the tubes and resuspended in appropriate amounts of lysis buffer. After 5 min incubation at 99°C denaturated proteins were cooled down on ice and protein concentrations were determined by BCA assay according to the microplate procedure of the Pierce BCA protein assay kit with 1:10 dilutions of the protein lysates.

2.8.2 Fractionation of total protein lysates

Total protein lysates were fractioned into nuclear and cytoplasmic components using the NE-PER Nuclear and Cytoplasmic Extraction Reagents according to the manufacturer's instructions. Reagents CER I and NER were supplemented with protease inhibitor cocktail from Sigma. To obtain a better fractionation the insoluble pellet of step 9 of the protocol, which contains the nucleic fraction, was rinsed twice with PBS before it was lysed with 35 µl ice-cold NER reagent.

2.8.3 SDS-PAGE gel electrophoresis

Protein gels were prepared in Mini-Protean Tetra System protein chambers. The resolving gel (8-10%) was prepared (see **Table 2.9**) and stacked with isopropanol to get an even surface. After polymerization the isopropanol was discarded, the resolving gel rinsed with dH_2O and the stacking gel was poured (see **Table 2.9**). Protein lysates were mixed with 4x loading buffer and lysis buffer (to adjust equal volume). The samples were heated to 99°C for 5 min and cooled down on ice for 1 min before they were loaded onto the gel. Per lane 40-100 µg protein lysate were applied and per gel at least one lane with a protein marker. 2.5 µl of PageRuler Prestained Protein Ladder was used for fluorescent western blots and 5 µl MagicMark XP Western Protein Standard for ECL western blots. The gel was run in 1x running buffer at 80 V until the loading buffer reached the lower end of the stacking gel and then a current of 120 V was applied.

2.8.4 Western blotting

2.8.4.1 ECL western blots

Protein lysates were separated on PAA gels and transferred to a PVDF membrane using the iBlot Dry Blotting System. The blots were incubated in milk blocking solution (**Table 2.9**) for 1 h at room temperature and overnight at 4°C with primary antibody dissolved in milk blocking solution. Thereafter, the membrane was extensively washed by shaking three times for 10 min in TBST before the HRP-conjugated secondary antibody dissolved in milk blocking solution was added and shaked for 1 h at room temperature. Again, the membrane was extensively washed in TBST and the bands were visualized using the ECL-Plus western blotting detection system for 5 min in the dark. Chemiluminescence was detected using the Luminescent Image Analyzer LAS-1000 with Image Reader LAS-1000 Pro V2.61 software. After stripping the membranes with 0.5 M NaOH for 15 min and incubation in milk blocking solution, membranes were incubated with primary antibody against GAPDH or β-Tubulin as housekeeping genes for 1 h at room temperature. Washing, secondary antibody incubation and chemiluminescence detection were performed as described above. Primary and secondary antibodies used are listed in **Table 2.3**.

2.8.4.2 Fluorescent western blots

After separation of protein lysates they were blotted on a nitrocellulose membrane using the iBlot Dry Blotting System. Blocking of the membrane was performed for 1 h at room temperature in LI-COR blocking buffer. Primary antibodies were incubated in LI-COR blocking buffer supplemented with 0.1% Tween-20 at 4°C overnight and membrane extensively washed by shaking three times for 10 min in PBST. Subsequently, IRDye

secondary antibodies diluted 1:10000 in LI-COR blocking buffer supplemented with 0.1% Tween-20 were incubated for 1 h at room temperature in the dark. Again, the membrane was washed three times for 10 min in PBST and finally in PBS. Fluorescence was detected using the Odyssey Infrared Imaging System. Primary and secondary antibodies used are listed in **Table 2.3**.

2.8.5 Immunocytochemistry

2.8.5.1 Immunofluorescence staining with anti-OCT4-488 antibody

For immunofluorescence staining cells were seeded in 24 well plates on glass coverslips and cultivated for 24 h at 37°C and 5% CO_2. Subsequently, they were washed with PBS and fixed for 30 min in 4% PFA in PBS at room temperature and 30 min in methanol at 4°C. After two washing steps cells were permeabilized with ice-cold 0.1% Triton X-100 in PBS for 10 min and washed again twice. Blocking was performed for 1 h at room temperature with LI-COR blocking buffer followed by overnight incubation at 4°C with the Stemgent DyLight 488 rabbit anti-OCT4 antibody diluted 1:100 with LI-COR blocking buffer supplemented with 0.1% Tween-20. Finally, the cells were washed four times for 5 min with PBS thereby diluting the PBS at the second washing step 1:1 with DAPI-solution (200 ng/ml) and mounted in VECTASHIELD mounting medium. Fluorescence images were visualized with a Zeiss Axiovert 40 CFL microscope with illuminator HPX 120C and AxioVision Rel.4.8 software.

2.8.5.2 Alkaline Phosphatase Staining

Staining of alkaline phosphatase in cell cultures was carried out in 24 well plates by using the Stemgent Alkaline Phosphatase Kit II according to the manual. The substrate solution was incubated for 15 min to obtain the maximum color reaction.

2.9 Functional assays

2.9.1 Dye exclusion assay

After incubating cell culture flasks for 5 min on ice cells were detached by scraping and resuspended to a concentration of 1x 10^6 cells/ml in media containing 1.5 µg/ml Hoechst 33342. For the control experiments, 100 µM verapamil was also included. Solutions were maintained at 37°C for 1 h with repeated mixing. Stained cells were centrifuged for 5 min at 1000 g at 4°C and resuspended in ice-cold HBSS+ buffer. Directly before analysis 1 µg/ml PI was added to the samples to allow the exclusion of dead cells. Presence of a side population was evaluated on the LSR II flow cytometer system with an excitation wavelength of 355 nm and analyzed with FlowJo software 6.4.7.

2.9.2 Drug resistance analyses

2.9.2.1 Drug treatment

6500 ChaMel91 cells, 5000 neonatal melanocytes and 7000 ChaMel47 cells were seeded in 200 µl medium on 96 well plates, respectively. After 24 h one half of the medium per well was removed and replaced by different concentrations of kinase inhibitors (see

Table 2.5) diluted with 100 µl medium. Each concentration was tested in technical triplicates.

2.9.2.2 Apoptosis assay

48 h post drug addition the induction of apoptosis was measured by use of the Cell Death Detection ELISA Plus following the manufacturer's instructions. The Cell Death Detection ELISA Plus is a photometric enzyme-immunoassay for the quantitative *in vitro* determination of cytoplasmic histone-associated-DNA-fragments after induced cell death. Untreated cells served as negative controls. ELISA plates were read by the microplate spectrophotometer Benchmark Plus at 450 nm with a reference wavelength of 490 nm.

2.9.2.3 Viability assay

72 h after the addition of kinase inhibitors viability of treated and untreated cells was determined by alamarBlue assay. 20 µl alamarBlue was added to each 96 well and plates were incubated for an additional 12 h at 37°C and 5% CO_2. Reduction of alamarBlue in each well was calculated using **Equation 2.1** after measuring the absorbance at 570 nm and 600 nm. Blanking of the reader was done with wells containing media only.

$$\%\ \textbf{AlamarBlue Reduction} = \frac{\mathbf{117.216}\times\mathbf{Abs.\,570\ nm} - \mathbf{80.586}\times\mathbf{Abs.\,600\ nm}}{\mathbf{155.677}\times\mathbf{Abs.'\ 600\ nm} - \mathbf{14.652}\times\mathbf{Abs.'\ 570\ nm}}\times\mathbf{100}$$

117.216	molar extinction coefficient of alamarBlue oxidized form [600 nm]
80.586	molar extinction coefficient of alamarBlue oxidized form [570 nm]
155.677	molar extinction coefficient of alamarBlue reduced form [600 nm]
14.652	molar extinction coefficient of alamarBlue reduced form [570 nm]
Abs.	absorbance of test wells
Abs.'	absorbance of negative control well (contains media + alamarBlue, but no cells)

Equation 2.1: Calculation of alamarBlue reduction.

Finally, IC_{50}s were determined using the sigmoidal ($LogEC_{50}$) model of the BioDataFit 1.02 software provided by Chang Bioscience (Retrieved 24 June 2011 <http:// www.changbioscience.com/stat/ec50.html>).

2.9.3 Anchorage-independent growth assay

To test the ability of tumor cells to grow anchorage-independent they were cultured in 25 cm^2 flasks filled with soft agar. Soft agar was prepared by dissolving 0.3% Difco Noble agar in dH_2O and autoclaving it at 121°C for 30 min. Soft agar was allowed to cool down to 60°C and stored at 45°C in a water bath until tumor cells were prepared. Cells growing in exponential phase were trypsinized, counted and serial dilutions of 1:10 dilution steps were made in 32 ml 2x RPMI medium. Cell suspensions were mixed with 32 ml 45°C agar solution in 25 cm^2 flasks by inverting several times. Subsequently, flasks were placed in ice-cold water for 10 min and finally incubated at 37°C 5% CO_2 in vertical orientation. After 4-6 weeks I analyzed anchorage-independent growth by counting and photo documenting the colony phenotype with a Zeiss Axiovert 40 CFL microscope and Axio Vision Rel.4.8 software.

2.9.4 Invasion and mobility assays

Invasion assays with BioCoat BD Matrigel Invasion Chambers allow for the assessment of cell invasiveness *in vitro*. These chambers have a PET membrane with a standard pore size of 8 µm with a thin layer of matrigel matrix, an equivalent to the basement membrane *in vivo* (see **Figure 2.2**). The matrigel matrix occludes the pores of the membrane, blocking non-invasive cells from migrating through the membrane. In contrast, invasive cells are able to invade through the matrix and the membrane pores. In parallel to each invasion assay migration assays with BioCoat Control Chambers were performed, which lack the matrigel matrix on the PET membrane.

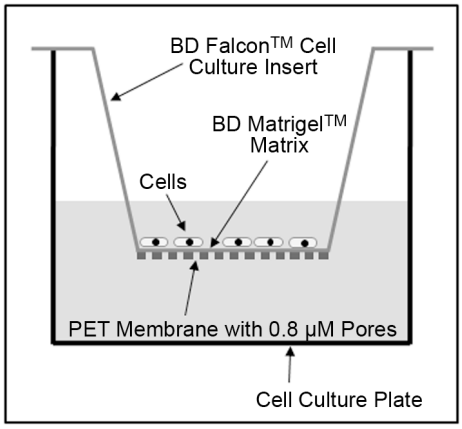

Figure 2.2: Illustration of an invasion assay.
Schematic diagraph of the invasion assay according to the description of BD Biosciences. BD Falcon Cell Culture Inserts are placed in a 24 well cell culture plate with medium supplemented with 10% FCS. Cells are seeded into the insert in medium with lower FCS concentration. Invasive cells are able to digest the matrigel matrix and invade through the pores of the membrane.

To rehydrate invasion and control chambers they were first acclimatized for 5 min at room temperature followed by 2 h incubation at 37°C and 5% CO_2 with 500 µl medium without supplements in insert and bottom of wells. After rehydration, medium was removed and 10^5 $CD133^+$ and $CD133^-$ cells seeded in 500 µl RPMI medium without phenol red supplemented with 1% FCS into the inserts, respectively. The inserts were placed into

wells containing 750 µl RPMI medium without phenol red with 10% FCS which served as chemoattractant for the cells seeded in 1% FCS-containing medium. After 24 h incubation at 37°C and 5% CO_2 the number of migrated or invaded cells was determined by the use of HE staining and MTT assay.

2.9.4.1 HE staining

First, the medium in inserts and wells was aspirated and cells that remained on the surface of the membrane were removed with a cotton bud. Subsequently, migrated or invaded cells were fixed with ice-cold 100% methanol for 10 min and rehydrated for 30 sec in 70% EtOH and 10 sec in dH_2O. Nuclei of the cells were then stained blue by swaying the inserts for 30 sec in 100% hematoxylin and 1 min in tap water. After 15 sec in dH_2O and 15 sec in 70% EtOH cytoplasms of the cells were counterstained in pink for 30 sec in 100% eosin. Finally, cells were dehydrated by two 30 sec incubation steps in 95% EtOH and air-dried for 2 min. Dry membranes were cut out of the inserts and covered on a glass slide with one drop of immersion oil.

2.9.4.2 MTT assay for cell number determination

The basic principle of the MTT assay is the conversion of water-soluble 3-(4,5-Dimethylthiazol-2-yl)-2,5-diphenyltetrazolium bromide (MTT) into purple-colored water insoluble formazan by metabolically active cells via a mitochondrial dehydrogenase. The purple formazan can in turn be solubilized by a SDS solution and quantified photometrically at 550 nm. The measured absorbance is directly proportional to the number of viable cells.

350 µl RPMI medium without phenol red was removed from the wells and the remaining 400 µl spiked with 43 µl MTT solution. BD Falcon Cell Culture Inserts were incubated in MTT solution for 4.5 h. After the formation of formazan was confirmed microscopically, 267 µl 10% SDS solution were added and the culture plate was shaken for 1 min. During an overnight incubation at 37°C and 5% CO_2 a clear solution formed and its absorbance at 550 nm was determined. To determine the number of migrated cells, which is correlated with the measured absorbance value, a standard curve with known cell numbers was generated in every experiment.

2.10 Xenotransplantation

EPO GmbH, Berlin, performed mouse transplantation experiments. Required numbers of melanoma cells were pelleted, resuspended in 50 µl PBS and mixed 1:1 with matrigel. The prepared cell suspension (100 µl) was then injected subcutaneously into the flank of gender-matched, 8-week-old immunodeficient NSG mice (NOD-SCID mice which lack the

interleukin 2 receptor gamma chain). Weight of transplanted mice as well as tumor volume was monitored and documented twice a week. Mice were maintained in the pathogen-free animal facility following institutional guidelines and with approval from the responsible authorities. The animals were housed under pathogen-free conditions in individually ventilated cages under standardized environmental conditions (22°C room temperature, 50 ± 10% relative humidity, 12 h light-dark rhythm). They received autoclaved food and bedding (Ssniff, Soest, Germany) and acidified (pH 4.0) drinking water *ad libitum*. Tumor size was measured in two dimensions with a caliper-like instrument. Individual tumor volumes (V) were calculated by the formula $V = 0.5 \times (\text{length} \times \text{width}^2)$ and related to the values at the first day of treatment (relative tumor volume, RTV).

3 Results

3.1 Identification of CSCs in malignant melanoma by established methods

In order to have full control of patient and tissue selection and to work with melanoma cell lines that resemble the tumor from which they originate from and not with well-established commercially available cell lines I started my work establishing low-passage melanoma cell lines from freshly excised metastases. After I raised ten primary melanoma cell cultures I started my work on melanoma CSCs with these cell lines by applying and comparing three different approaches, which have been described in literature to identify CSCs, which are "sphere formation analysis", "dye exclusion assay" and "expression analysis of well-described stem cell/CSC markers".

3.1.1 Spheroid formation under ES cell culture conditions

The formation of spherical colonies *in vitro* is a common feature of stem cells of various origins and degrees of maturation. In cancer cell lines, the ability to grow as spheres serves as an indicator for self-renewal and tumorigenicity and thus an approach to identify CSCs. I successfully established the sphere formation assay in our laboratory and investigated the melanoma cell lines established so far. For all ten primary melanoma cell lines routinely grown in Q263 the phenotype was that of epithelial cells which is adherent, elongated and spindle-like (**Figure 3.1**, left). After switching to hESC medium, which contains FGF2 (compare **Table 2.9** and section 2.2.4), six of the cell lines tested gradually changed their phenotype. Within five days the cells' morphology turned to small and round-shaped cells that began to grow in colonies (**Figure 3.1**, center). After ten days most cells of these six cell lines grew in suspension and formed large spheroids (**Figure 3.1**, right). This phenotype remained stable for at least four months. When switching back to the standard Q263 medium, the phenotype reverted into its original epithelial-like shape within a few days. In the other four melanoma cell lines sphere formation was not observed even after four months of cultivation in hESC medium. Thus, according to the sphere formation assay six melanoma cell lines exhibit CSC characteristics and four do not.

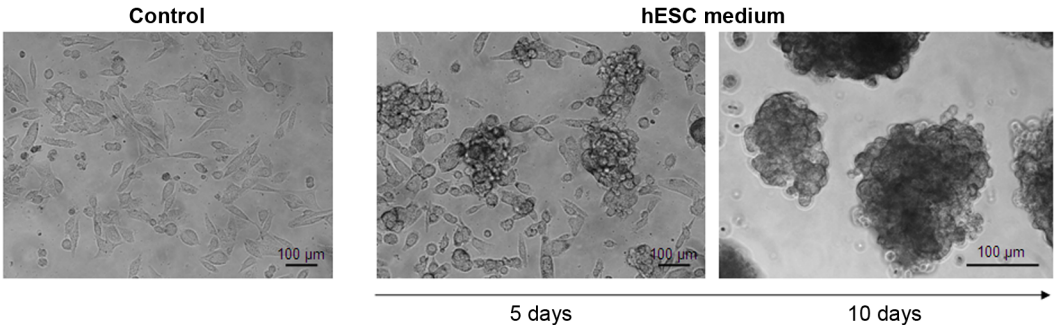

Figure 3.1: Change of phenotype of the melanoma cell line ChaMel115 in ES medium.
Within ten days of cultivation in hESC medium, originally adherent, large, elongated ChaMel115 cells (**A**) formed spheres of non-adherent, small, round-shaped cells (**B**). Under hESC culture condition this phenotype remained stable for at least four months whereas in standard medium an adherent monolayer was maintained.

3.1.2 Identification of a Hoechst SP in most melanoma cell lines

Another property of putative cancer stem cells is their ability to strongly efflux Hoechst 33342 fluorescent dye due to their high expression of ABC transporters. These cells are referred to as the Hoechst „side population" (SP). To identify such putative CSCs in the ten melanoma cell lines (compare 3.1.1), I stained the cells with pre-determined optimal concentrations of Hoechst 33342 and analyzed the emission by FACS (see section 2.9.1). After staining with Hoechst most cells retained the dye and emitted light in the blue and red spectra. In nine cell lines, however, a small SP of only weakly stained cells could be identified (**Figure 3.2**, A). In control experiments I blocked ABC transporters with the phenylalkylamine verapamil. In all nine melanoma cell lines verapamil effectively blocked the rapid efflux of Hoechst dye and decreased the SP significantly (**Figure 3.2**, B). The relative amount of observed side populations in the nine melanoma cell lines ranged from 0.81 to 3.81%. The results were briefly summarized in **Table 3.1** below.

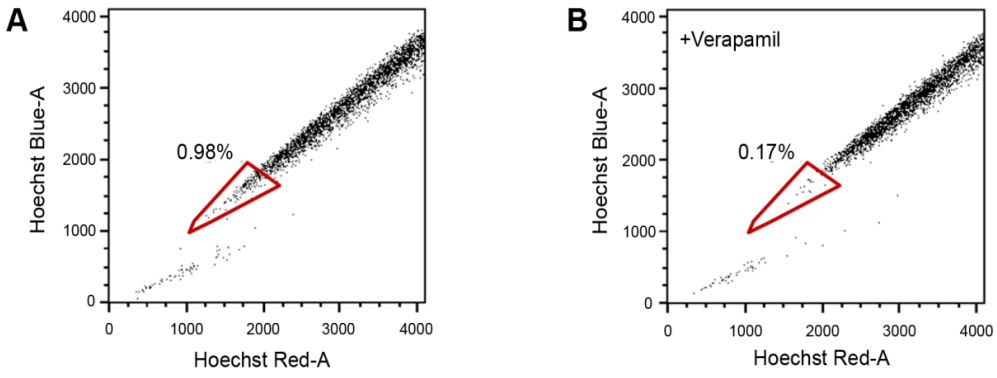

Figure 3.2: Presence of a Hoechst side population in dye exclusion assay.
Identification of CSCs as side population via Hoechst dye staining. Example of the melanoma cell line ChaMel91 containing 0.81% putative cancer stem cells (**A**). Inhibition of ABC transporters that efflux the Hoechst dye by verapamil led to a decrease of the side population (**B**).

One melanoma cell line (ChaMel115, compare **Table 2.6**) showed no SP in Q263 medium (**Figure 3.3**, A and B). But since this cell line showed efficient sphere formation in hESC medium, it was also cultivated in hESC medium prior to dye exclusion analysis. After 14 days the side population increased significantly from 0.04% to 5.97% (**Figure 3.3**, C and D).

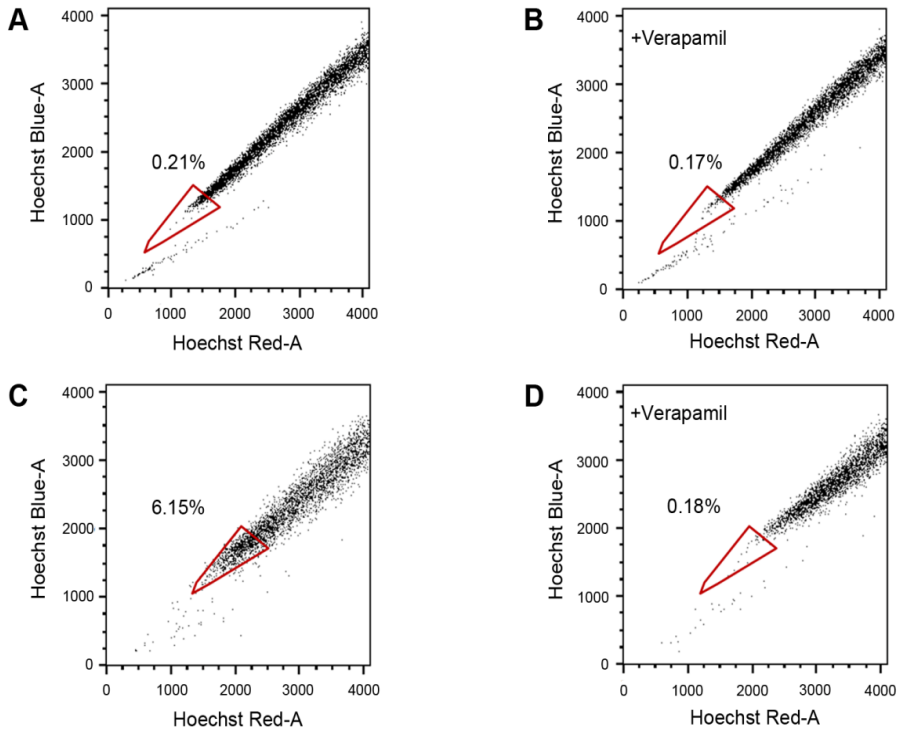

Figure 3.3: Enrichment of Hoechst SP under hESC culture condition.
Melanoma cell lines cultivated in standard medium (**A**) and hES Cmedium (**C**) were incubated with Hoechst 33342 dye and analyzed for Hoechst dye emission. Whereas in standard medium no SP of putative CSCs was detected, a SP of about 6 % emerged under hESC culture condition. **B** and **D** show the corresponding verapamil controls.

In summary, the Hoechst 33342 dye exclusion assay was implemented successfully and putative melanoma CSC subpopulations could be identified in nine of ten primary melanoma cell lines. Culturing melanoma cells in hESC medium drastically increased the percentage of these putative CSCs.

3.1.3 Expression of putative CSC markers in melanoma cell lines

The expression of several markers characteristic of melanoma cells and hESCs, which might also serve as putative melanoma CSC markers, was analyzed by RT-PCR. The original ten melanoma cell lines as well as one well-established melanoma cell line (A375), neonatal and adult melanocytes and the embryonic carcinoma cell line NCCIT), which served as a positive control for stem cell markers were used. Additionally, I investigated four low-passage melanoma cell lines (ChaMel19, ChaMel73, ChaMel81, Pat1T1k), which were newly established during the course of my thesis. The analyzed markers

encompassed genes related to the development of melanocytes and melanoma progression (*TYR, CSPG4, MITF*), ABC transporters (*ABCB1, ABCB5, ABCC2, ABCG2*), common cancer-related genes (*C-MYC, C-KIT, BMI-1*), genes involved in proliferation, migration, angiogenesis and tumor progression (e.g. *TNC, CD166, FGF2, MSI-1, JARID1B*) and genes crucial for stemness and asymmetric cell division (e.g. *CD133, NESTIN, SOX2, NANOG, LIN28*). *HPRT* was used as loading control.

The results confirmed that all cell lines were indeed of neoplastic origin (positive for *TNC, CD166, FGF2, MSI-1* and/or *JARID1B*) and melanoma derived (positive for *TYR, CSPG4* and/or *MITF*). Most cell lines showed a strong expression of ABC transporters and were relatively undifferentiated (expression of *SOX2* and *NANOG*). Furthermore, all cell lines expressed well-described genes crucial for stemness (e.g. *NESTIN*) and asymmetric cell division (*CD133*) as well as the common cancer-related genes *C-MYC* and *C-KIT* (**Figure 3.4**). Of the genes investigated, *CD20* and *LIN28* were the only genes that I could not detect in any of the tested cell lines. *GDF3*, a gene only active in development was exclusively shown in NCCIT cells (**Figure 3.4**).

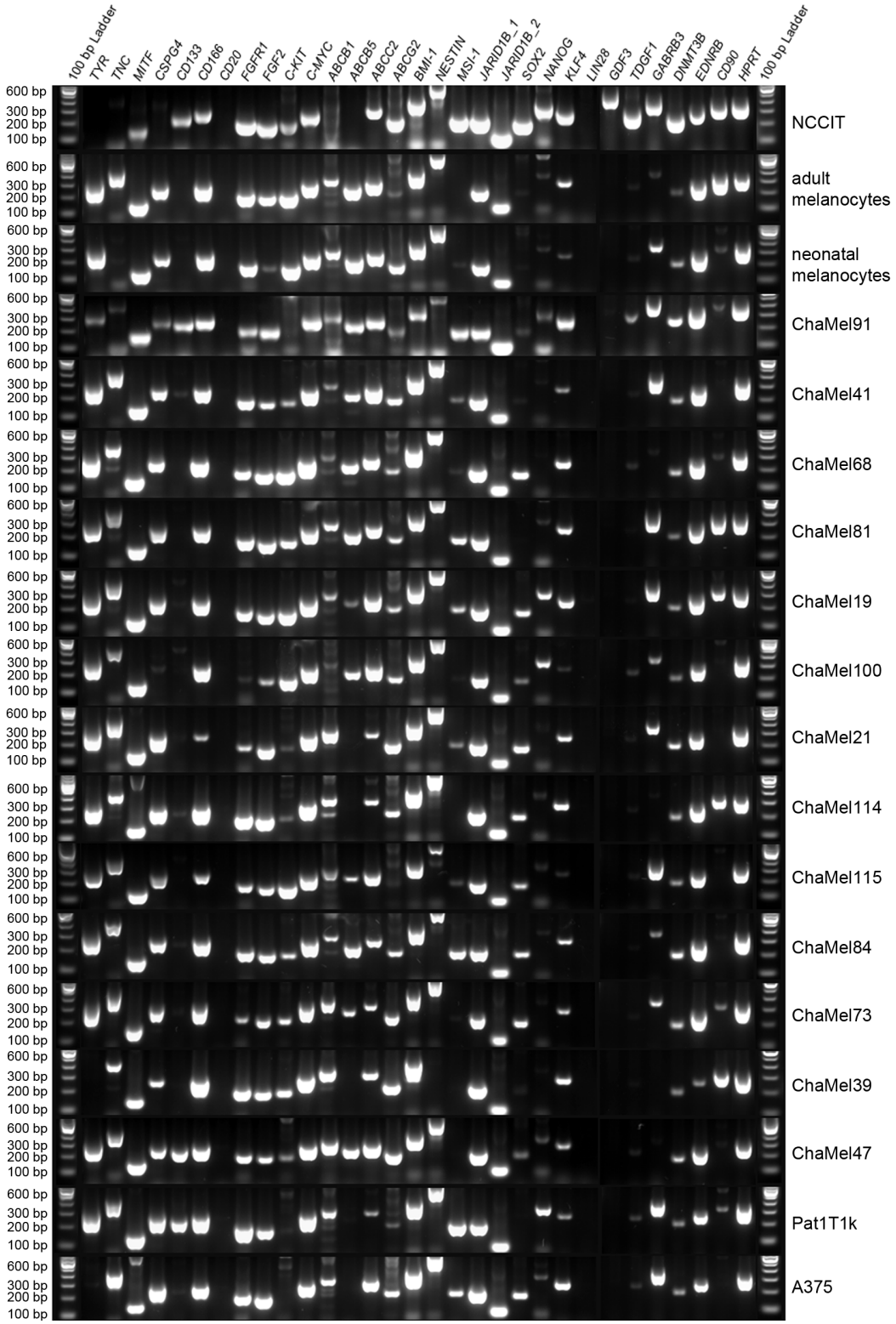

Figure 3.4: Expression analysis of 15 melanoma cell lines, NCCIT and melanocytes.
RT-PCR analysis of genes related to melanocyte development and melanoma progression (e.g. *TYR, MITF*), ABC transporters, cancer-related genes (e.g. *C-KIT, BMI-1*), genes involved in tumor progression (e.g. *TNC, CD166*) and genes crucial for stemness and asymmetric cell division (e.g. *CD133, NESTIN*) showed a heterogeneous expression pattern of all markers in melanoma cell lines. *HPRT* was used as loading control.

Cluster analysis was performed with all analyzed cell lines and transcripts to find putative CSC markers or a set of markers, which define stem cell characteristics similar to the properties of the embryonic carcinoma cell line NCCIT. The resulting dendrogram illustrates that none of these markers or groups of markers are able to define stemness since all clusters of cell lines have the same distance from NCCIT (Figure 3.5).

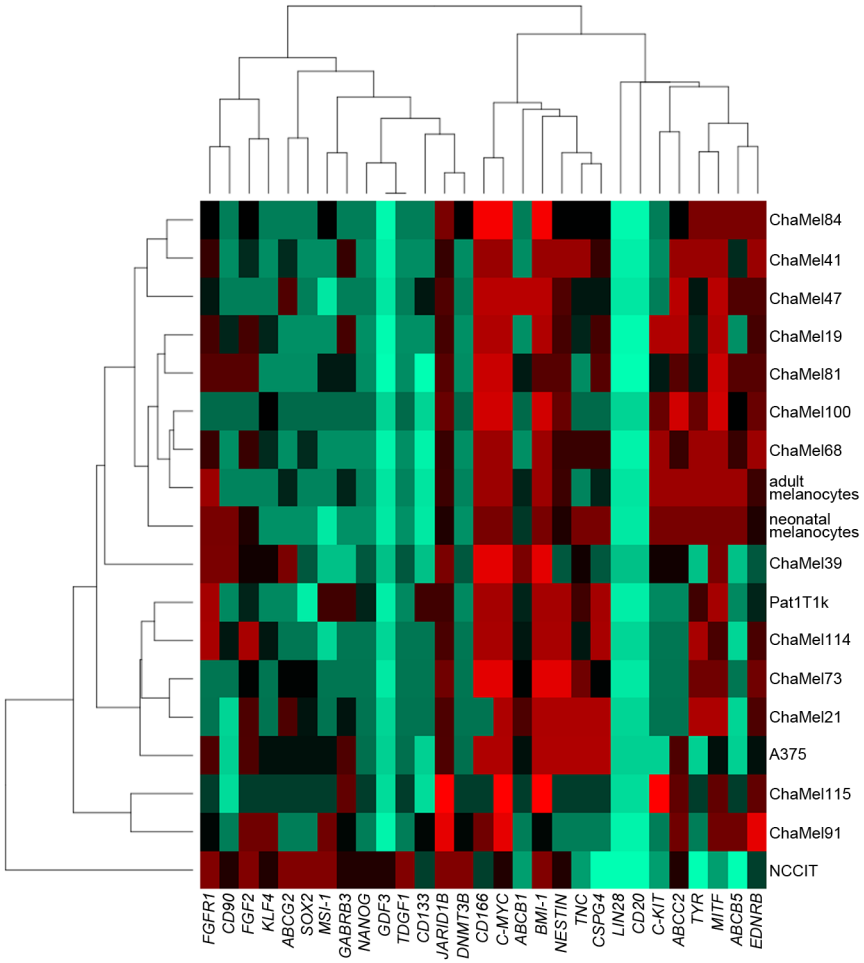

Figure 3.5: Cluster analysis of putative CSC markers and investigated melanoma cell lines.
Hierarchical clustering of all analyzed putative CSC markers and melanoma cell lines represented as dendrogram. Spearman correlation was used as distance measure to determine the similarity between the markers and cell lines and above all to find similarities to the embryonal carcinoma cell line NCCIT. No putative CSC marker or set of markers was found that defines characteristics more similar to the stem cell characteristics of NCCIT than others.

The results of the identification of stem-like populations from the ten cultivated melanoma cell lines on which all established methods were applied and NCCIT are summarized in **Table 3.1**. These findings indicated no direct correlation between the three methods applied. Whereas, nine of ten analyzed cell lines exhibited a side population by Hoechst staining only six of these cell lines grew in spheres under hESC culture conditions. E.g., the only cell line (ChaMel115) which had no defined SP, established the largest spheres under

hESC culture conditions and expressed stem cell and precursor markers like *NESTIN*, *SOX2*, *NANOG* and *TDGF1*. Furthermore, cell lines which had a SP after Hoechst staining or which developed spheroids in hESC medium are evenly distributed in all groups of the cluster analysis and do not define similarity to the stemness of NCCIT. Expression levels of the investigated ABC transporters and of every other marker investigated did not correlate with the size of the Hoechst SP. Also, the formation of spherical colonies did not correlate with the expression of any gene analyzed by RT-PCR.

Table 3.1: Summary of CSC characteristics.
Overview of the expression pattern of different putative cancer stem cell markers, the presence of a Hoechst side population and spheres in hESC medium in ten melanoma cell lines and NCCIT (0-4 emblematize the signal intensity after RT-PCR; 0: no expression; 1: very weak expression; 4: very strong expression; + presence of Hoechst SP and spheres in hESC medium; - absence of Hoechst SP and spheres in hESC medium).

Cell line / CSC marker	NCCIT	ChaMel21	ChaMel39	ChaMel41	ChaMel47	ChaMel68	ChaMel84	ChaMel91	ChaMel100	ChaMel114	ChaMel115
TYR	0	4	0	4	2	4	3	1	3	4	1
TNC	1	4	2	4	2	3	2	1	1	2	1
MITF	1	4	3	4	4	4	3	3	4	3	2
CSPG4	0	4	1	3	2	3	2	1	1	4	1
CD133	2	1	0	1	2	0	1	2	0	1	0
CD166	2	1	4	4	4	4	4	3	4	4	1
CD20	0	0	0	0	0	0	0	0	0	0	0
FGFR1	4	1	3	3	2	3	2	2	1	4	1
FGF2	4	3	2	2	1	3	2	3	1	4	1
c-KIT	1	1	2	1	1	4	1	1	3	1	3
c-MYC	3	4	4	4	4	4	4	4	4	4	3
ABCB1	1	3	3	1	4	1	1	1	1	2	1
ABCB5	0	0	0	2	3	3	3	3	2	0	1
ABCC2	3	1	2	4	4	3	2	3	4	1	2
ABCG2	4	3	3	2	3	1	1	1	1	1	1
BMI-1	4	4	4	4	4	4	4	2	4	4	3
NESTIN	3	4	1	4	3	3	2	1	3	4	1
MSI-1	4	1	0	1	0	1	2	3	1	0	1
JARID1B	4	3	3	3	3	3	3	4	3	3	3
SOX2	4	2	1	1	1	2	1	1	1	1	1
NANOG	3	1	1	1	1	1	1	1	1	1	1
KLF4	3	1	2	1	1	2	1	3	1	2	1
LIN28	0	0	0	0	0	0	0	0	0	0	0
GDF3	3	0	0	0	0	0	0	0	0	0	0
TDGF1	4	1	1	1	1	1	1	1	1	1	1
GABRB3	3	2	0	3	1	1	1	2	1	1	2
DNMT3B	4	1	1	1	1	1	2	2	1	1	1
EDNRB	2	3	1	4	3	4	3	4	3	3	2
CD90	3	0	3	1	1	1	1	1	1	2	0
SP	+	+	+	+	+	+	+	+	+	+	-
Spheres	+	-	+	+	+	-	+	-	+	-	+

To investigate the correlation of *BRAF* mutations in melanoma cell lines with the clustering of these cell lines in similarity groups, cycle sequencing was performed with genomic DNA. According to the literature 50-70% of melanomas have a *BRAF* mutation (refer to 1.2.2.1). Of the melanoma cell lines I investigated, 75% were *BRAF* mutated (see **Table 3.2**). Cell lines with wild type *BRAF* as well as homozygous and heterozygous mutated *BRAF* were equally distributed between the different cell line clusters illustrated in the dendrogram (**Figure 3.5**).

Table 3.2: Sequence analysis of the BRAF gene in melanoma cell lines.

Cell line	*BRAF* status	Type of mutation	Zygosity
ChaMel19	Wild type	NA	Homozygous
ChaMel21	Mutated	V600E	Heterozygous
ChaMel47	Mutated	V600R	Heterozygous
ChaMel68	Wild type	NA	Homozygous
ChaMel73	Wild type	NA	Homozygous
ChaMel81	Mutated	V600E	Heterozygous
ChaMel84	Mutated	V600E	Homozygous
ChaMel91	Mutated	V600E	Heterozygous
ChaMel100	Mutated	V600E	Heterozygous
ChaMel115	Mutated	V600K	Homozygous
Pat1T1k	Mutated	V600E	Homozygous

3.2 Comparison of CD133$^+$ and CD133$^-$ melanoma cells

The transmembrane protein CD133 has been widely used to isolate putative CSC populations in several cancer types. In order to further characterize the molecular properties of CSCs, I used magnetic cell sorting against CD133 to enrich for putative CSCs in ChaMel47, ChaMel91 and PatT1k melanoma cells. These cell lines had the highest expression of CD133 as observed in PCR experiments.

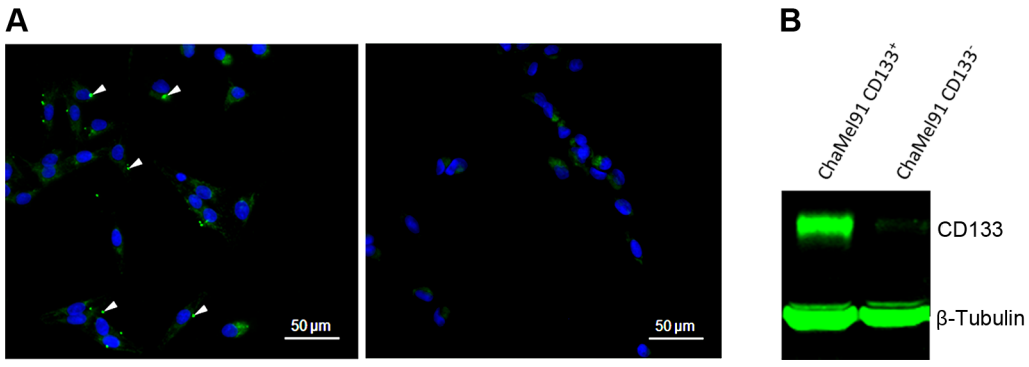

Figure 3.6: Verification of MACS via immunofluorescence staining and western blotting.
A: Immunofluorescence micrographs from ChaMel91 cells 24 h after sorting with the Indirect CD133 Microbead Kit from Miltenyi. Cells were seeded on cover slips and stained with Alexa Fluor 488 goat anti-rabbit secondary antibody, which bound to the anti-CD133 microbeads. Only in the CD133$^+$ fraction a specific signal at the cell membrane was observed as indicated by white arrows (left panel). CD133$^-$ cells did not stain for the presence of the protein (right panel). **B:** Confirmation of sorting purity by quantitative fluorescent western blotting. A strong CD133 signal was detected in the CD133$^+$ fraction, whereas a very weak CD133 expression was observed in the CD133$^-$ population.

CD133+ cells were then compared with the bulk tumor cells in the CD133- fraction on the level of mRNA transcripts and proteins as well as in functional assays. With the modified protocol from the Indirect CD133 Microbead Kit (see 2.3.1), a high purity (>99.75%) and yield of CD133+ and CD133- fraction as well as a high viability of both fractions after sorting was achieved. Sorting efficacy and purity was always verified by immunofluoresence staining or western blot analysis (**Figure 3.6**). The average yield of CD133+ cells was cell line specific: 6.75% (SD 2.06) in ChaMel91, 3.60% (SD 0.49) in ChaMel47 and 4.63% (SD 1.40) in Pat1T1k.

3.2.1 CD133 related gene expression profiling

3.2.1.1 Realtime analysis of commonly used putative CSC markers

To depict if CD133 correlates with other commonly used putative CSC markers I analyzed the expression of a panel of putative CSC markers such as ABCB1, ABCB5, ABCG2, BMI-1, CD166, CD90, CSPG4, MITF, MSI-1, NESTIN and TNC (Cheli *et al.* 2011, Fukunaga-Kalabis *et al.* 2010, Jiang *et al.* 2009, Legg *et al.* 2003, Lim *et al.* 2011, Moitra *et al.* 2011, Schatton *et al.* 2009b, Wang *et al.* 2010), the stem cell mediators FGF2, FGFR1 as well as the differentiation marker TYR. Gene expression data of CD133+ and CD133- ChaMel91 cells as well as neonatal melanocytes were investigated by real-time PCR, normalized and calculated relative to NCCIT cells (see 2.4.6). For none of the selected markers could I detect a significantly differential expression between CD133+ and CD133- ChaMel91 cells. **Figure 3.7** exemplarily shows expression of ten of the investigated genes.

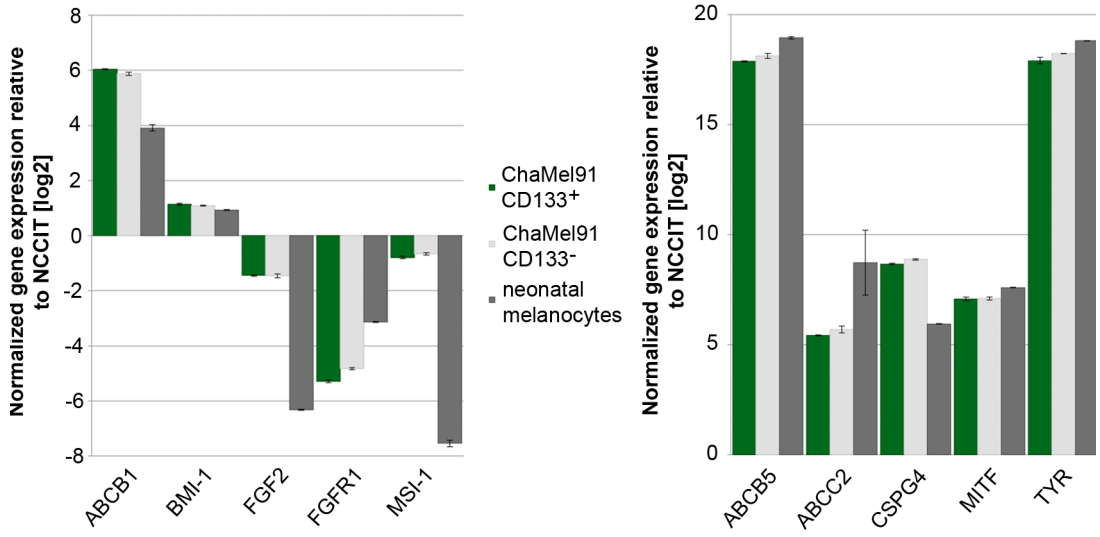

Figure 3.7: Real-time PCR results of CD133+ and CD133- ChaMel91 cells.
Gene expression data of CD133+ and CD133- ChaMel91 cells as well as neonatal melanocytes were normalized and calculated relative to NCCIT cells. There was no significant difference in gene expession between CD133+ and CD133- ChaMel91 cells.

3.2.1.2 Genome-wide expression profiling using Illumina BeadChips

To determine further differences between CD133+ and CD133- melanoma cells genome-wide expression profiling was performed using the Illumina BeadChip technology with HumanRef-8_V3 Expression BeadChips (see 2.4.9). Only RNA of very high purity and yield was used for gene expression profiling. This was ensured by sharp 28S and 18S rRNA signals and by a 2:1 ratio of 28S to 18S rRNA in the agarose gel. Amplified RNA for chip hybridization was also checked using a NanoDrop spectrophotometer. Only RNA with a 260:280 nm ratio of around 2 was processed.

Gene expression data were normalized and analyzed for significant gene expression differences between CD133+ and CD133- Pat1T1k melanoma cells (detection p-value <0.01, p-value <0.05). 599 genes were at least 1.5-fold upregulated in CD133+ compared to CD133- cells. **Figure 3.8** shows the 185 genes, which were at least 2-fold upregulated in CD133+ cells. This gene list was further analyzed using gene annotation tools to identify gene ontologies (GOs) and KEGG pathways significantly overrepresented in CD133+ melanoma cells (see 2.4.10). I found that genes involved in angiogenesis, inhibition of apoptosis, adhesion, cellular migration and invasion as well as cell cycle regulation were upregulated and overrepresented in the CD133+ melanoma fraction. Also, members from the MAPK, WNT, NOTCH, Hedgehog and TGF-β signaling pathway were overrepresented in the CD133+ melanoma fraction compared to CD133- melanoma cells (not significant). The total list of these overrepresented GOs is shown in **Table S 1**.

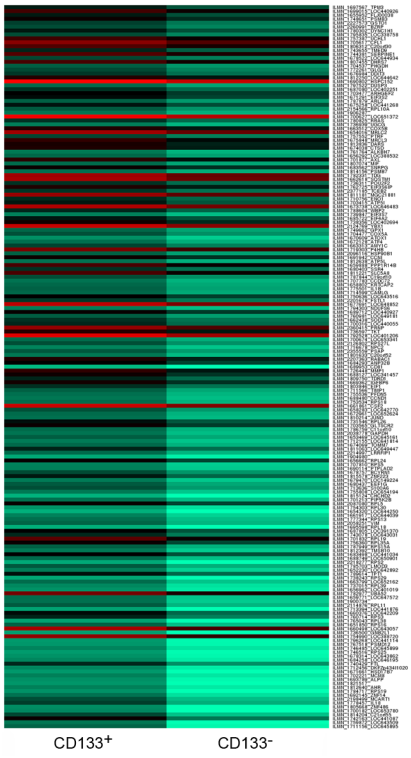

Figure 3.8: Heatmap of gene expression profile from CD133+ and CD133- melanoma cells.
Gene expression analysis of CD133+ and CD133- melanoma cells revealed that 185 genes are >2-fold upregulated in the CD133+ compared to the CD133- subpopulation. As analysis parame-ters a detection p-value <0.05 in at least one subpopulation and a p-value <0.05 for differential gene expression were chosen.

3.2.2 Activated FGF pathway in CD133+ melanoma cells

In the following experiment I focused on the TGF-β signaling cascade, to validate the differences between CD133+ and CD133- melanoma cells on protein level exemplarily for one signaling cascade (compare 3.2.1.2). The TGF-β signaling cascade is closely related to the FGF pathway as shown by Greber *et al.* and described in 1.4.2. To prevent differentiation and maintain self-renewal in hESCs the FGF pathway needs to be activated and is characterized by exogenous and autocrine FGF2 modulating the expression of TGF-β ligands and activating the MEK1/ERK pathway (Greber *et al.* 2007a). The read-out for activation is the phosphorylation of the protein kinase ERK, which was consequently analyzed in melanoma subpopulations. In unsorted melanoma cells I was only able to detect phosphorylated ERK when the cells were cultivated in hESC medium for at least ten days. Under normal growth conditions in RPMI medium almost no phosphorylated ERK was detected (**Figure 3.9**, A). Sorting of melanoma cells into CD133+ and CD133- fraction revealed that phosphorylated ERK is indeed expressed when cultivating the cells in RPMI medium, but preferentially in CD133+ cells (**Figure 3.9**, B). In contrast to the non-phosphorylated form of ERK it was not detected in CD133- ChaMel91 and CD133- ChaMel47 melanoma cells.

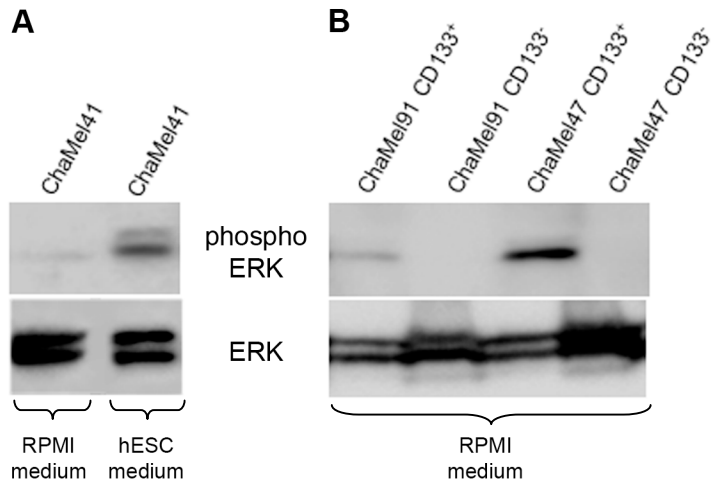

Figure 3.9: Activated FGF signaling cascade in putative melanoma CSCs. Whereas the expression of ERK can be detected in melanoma cells cultivated under both culture conditions, activated phosphorylated ERK can only be detected under hESC culture conditions (**A**) or in the CD133+ fraction after normal culture conditions in RPMI (**B**). It is not expressed in CD133- cells.

3.2.3 Whole transcriptome mRNA sequencing of CD133+ and CD133- melanoma cells

Whole transcriptome mRNA sequencing (see section 2.6) revealed that the differences found during gene expression analysis could not only be caused by mutations or genomic aberrations at the sequence level. Only rare single nucleotide polymorphisms (SNPs) were found to be different between CD133+ and CD133- ChaMel91 melanoma fractions. Most of these SNPs were non-genic or located within the 5'UTR or 3'UTR of a gene.

SNPs located in the coding region of a gene were mostly synonymous nucleotide exchanges (see **Table S 2**). Only one non-synonymous mutation located in the coding region of the CoA synthase gene was SIFT predicted to affect the protein function (damaging). In this case the amino acid substitution S55Y was caused by the homozygous nucleotide exchange *C* > *A* in CD133⁺ cells as shown in **Figure 3.10**. CD133⁻ cells show a heterozygous phenotype at this position (C and A).

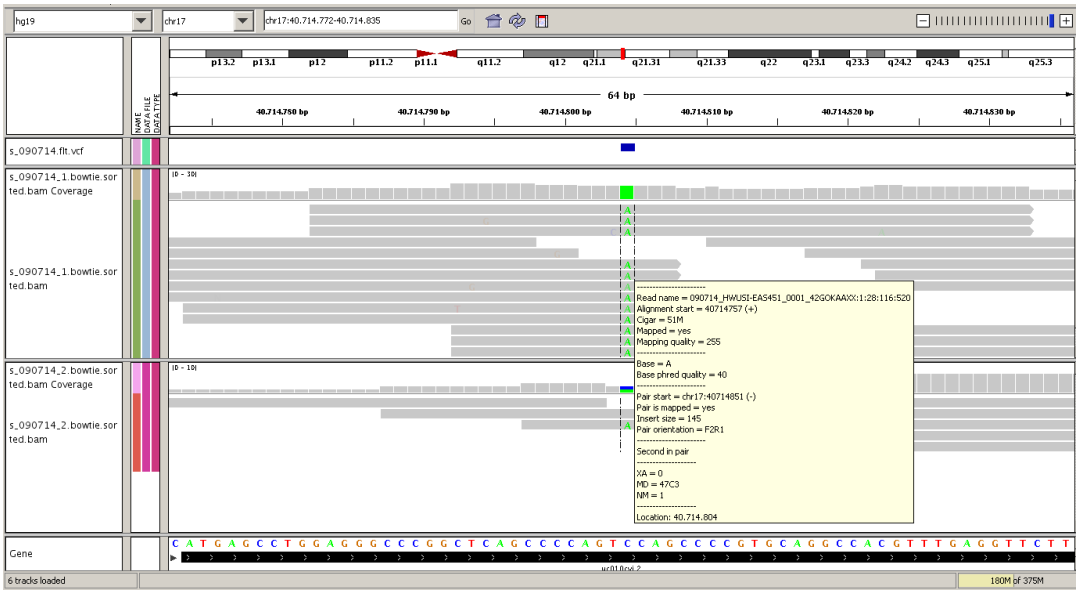

Figure 3.10: Reads for gene COASY displayed by the IGV software package (Robinson *et al.* 2011). In the track at the bottom the reference sequence of *COASY* is indicated (UCSC HG19) showing a *C* at the location of interest. In the first sample (CD133⁺ cells) the reads consistently gave evidence to the alternative base *A*. The second sample (CD133⁻ cells) showed a heterozygous phenotype of the wildtype sequence and a SNP from *C* to *A*.

3.2.4 Is the CD133 expression epigenetically regulated?

Since I could not detect any coding mutations at the genome or transcriptome level that could explain the differences between CD133⁺ and CD133⁻ melanoma cells found by genome-wide expression profiling and western blot analysis of the FGF pathway, I was interested in a putative epigenetic regulation of CD133 and if CpG methylation facilitates the maintenance of the phenotype. After magnetic cell sorting CD133⁻ cells were either grown in Q263 medium alone or in Q263 medium supplemented with 0.1 µM of the DNA methyltransferase inhibitor 5-aza-2'-deoxycytidine for seven days. In preexperiments with different concentrations of 5-aza-2'-deoxycytidine I determined 0.1 µM as the most suitable concentration since 0.1 µM 5-aza-2'-deoxycytidine reduced the expression of DNMT1 the most abundant and key maintenance DNA methyltransferase in mammalian cells to a level below western blot detection threshold without reducing cell viability as determined by alamarBlue assays. In parallel control experiments cells were treated with 1 µg/ml of the DNA crosslinker mitomycin C.

Western blot analysis of the cultured cells revealed that the CD133 expression in untreated cells had doubled within seven days. In contrast, CD133 expression increased only during the first two days in cells treated with 5-aza-2'-deoxycytidine but not above the level of untreated cells. Subsequently, CD133 expression in 5-aza-2'-deoxycytidine treated cells decreased significantly below the CD133 expression level of untreated cells (**Figure 3.11**, A). This effect could not be credited to the demethylating activity of 5-aza-2'-deoxycytidine since similar results were obtained when treating the melanoma cells with mitomycin C. As shown in **Figure 3.11**, B DNA demethylation via the treatment with 5-aza-2'-deoxycytidine and crosslinking of DNA using mitomycin C resulted in a slower proliferation of ChaMel91 cell when compared to untreated cells, resulting in remarkably lower cell confluence after seven days of cultivation.

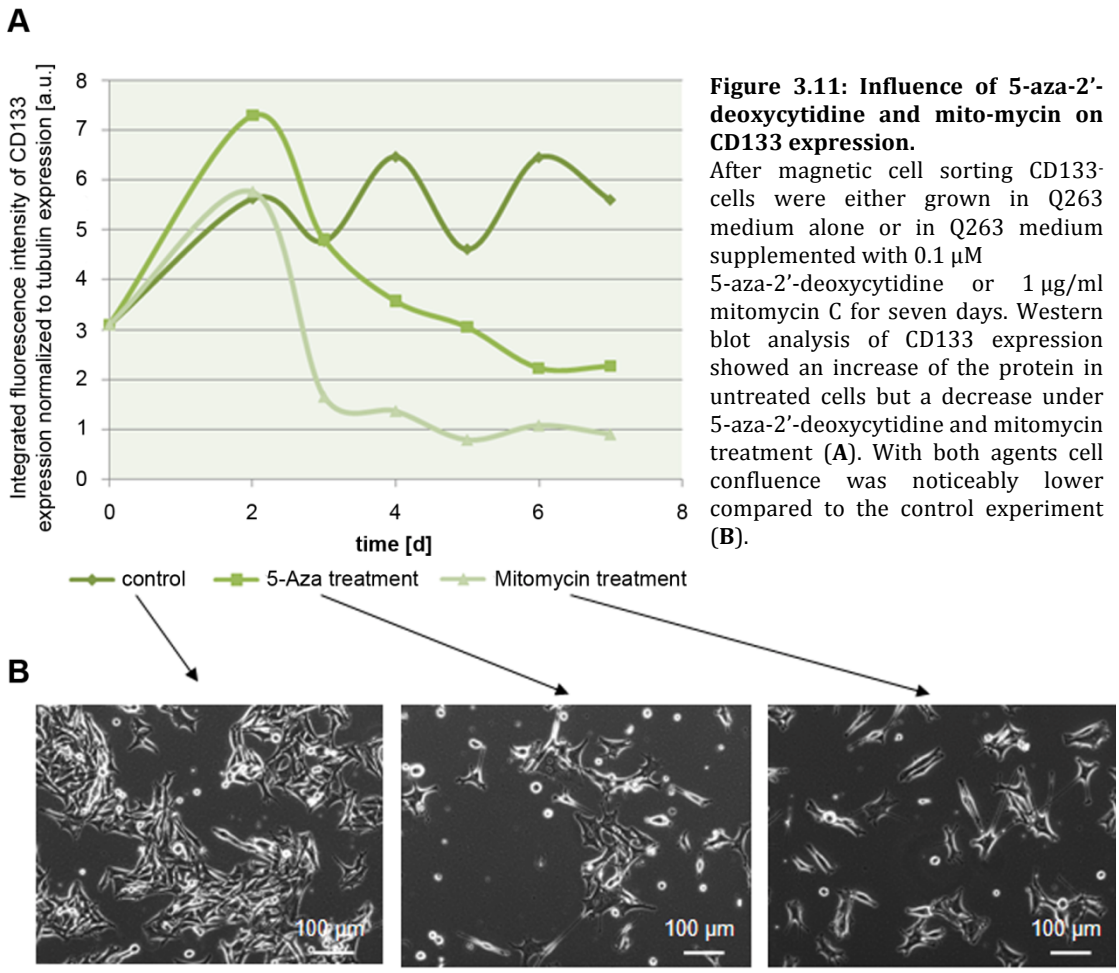

Figure 3.11: Influence of 5-aza-2'-deoxycytidine and mito-mycin on CD133 expression.
After magnetic cell sorting CD133$^-$ cells were either grown in Q263 medium alone or in Q263 medium supplemented with 0.1 µM 5-aza-2'-deoxycytidine or 1 µg/ml mitomycin C for seven days. Western blot analysis of CD133 expression showed an increase of the protein in untreated cells but a decrease under 5-aza-2'-deoxycytidine and mitomycin treatment (**A**). With both agents cell confluence was noticeably lower compared to the control experiment (**B**).

3.2.5 Functional comparison of CD133+ and CD133- cells

To elucidate the implications of the observed differences between CD133+ and CD133- melanoma cells on cancer- and stem cell-related capabilities I performed various functional assays with both subpopulations as well as unsorted melanoma cells.

3.2.5.1 Tumor initiation capability of CD133+ and CD133- cells

The ultimate functional assay to depict differences between CD133+ and CD133- melanoma cells is xenotransplantation of both subpopulations (see 2.10). After magnetic cell sorting 10^5 CD133+, CD133- and unsorted ChaMel91 cells were injected into three male NSR mice, respectively. Nine weeks thereafter, a difference in the tumor growth capability between CD133+ and CD133- was examined. CD133+ cells formed significantly bigger tumors compared to CD133- and unsorted cells (**Figure 3.12**).

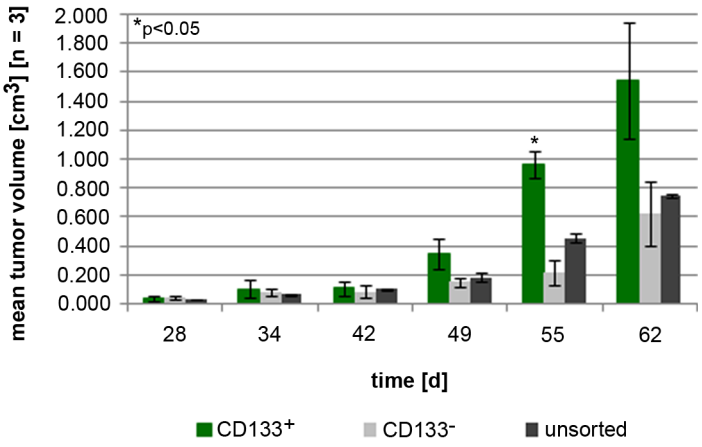

Figure 3.12: Tumor formation capability of CD133 sorted ChaMel91 cells.
On average, injection of 10^5 CD133+ ChaMel91 cells into NSR mice led to the formation of significantly larger tumors compared to CD133- and unsorted cells.
Tumor formation was monitored for 62 days. Error bars indicate the standard deviation among the group of three mice. p-values were determined for unpaired samples of CD133+ and CD133- cells by the Student's *t*-test.

Using different *in vitro* assays these differences in tumor growth capabilities between CD133+ and CD133- melanoma cells as well as its other disparities were further investigated.

3.2.5.2 Anchorage-independent growth

The ability of cell lines to form tumors is highly correlated with the ability of anchorage-independent growth *in vitro*, which was analyzed by means of softagar assays (see 2.9.3). Different numbers of NCCIT cells served as positive control and were tested for their colony formation capability as well. Whereas, 10^3 seeded NCCIT cells formed dozens of large 0.5-1.7 mm colonies after five weeks in softagar, ten times more melanoma cells were necessary to form colonies, initially. A minimum of 10^4 ChaMel91 cells was required to form colonies in the performed softagar assays. Comparison of CD133+ and CD133- ChaMel91 cells evinced that there was no difference in the colony-forming capability between these two fractions. An example with 5x 10^4 seeded cells is shown in **Figure 3.13**.

Compared to NCCIT, colonies formed by ChaMel91 were on average much smaller (maximum 0.5 mm).

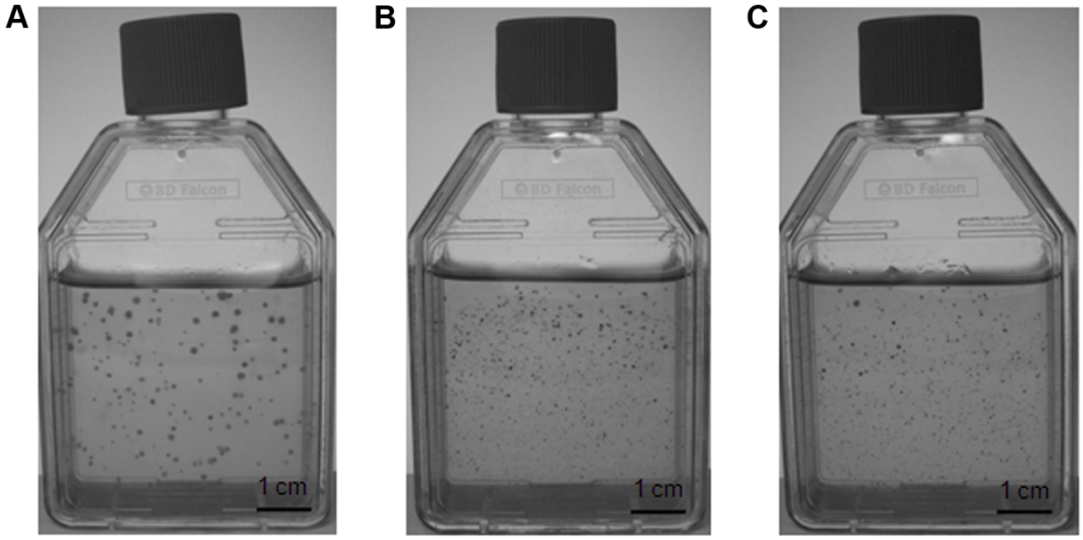

Figure 3.13: Soft agar assays from CD133$^+$ and CD133$^-$ ChaMel91 cells.
10^3 seeded NCCIT cells built dozens of large colonies after five weeks in soft agar (**A**). ChaMel91 showed anchorage-independent growth only after seeding at least 10^4 cells. No difference in colony formation was visible between CD133$^+$ (**B**) and CD133$^-$ (**C**) ChaMel91 cells when 5x 10^4 were seeded and cultivated for five weeks. Both fractions built hundreds of small colonies.

3.2.5.3 Alkaline phosphatase activity

An additional indicator for an undifferentiated phenotype is alkaline phosphatase (AP) activity. I investigated the activity of AP in CD133$^+$ and CD133$^-$ ChaMel91 cells and compared it to NCCIT cells. Whereas the embryonic carcinoma cell line showed a very strong staining for AP in 100% of cells nearly no AP activity was detected in ChaMel91 cells. Only a small number of ChaMel91 cells stained positive for AP, which was very weak in contrast to NCCIT cells (**Figure 3.14**) and not significantly different between CD133$^+$ and CD133$^-$ cells$^-$. No AP activity was seen in neonatal melanocytes (data not shown).

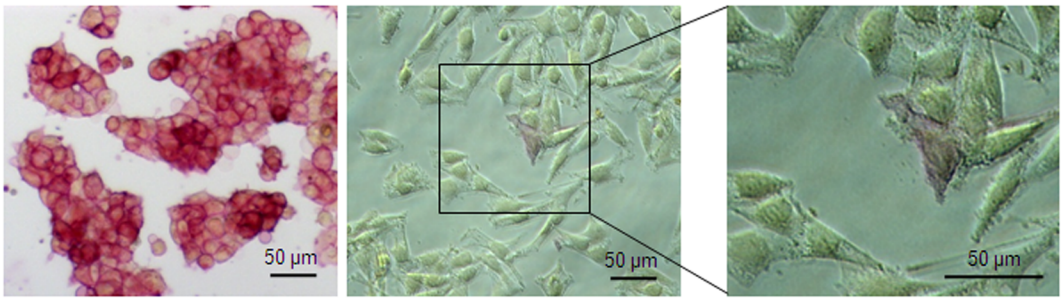

Figure 3.14: AP staining of NCCIT and ChaMel91 cells.
NCCIT cells (left) showed strong staining for alkaline phosphatase in 100% of cells. Whereas in ChaMel91 only rare melanoma cells stained weakly for AP (middle and right). No AP activity was seen in neonatal melanocytes (data not shown).

3.2.5.4 Migration and invasion capability

To investigate the cell invasiveness *in vitro* migration and invasion assays were performed with CD133+, CD133- and unsorted ChaMel91 cells and analyzed microscopically as well as via MTT assays (see 2.9.4). ChaMel91 melanoma cells had migratory and invasion capacity, which was higher in unsorted cells (data not shown) but did not differ between the CD133+ and CD133- fractions as shown in **Figure 3.15**. On average, about 5% of the cells migrated through the PET membrane of the BD BioCoat Control Chambers within 24 h. The invasion capacity of these cells was even smaller. Only very few cells were able to invade through the matrigel matrix and the membrane pores of the invasion chambers.

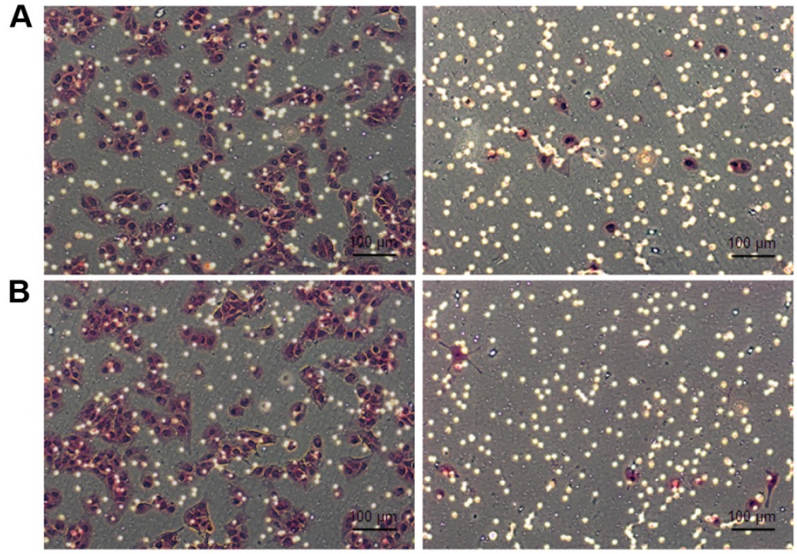

Figure 3.15: Invasion and mobility assays of ChaMel91 melanoma cells.
Invasion (right panels) and mobility (left panels) capacity was analyzed *in vitro* for CD133+ (**A**) and CD133- (**B**) ChaMel91 cells, respectively. Invaded and migrated tumor cells were HE stained and documented microscopically.

3.2.5.5 Chemoresistance

To further investigate main signaling pathways, which drive tumorigenesis key signaling pathways such as RAS, WNT or PI3K pathways were inhibited to learn about their specific effects on CSCs and bulk melanoma cells. Targeted protein kinase inhibitors, most of them in clinical evaluation, were used to inhibit crucial signaling molecules from these pathways such as SRC, ABL which were inhibited with dasatinib and bosutinib, MEK with PD184352, FGFR1 with SU5402, EGFR with erlotinib, PDGFR, VEGFR, RAF with sorafenib and sunitinib, and PI3K with GDC-0941. After magnetic sorting CD133+ and CD133- cell populations were treated with different concentrations of the inhibitors and viability and apoptosis were assessed by reduction of alamarBlue reagent and Cell Death Detection ELISA^{Plus}, respectively (refer to 2.9.2). The calculated IC_{50} values (**Equation 2.1**) for the viability experiments showed no significant difference in resistance to any of the tested compounds between CD133+ and CD133- cells (**Table 3.3**). When comparing the kinase inhibitors used three different kinetics were observed. Some inhibitors like dasatinib, lapatinib and sorafenib (sorafenib is shown in **Figure 3.16**) induced a high apoptosis rate

in all melanoma cells and led to 100% mortality. Other kinase inhibitors like PD98059 and SU5402 had only a light effect on viability and apoptosis of the tested melanoma cells. Even high concentrations of these compounds (up to 100 µM) reduced the viability only by about 20% (see SU5402 as an example in **Figure 3.16**). And few inhibitors, e.g. GDC-0941 reduced the viability and induced apoptosis of melanoma cells already at very low concentrations clearly but did not reduce viability further at increasing concentrations. That means a very high and stable amount of melanoma cells survived these kinase inhibitors also at high concentrations. As an example the effect of GDC-0941 on ChaMel47 is shown in **Figure 3.16**. Concentrations up to 10 µM GDC-0941 reduced the viability of ChaMel47 continuously by 20% and induced apoptosis remarkably. This level remained stable for all higher concentrations tested. The phenotype of the surviving melanoma cells did not differ from the one of untreated control cells.

Table 3.3: Summary of *in vitro* cytotoxicity assays.
IC_{50} values of $CD133^+$ and $CD133^-$ fraction from ChaMel91 and ChaMel47 melanoma cells did not differ in any tested kinase inhibitor. Neonatal melanocytes served as normal control cells.

Compound	Target	ChaMel91 $CD133^+$	ChaMel91 $CD133^-$	ChaMel47 $CD133^+$	ChaMel47 $CD133^-$	neonatal melanocyte
Bosutinib	SRC, ABL	5.20 µM	5.20 µM	9.70 µM	9.45 µM	4.60 µM
Dasatinib	ABL, SRC	15.10 µM	15.00 µM	29.76 µM	29.68 µM	14.80 µM
Sunitinib	PDGFR, VEGFR	9.70 µM	9.80 µM	9.76 µM	10.00 µM	4.90 µM
Sorafenib	PDGFR, VEGFR, RAF	9.80 µM	9.90 µM	9.94 µM	9.98 µM	2.10 µM
Vandetanib	VEGFR, EGFR	10.00 µM	9.90 µM	7.45 µM	7.62 µM	7.30 µM
Lapatinib	EGFR, HER2	11.20 µM	11.10 µM	14.49 µM	15.01 µM	3.20 µM
Gefitinib	EGFR	14.70 µM	10.30 µM	15.25 µM	15.25 µM	7.50 µM
Nilotinib	ABL	10.20 µM	9.80 µM	10.35 µM	14.77 µM	2.50 µM
Rapamycin	MTOR	19.60 µM	19.70 µM	19.88 µM	20.59 µM	10.70 µM
Staurosporin	Broad Spectrum	25.30 nM	26.80 nM	136.10 nM	110.50 nM	50.90 nM
Imatinib	ABL, KIT, PDGF	30.01 µM	29.80 µM	49.56 µM	49.60 µM	39,87 µM
U0126	MEK1	1.93 µM	4.36 µM	1.22 µM	1.78 µM	1.19 µM
ABT-869	VEGFR, PDGFR	9.77 µM	9.86 µM	10.09 µM	10.22 µM	nd
SU5402	FGFR1	30.73 µM	30.76 µM	29.99 µM	30.09 µM	29.03 µM
PD98059	p38 MAPK	19.80 µM	20.10 µM	20.06 µM	19.98 µM	3.22 µM
PLX-4032	BRAF	1.01 µM	0.74 µM	4.13 µM	7.57 µM	nd
PD184352	MEK	2.00 µM	2.10 µM	2.17 µM	2.32 µM	1.87 µM
GDC-0941	PI3K	NaN	NaN	NaN	NaN	NaN
PI-103	PI3K, DNA-PK, mTOR1/2	0.74 µM	0.58 µM	0.32 µM	0.44 µM	0.40 µM

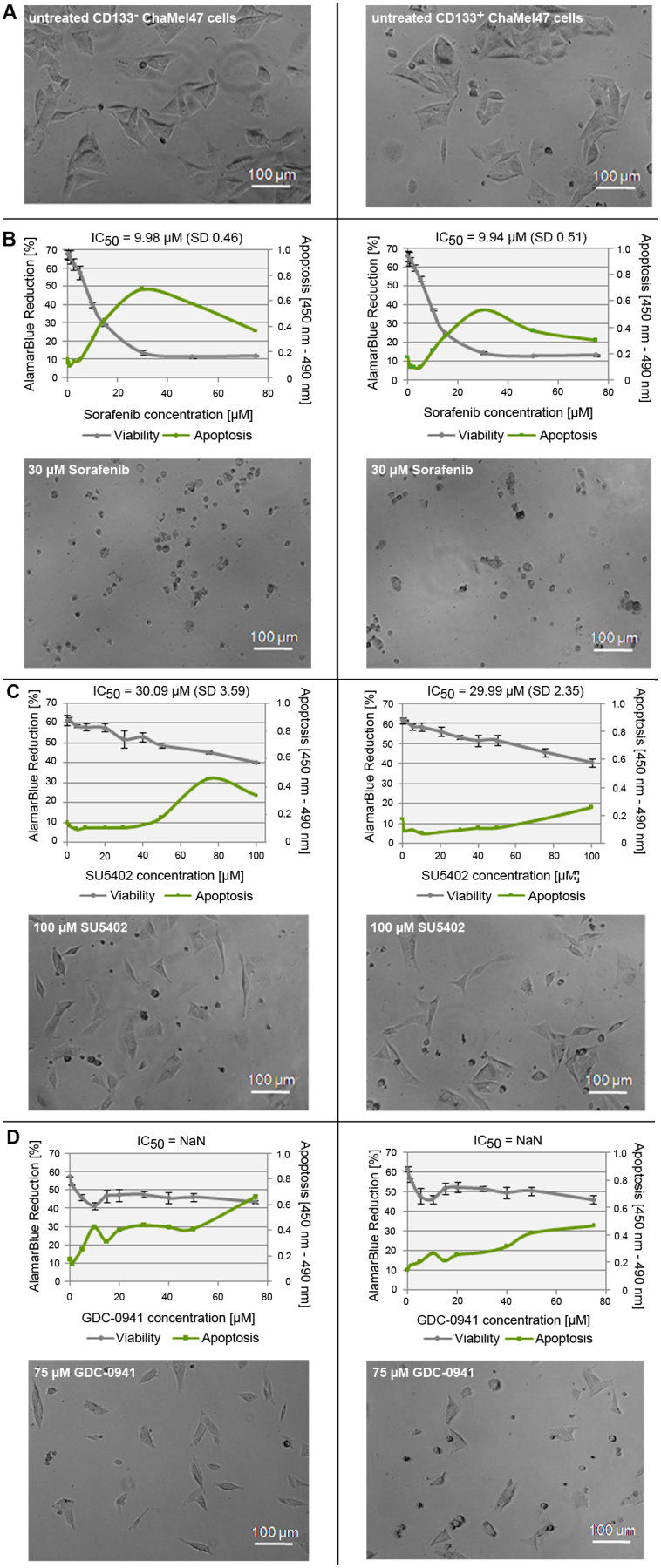

Figure 3.16: Effect of kinase inhibitors on viability and apoptosis of ChaMel47.
A shows the typical phenotype of untreated ChaMel47 melanoma cells after sorting in $CD133^-$ (left) and $CD133^+$ (right) subpopulations.
Treatment of these cells with kinase inhibitors (**B-D**) resulted in no significant differences in the IC_{50} values for viability of $CD133^-$ (left) and $CD133^+$ (right) cells.
B-D also compares viability and apoptosis rate of ChaMel47 cells after treatment with the kinase inhibitors sorafenib, SU5402 and GDC-0941.
Sorafenib induced a high apoptosis rate in ChaMel47 cells and resulted in 100% mortality after treatment with 30 µM (**B**). SU5402 had only a light effect on viability and apoptosis of ChaMel47. Even 100 µM reduced the viability only by about 20% (**C**). GDC-0941 reduced viability and induced apoptosis of ChaMel47 cells already at very low concentrations but had no increasing effects on the cells with increasing concentrations. Many cells survived even high concentrations of GDC-0941 (**D**).
Phenotype and amount of surviving cells was recorded microscopically and is shown exemplary for one concentration of sorafenib, SU5402 and GCD-0941, respectively.
Error bars indicate standard deviations of technical triplicates.

3.2.5.6 Influence of kinase inhibitors on CD133 expression

Since no significant difference in chemoresistance for the tested substances was observed between $CD133^+$ and $CD133^-$ melanoma cells, the influence of three kinase inhibitors on the expression of CD133 was examined. Sorafenib, SU5402 and GDC-0941 were tested, representative for effective kinase inhibitors (sorafenib), non-effective kinase inhibitors (SU5402) and effective only on a small fraction of the melanoma population (GDC-0941). ChaMel91 cells were sorted into $CD133^+$ and $CD133^-$ fraction and treated with two concentrations of each compound (IC_{50} and IC_{80} concentrations in unsorted ChaMel91 cells, which were calculated from previous experiments; for GDC-0941 concentrations correspond to the range of the inhibitor, where an effect on a small ChaMel91 subpopulation was observed). 48 h later CD133 expression of the treated cells was examined and compared with untreated control cells. Whereas upon sorafenib treatment the CD133 expression was reduced significantly in $CD133^+$ and $CD133^-$ ChaMel91 cells, SU5402 and GDC-0941 increased the CD133 expression remarkably at both tested concentrations but only in the $CD133^+$ fraction (**Figure 3.17**).

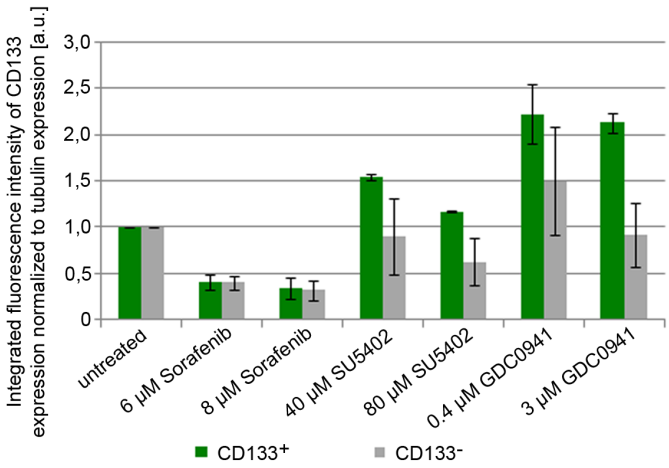

Figure 3.17: Effect of kinase inhibitors on CD133 expression. Whereas sorafenib reduced the CD133 expression compared to the untreated control in ChaMel91 cells, SU5402 and GDC-0941 increased the CD133 expression significantly in the $CD133^+$ fraction. In $CD133^-$ ChaMel91 cells there was no effect of SU5402 and GDC-0941. CD133 expression of untreated $CD133^+$ and $CD133^-$ cells was set to 1 independently. Error bars indicate the standard deviation of two biological replicates.

3.3 Dynamic of CD133 expression

Yield of $CD133^+$ melanoma cells varied from 2.8-10% in ChaMel91 in all magnetic sorting procedures performed. It turned out that these differences were independent of the cell density in the culture flasks (see **Figure 3.18**) or cell number loaded on the MACS columns (within the range indicated by the company, data not shown). These observations were followed in more depth by long-term experiments with sorted ChaMel91 cells. After magnetic cell sorting $CD133^+$, $CD133^-$ and unsorted cells were seeded and subcultured for 38 days. Every 2-4 days about 2x 10^6 cells were pelleted and analyzed for their CD133 expression via fluorescent western blot (see 2.8.4.2).

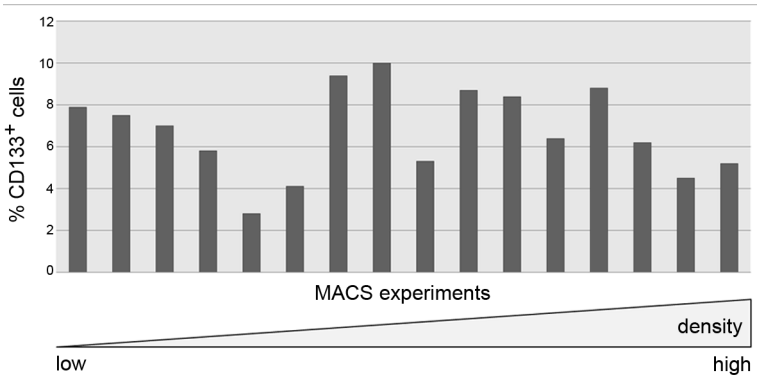

Figure 3.18: Correlation of cell confluence and yield of CD133+ ChaMel91 cells.
Evaluation of twelve independent magnetic sortings of ChaMel91 showed that no correlation between the confluence of melanoma cells in culture and yield of CD133+ cells exists.

Throughout the experiment CD133 expression was highest in CD133+ ChaMel91 cells. After 38 days the different fractions (CD133+, CD133- and unsorted cells) still did not reach the same CD133 expression level compared to each other. However, in all three melanoma fractions a cyclic increase and decrease of CD133 was seen (**Figure 3.19**). The length of the observed period differed in the three populations and also within each population. The half-period ranged from 3-11 days from the minimal to the maximal CD133 expression. CD133+ cells had the longest CD133 fluctuation period. About three cycles of CD133 fluctuation were observed within the 38 days of the experiment and are indicated by the grey-to-white shadings in **Figure 3.19**. The difference between CD133 minimum and maximum expression was about 2-4 (a.u.).

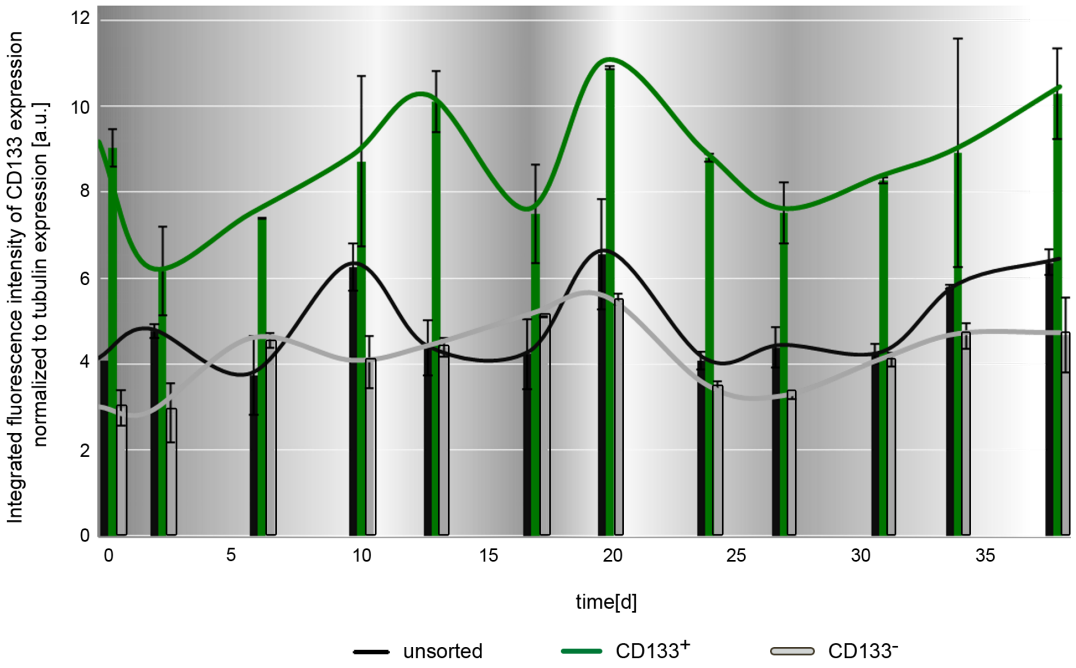

Figure 3.19: Long-term analysis of CD133 expression.
CD133 expression behaved cyclic in the observed period of 38 days in sorted and unsorted cells of ChaMel91 with a difference between minimum and maximum expression of about 2-4. Error bars indicate the standard deviations of three biological replicates.

This cyclic behavior could not directly be correlated with routine cell culture handling such as splitting or medium change since anti-cyclic shifting of the routine handling by 4 days during the biological triplicates did not change the cyclic behavior of CD133 expression. In further experiments the cell cycle distribution of CD133$^+$, CD133$^-$ and unsorted ChaMel91 cells as well as the doubling time of these fractions were investigated to test for a correlation with the observed cyclic CD133 expression. These experiments were performed in collaboration with the department of Molecular Cell Biology at the Elbeklinikum Buxtehude. No significant difference in doubling times between CD133$^+$ and CD133$^-$ populations was observed. It was 31.7 h for CD133$^+$ cells and 32.1 h for CD133$^-$ cells respectively (data not shown).

Also, neither significant differences in the cell cycle distribution between the populations nor a correlation of the individual cell cycle phases with the CD133 expression was observed using PI staining and FACS analysis on an EPICS XL-MCL flow cytometer (see section 2.4.11). On average about 74% of cells from all fractions were in G1-phase, 20% in S-phase and the remainder in G2-phase. **Figure 3.20** exemplarily shows the cell cycle distribution of CD133$^+$ cells plotted together with the CD133 expression measured at the same time points during the long-term experiment. This analysis did not show any change of the CD133 expression in dependence of a certain cell cycle phase. In summary, doubling times and cell cycle distribution of CD133$^+$, CD133$^-$ and unsorted ChaMel91 cells did not account for the cyclic behavior of CD133 expression.

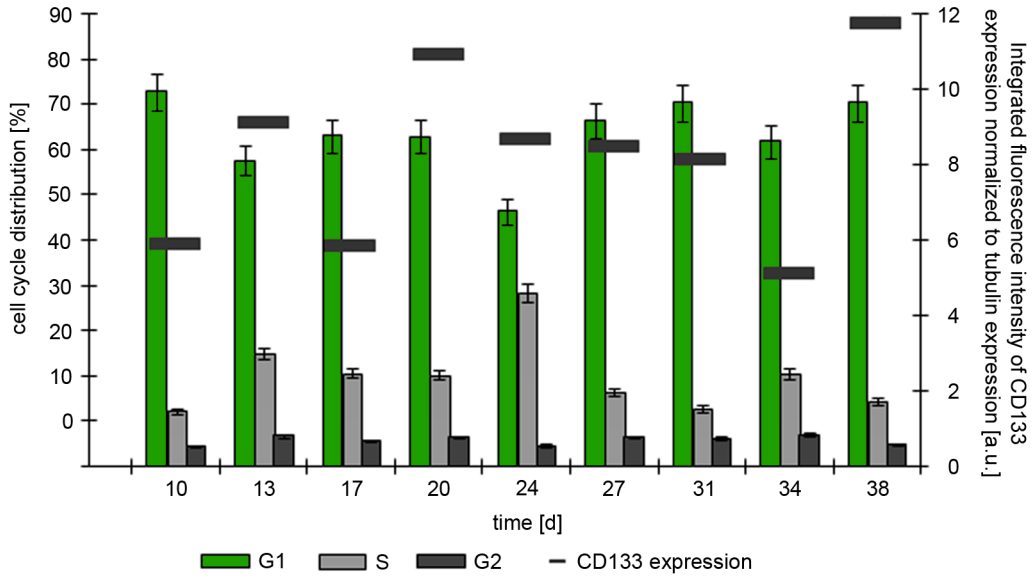

Figure 3.20: Independence of CD133 expression from cell cycle distribution.
Illustrated is the CD133 expression in CD133$^+$ ChaMel91 cells at nine different time points during the long-term experiment described in **Figure 3.19** and the corresponding cell cycle distribution. No correlation of CD133 expression with G1-, S- nor G2-phase could be observed. Error bars indicate assumed standard deviations of 5%.

To elucidate if the CD133 fluctuations result from overgrowing of one subpopulation over the other or from an interconversion of $CD133^+$ and $CD133^-$ cells I then sorted CD133 populations and cultivated the populations separately for seven days before the next sorting round. By six repetitive sorting cycles I aimed to dilute the amount of false negative cells (= $CD133^+$) within the $CD133^-$ subpopulation subsequently. During six cycles of sorting and with an average of 0.25% false negative cells after each sorting round I theoretically should have diluted the false negative cells down to 7.8^{-8} %. But still, I ended up with an average of 5-10% $CD133^+$ cells in the $CD133^-$ subpopulation. In order to explain this observation by an increased cell cycle rate of $CD133^+$ cells, the cells would have needed to double two times as fast as the $CD133^-$ cells, meaning the average duration of the cell cycle in $CD133^+$ would be as short as 16.5 minutes.

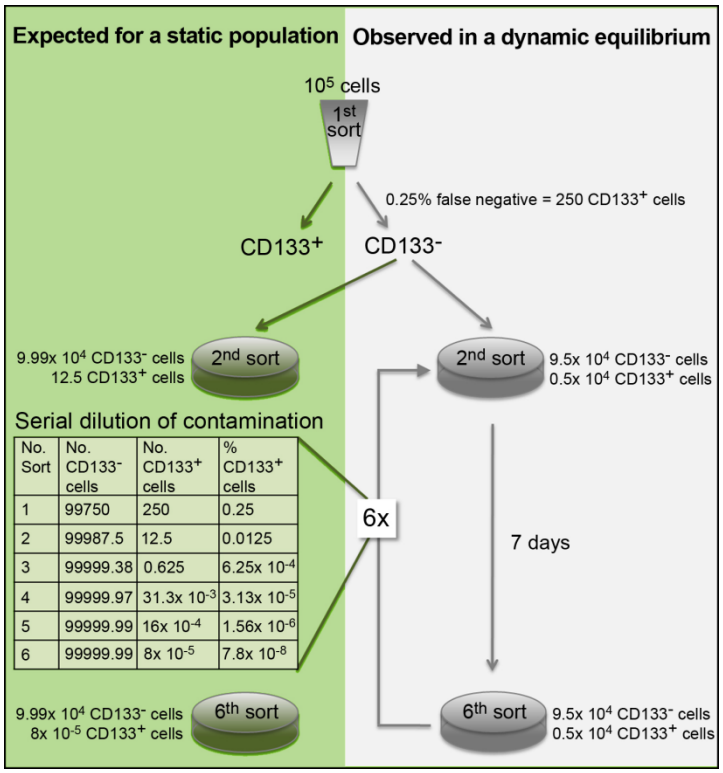

Figure 3.21: Bidirectional interconversion of $CD133^+$ and $CD133^-$ melanoma cells. In a proposed static population serial MACS experiments would result in subsequent dilution of false negative cells in the $CD133^-$ fraction. Theoretical amount of cells was calculated as shown on the left. Shown on the right is the measured percentage of $CD133^+$ cells, which in our experiments always returned towards initial proportions over time. This indicates a dynamic equilibrium of CD133 expressing cells in melanoma and a bidirectional interconversion of $CD133^+$ and $CD133^-$ melanoma cells.

To study whether the cell density and/or frequency of fresh medium-supply during culture could influence expression of CD133 and the observed plasticity of $CD133^+$ and $CD133^-$ cells, we modified the experimental conditions. In comparative experiments we seeded only half the number of cells or changed the cell culture medium daily instead of every three days. In both experiments we observed a comparable periodic behavior as before in terms of the amplitude, however, with altered dynamics of CD133 expression. While one half-period of the CD133 fluctuation in unsorted ChaMel91 cells was seven days (max) in the original experiment, we saw that under the conditions of sparser cell seeding

(data not shown) and frequent medium supplements the half-period was increased to >14 days (**Figure 3.22**).

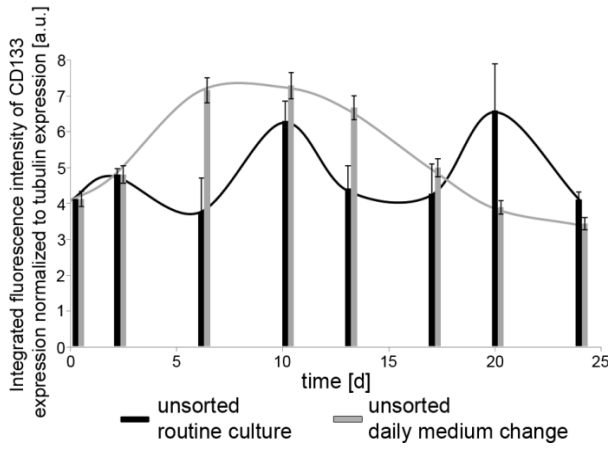

Figure 3.22: CD133 fluctuation is significantly influenced by change of routine culture conditions.
In comparative experiments we changed the cell culture medium either every three days (routine culture) or daily. In both experiments we observed a comparable periodic behavior of CD133 expression in terms of the amplitude. But daily medium change decreased the frequency of the CD133 dynamic. While in the original experiment one half-period of the CD133 fluctuation was 7 d (max), we saw that upon daily medium supply the half-period was significantly longer (>14 d).

3.4 Analysis of OCT4A expression in melanoma cells

3.4.1 *OCT4A* is expressed in melanoma cells

Standard PCR with *OCT4A* primers (see section 2.4.5) and cDNA revealed that all melanoma cell lines tested as well as adult and neonatal melanocytes express *OCT4*. To verify that the weak signals from the PCRs are really due to *OCT4A* expression and not the amplification products of other *OCT4* splice variants or even pseudogenes, the PCR products were re-amplified with *OCT4A* nested primers to increase the putative *OCT4A* product. Then, resulting PCR products were purified and digested with the restriction enzymes *Apa*I and *Tsp*45I (see protocol in section 2.4.8). The *OCT4A* transcript specifically encodes the recognition sites of both enzymes. In **Figure 3.23** A the restriction digests of the *OCT4A* PCR products from the melanoma cell line ChaMel91 and the positive control NCCIT is shown exemplarily (in this example no re-amplification with *OCT4A* nested primers was performed). Digest of the 474 bp products with *Apa*I resulted in the two expected fragments of 288 bp and 185 bp and with *Tsp*45I in a 403 bp and 70 bp fragment. The *OCT4A* PCR products of all tested cell lines could be digested by the two restriction enzymes, which indicated the presence of *OCT4A* specific mRNA sequence.

To verify these results, all PCR products generated by *OCT4A* nested primers were sequenced by means of BigDye Terminator v3.1 Cycle Sequencing Kit and the 3730xl DNA Analyzer (compare section 2.5). In the range investigated, the analyzed sequences of all tested cell lines were 100% identical to the annotated *OCT4A* sequence on the Ensembl Genome Browser.

3.4.2 Differential expression of OCT4A between CD133$^+$ and CD133$^-$ melanoma cells

The expression of *OCT4A* was then analyzed on transcript and protein level in CD133$^+$, CD133$^-$ and unsorted ChaMel91 cells. Whereas standard PCR from cDNA of these three cell fractions revealed only a very weak *OCT4A* expression in unsorted melanoma cells, the signal was much stronger in CD133$^+$ ChaMel91 cells (**Figure 3.23** B). Restriction digest of the *OCT4* PCR product with restriction enzymes *Apa*I and *Tsp*45I revealed that the transcript of the pluripotency related *OCT4A* and not *OCT4B* or any other alternatively spliced transcript was amplified. In CD133$^-$ melanoma cells no *OCT4A* transcript could be detected. The same held true for the OCT4 protein, which by western blotting could only be detected in CD133$^+$ ChaMel91 cells and not in CD133$^-$ cells (**Figure 3.23** C). *OCT4A* transcript as well as protein expression was much higher in NCCIT cells compared to CD133$^+$ melanoma cells.

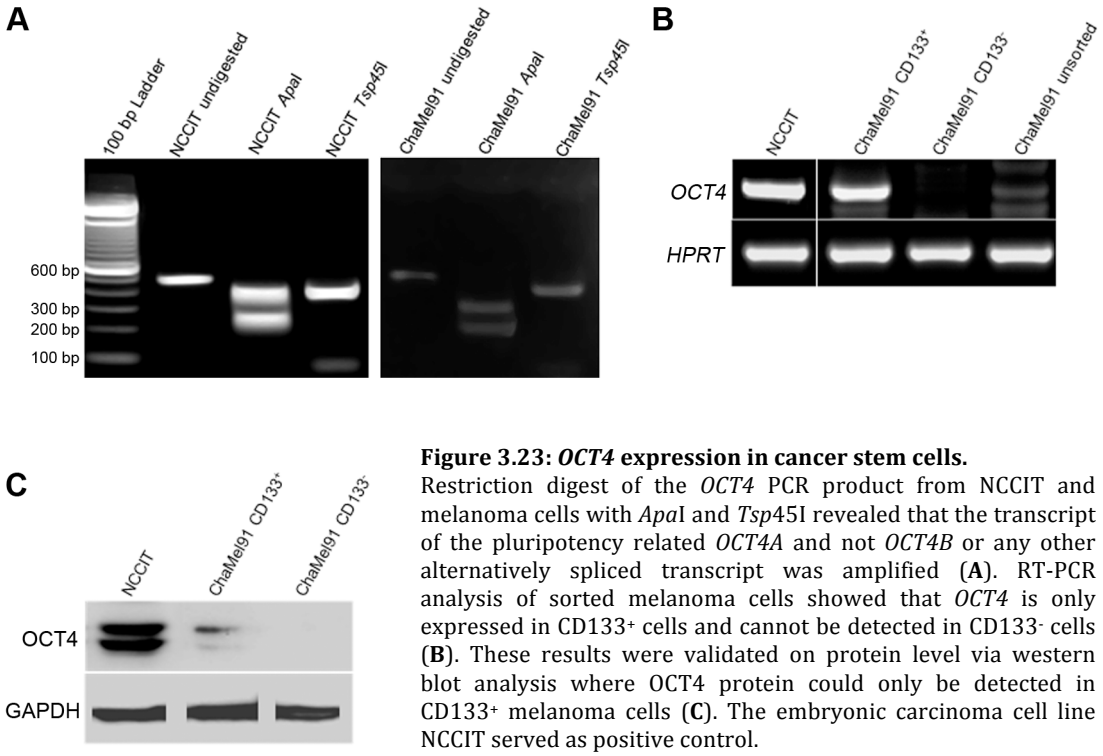

Figure 3.23: *OCT4* expression in cancer stem cells.
Restriction digest of the *OCT4* PCR product from NCCIT and melanoma cells with *Apa*I and *Tsp*45I revealed that the transcript of the pluripotency related *OCT4A* and not *OCT4B* or any other alternatively spliced transcript was amplified (**A**). RT-PCR analysis of sorted melanoma cells showed that *OCT4* is only expressed in CD133$^+$ cells and cannot be detected in CD133$^-$ cells (**B**). These results were validated on protein level via western blot analysis where OCT4 protein could only be detected in CD133$^+$ melanoma cells (**C**). The embryonic carcinoma cell line NCCIT served as positive control.

To be able to sort ChaMel91 into OCT4A$^+$ and OCT4A$^-$ cells and examine the differences between both fractions as well as their similarities to hESCs or the embryonic carcinoma cell line NCCIT, I stably transfected ChaMel91 cells with a plasmid expressing the EGFP reporter gene under the control of the OCT4 promoter (phOCT4-EGFP-1 plasmid) (see section 2.7). Microscopic and flow cytometric analysis (at FACSCalibur System with CellQuest Pro Software 4.0.1) of these cells revealed a small subpopulation of about 2-10% cells which express EGFP. The percentage of OCT4-EGFP$^+$ cells was shown to increase with

decreasing cell density. After decreasing the cell number below 5x 10^4 cells per cm^2 the fraction of OCT4-EGFP expressing cells was even increased to more than 10% as shown in **Figure 3.24**. Most notably, the subpopulation of OCT4-EGFP$^+$ cells is significantly greater in CD133$^+$ ChaMel91 cells when compared to CD133$^-$ cells as already observed in previous experiments (compare **Figure 3.23**).

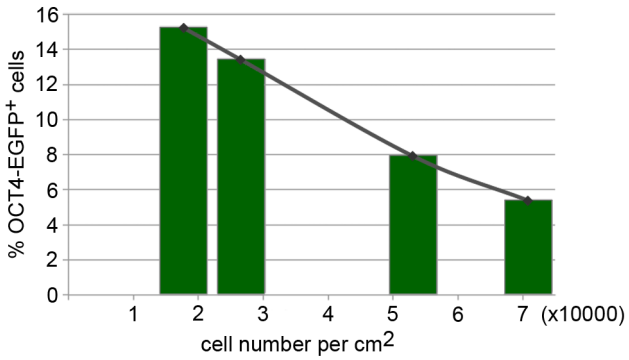

Figure 3.24: Correlation of OCT4-EGFP expression and cell density. ChaMel91 cells were transiently transfected with the phOCT4-EGFP-1 plasmid. 5 h post transfection different cell numbers were seeded into cell culture dishes. After incubation for 48 h OCT4-EGFP expression was analyzed by flow cytometry and plotted together with the cell number per cm^2. Decreasing cell density correlated with an increase of OCT4-EGFP$^+$ cells.

3.4.3 Sorting of OCT4-EGFP$^+$ and OCT4-EGFP$^-$ melanoma cells

ChaMel91 cells stably transfected with the phOCT4-EGFP-1 plasmid were sorted into OCT4-EGFP$^+$ and OCT4-EGFP$^-$ cells using a FACSDiva Flow Cytometer & Cell Sorter with BD FACSDiva Software 6.0. A representative example for the sorting is shown in **Figure 3.25**. First, melanoma cells were analyzed in forward and side scatter to find the main population of viable, isolated cells (**Figure 3.25** A). This population was then gated and analyzed for its EGFP expression. Cells, strongly expressing EGFP (gate P2) and cells that did not express EGFP (gate P1) (**Figure 3.25** B) were sorted into two different tubes and seeded in appropriate culture flasks. 48 h after sorting accuracy of the flow cytometer and instrument settings was verified microscopically (**Figure 3.25** C). Nearly all cells of gate P2 expressed EGFP whereas no EGFP expression was observed in cells of gate P1. Even five days post sorting this result had not changed.

As an additional control, the sorting efficiency and consistency was evaluated on transcript level by standard PCR and on protein level using fluorescent western blot (**Figure 3.26**). Even 72 h post sorting the EGFP transcript was much higher expressed in the OCT4-EGFP$^+$ fraction compared to the OCT4-EGFP$^-$ fraction. Furthermore, the EGFP signal intensity of unsorted ChaMel91 cells was intermediate of both sorted fractions (**Figure 3.26** A). This result was validated on protein level via fluorescent western blot where the EGFP signal was 85% lower in the OCT4-EGFP$^-$ fraction compared to the OCT4-EGFP$^+$ fraction (**Figure 3.26** B).

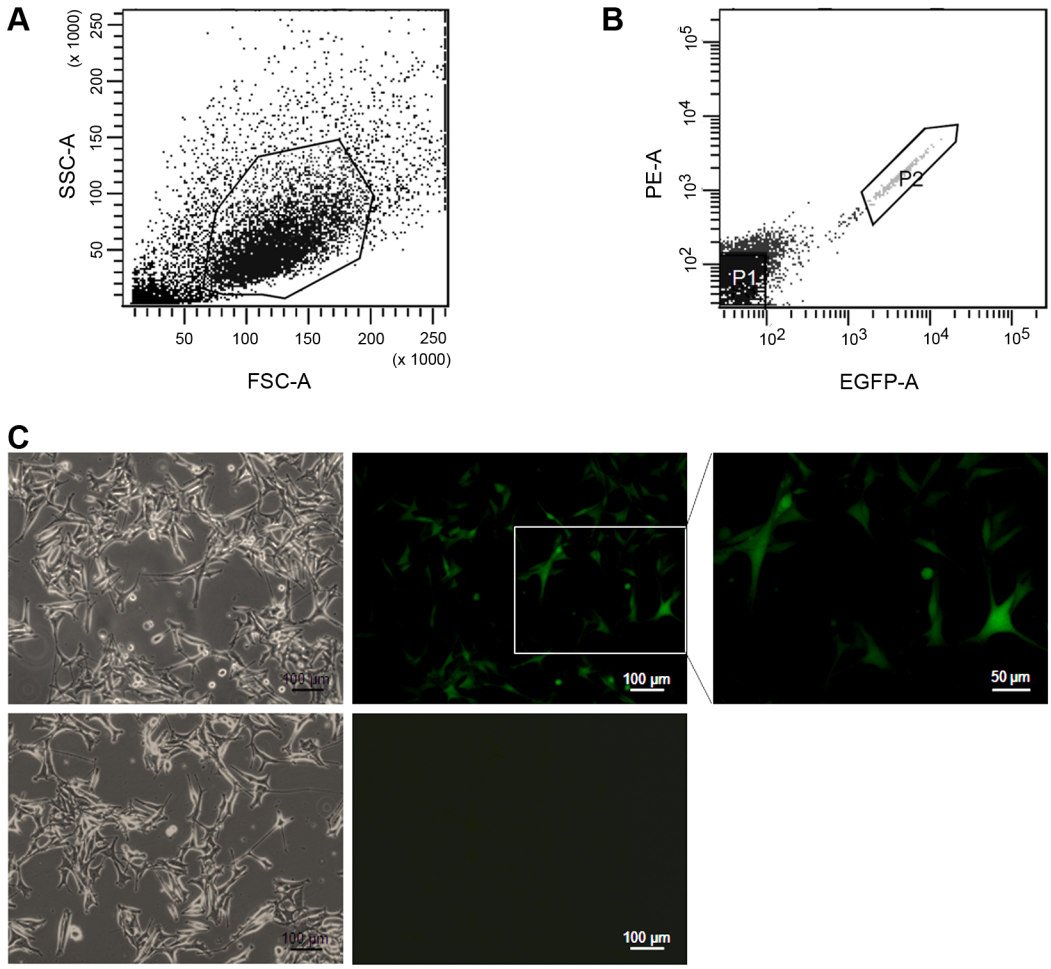

Figure 3.25: FACS of ChaMel91 into OCT4-EGFP⁺ and OCT4-EGFP⁻ cells.
ChaMel91 melanoma cells were stably transfected with the phOCT4-EGFP-1 plasmid and sorted with FACSDiva Flow Cytometer & Cell Sorter. First, the main population of ChaMel91 was gated in forward and side scatter plot (**A**). Then, OCT4-EGFP⁺ (gate P2) and OCT4-EGFP⁻ cells (gate P1) were separated. In the sort shown here, 2.5% of all cells were located in gate P2 (**B**). Accuracy of the cytometer and instrument settings was verified microscopically 48 h after sorting (**C**). Nearly all cells of gate P2 express EGFP (upper panels) whereas no cells of gate P1 do so (lower panels).

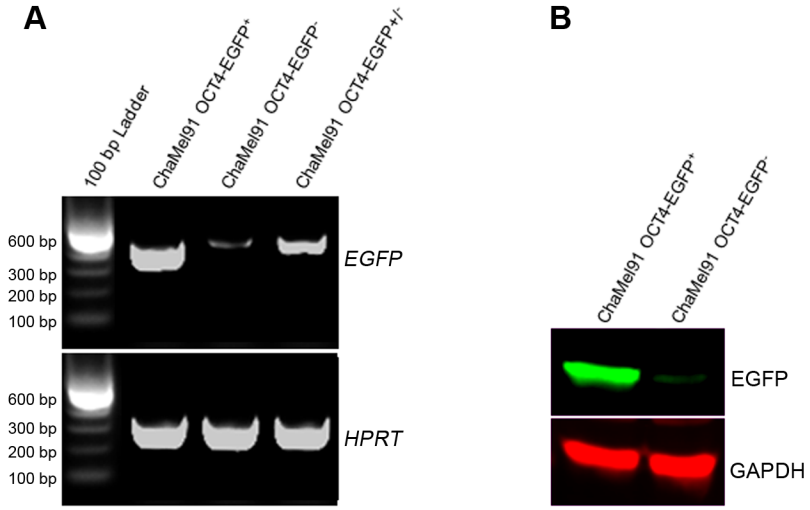

Figure 3.26: Verification of OCT4-EGFP sorting via RT-PCR and western blot analysis.
RT-PCR with EGFP-specific primers showed that cells sorted with FACS DIVA as OCT4-EGFP⁺ strongly expressed EGFP while OCT4-EGFP⁻ cells showed nearly no EGFP expression on mRNA level (**A**). This result was verified also on protein level via western blot analysis (**B**).

3.4.3.1 Nuclear expression of OCT4A in OCT4-EGFP$^+$ melanoma cells

To confirm that EGFP expression in sorted ChaMel91 correlated with their endogenous expression of OCT4A, cells were cultivated for 120 h after sorting into OCT4-EGFP$^+$ and OCT4-EGFP$^-$ fractions to recover from the procedure and then stained with an OCT4A-specific antibody conjugated to AlexaFluor488. Whereas OCT4-EGFP$^-$ cells showed only a weak and diffuse unspecific staining all over the cell body with this antibody (**Figure 3.27** A), a distinct and strong staining for OCT4A in the nuclei was demonstrated in OCT4-EGFP$^+$ cells (**Figure 3.27** B). NCCIT, which served as positive control for OCT4A showed also a strong staining for OCT4A in the nuclei and neonatal melanocytes were negative for OCT4A (data not shown).

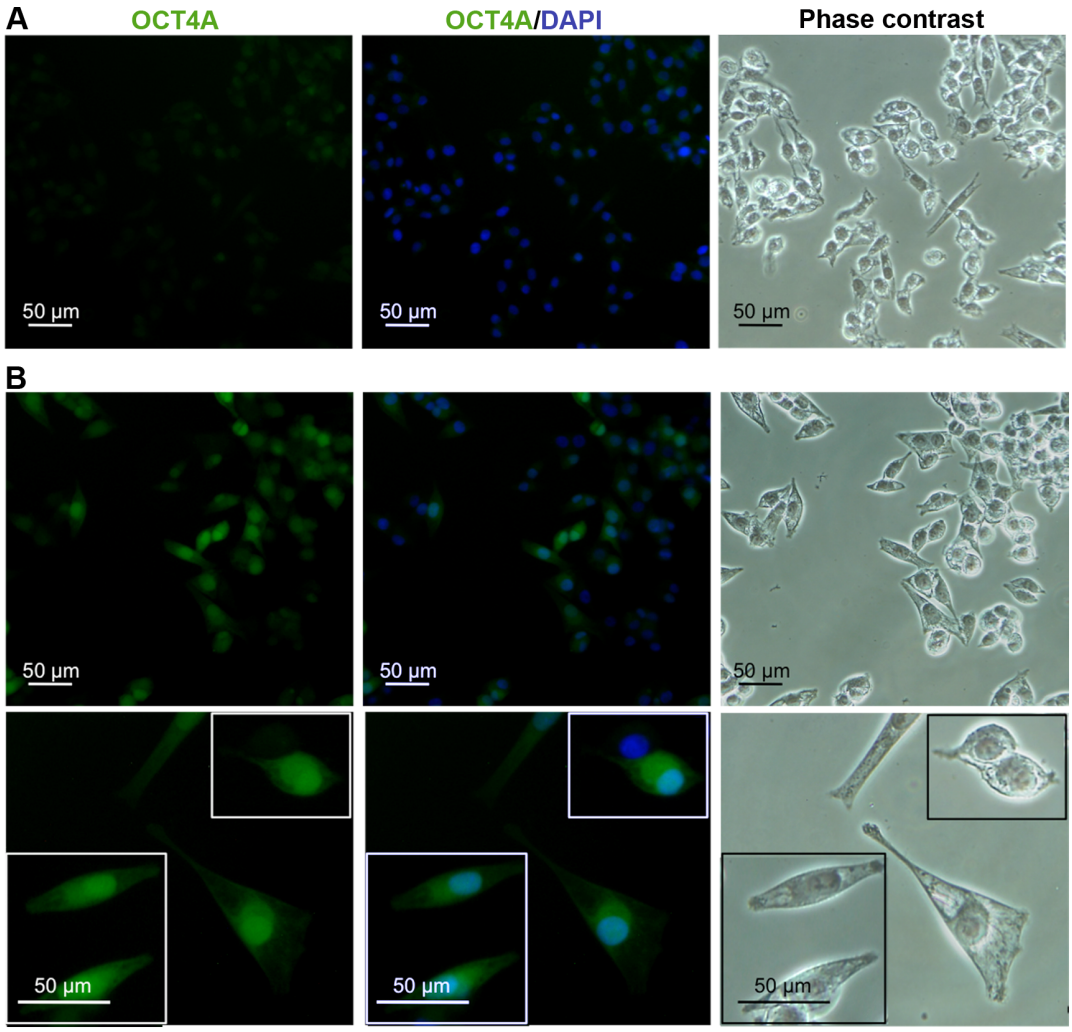

Figure 3.27: OCT4A immunofluorescence staining of ChaMel91.
After sorting ChaMel91 cells with FACSDivaflow cytometer into OCT4-EGFP$^+$ and OCT4-EGFP$^-$ fractions, cells were cultivated for 120 h to recover from sorting procedure. Thereafter, cells were stained with an OCT4A-specific antibody conjugated to AlexaFluor488 (green). Left: Whereas OCT4-EGFP$^-$ cells show only a weak and diffuse unspecific staining (**A**) a distinct and strong staining for OCT4A in the nuclei is demonstrated in OCT4-EGFP positive cells (**B**). Middle: Co-staining with the nuclear stain DAPI (blue). Right: Corresponding phase contrast micrographs of ChaMel91 cells.

3.4.4 Comparison of OCT4-EGFP$^+$ and OCT4-EGFP$^-$ melanoma cells

3.4.4.1 Gene expression analysis of OCT4-EGFP$^+$ and OCT4-EGFP$^-$ cells

Genome-wide expression analysis of OCT4-EGFP$^+$ and OCT4-EGFP$^-$ ChaMel91 cells was performed with cells harvested five days post sorting. Sustained differential expression of EGFP in the sorted cells was confirmed by fluorescent microscopy. cRNA samples were hybridized on Illumina HumanHT-12 v4 and HumanWG-6_V3 Expression BeadChips and analyzed as described in section 2.4.10. Gene expression data were normalized and analyzed for significant gene expression differences (detection p-value <0.05, p-value <0.05). The transcriptome of OCT4-EGFP$^+$ and OCT4-EGFP$^-$ was than compared with hESCs to find genes exclusively expressed in OCT4-EGFP$^+$ and hESCs but not in OCT4-EGFP$^-$ melanoma cells. 156 genes were at least 1.5-fold upregulated in OCT4-EGFP$^+$ and hESCs compared to OCT4-EGFP$^-$ cells (**Figure 3.28**). This gene list was further analyzed using gene annotation tools to identify gene ontologies (GOs) and KEGG pathways significantly overrepresented in OCT4-EGFP$^+$ melanoma cells. KEGG pathway analysis revealed that key developmental pathways such as Wnt, Notch and Hedgehog signaling (overexpressed genes were e.g. *DVL1, TCF7L2, CTBP1, CSNK1A1*) were amongst the overrepresented pathways in OCT4-EGFP$^+$ as well as hES cells. Besides, I found that genes involved in the inhibition of apoptosis, cellular migration as well as cell cycle regulation were upregulated and overrepresented in the OCT4-EGFP$^+$ melanoma fraction. Total lists of these overrepresented GOs and KEGG pathways are shown in **Table S 3** and **Table S 4**. These results are similar to the expression data obtained for CD133$^+$ and CD133$^-$ cells. The important cancer- and stem cell-related WNT, NOTCH, Hedgehog pathways as well as genes involved in apoptosis, cellular migration and cell cycle regulation are overrepresented in CD133$^+$ and OCT4-EGFP$^+$ putative melanoma CSC fractions compared to their negative counterparts.

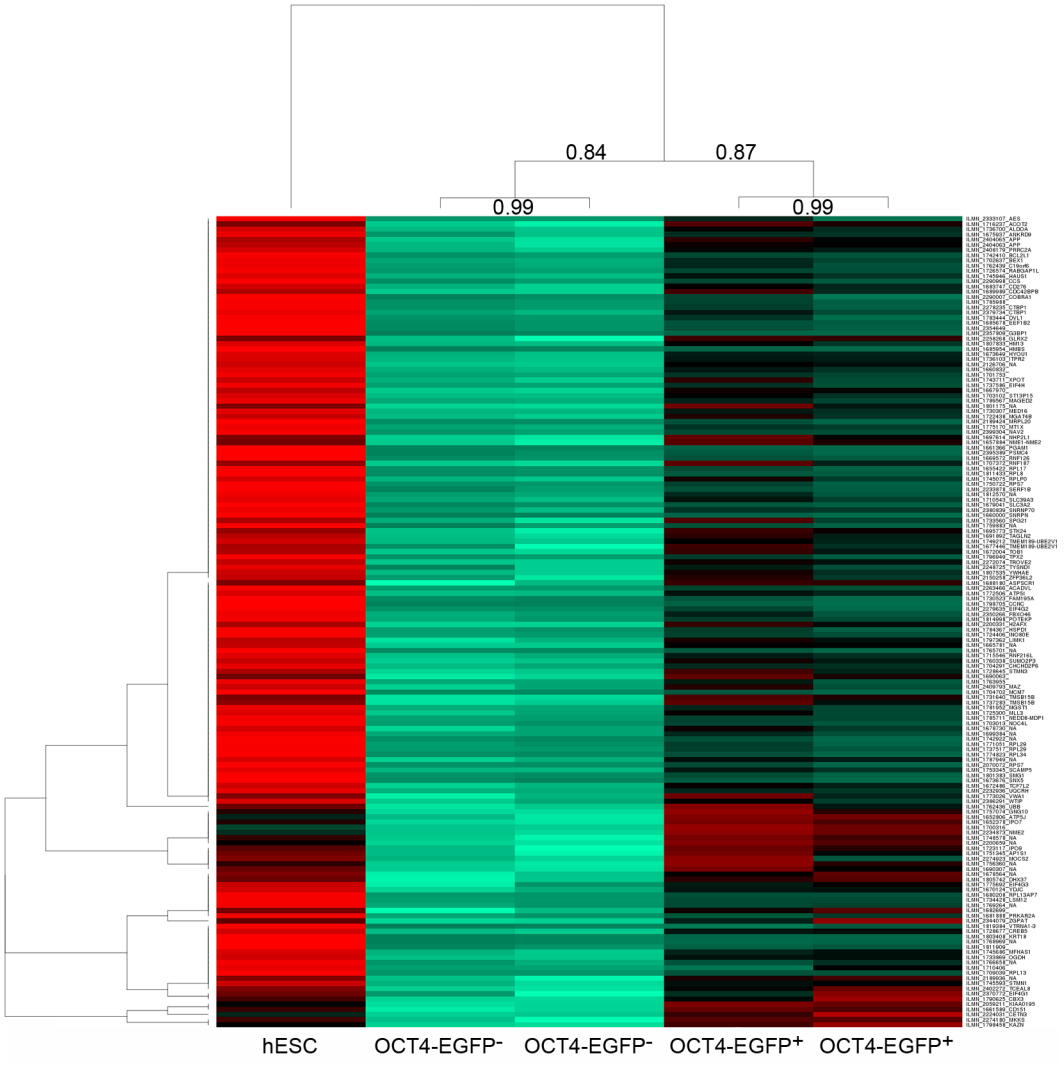

Figure 3.28: Heatmap of hESCs, OCT-EGFP$^+$ and OCT4-EGFP$^-$ cells.
Gene expression analysis of hESC cells as well as OCT-EGFP$^+$ and OCT4-EGFP$^-$ melanoma cells revealed that 156 genes are at least 1.5-fold upregulated in hESCs and OCT-EGFP$^+$ cells compared to OCT4-EGFP$^-$ cells. Numbers on top of the heatmap represent correlation coefficients of the OCT4-EGFP subpopulation duplicates and of these subpopulations with hESCs.

3.4.4.2 Tumor initiation capability of OCT4-EGFP$^+$ and OCT4-EGFP$^-$ cells

In comparison to CD133$^+$ and CD133$^-$ ChaMel91 cells tumor formation capability of OCT4-EGFP$^+$ and OCT4-EGFP$^-$ cells was also examined and compared (see 2.10). Five days after fluorescent activated cell sorting 10^5 OCT4-EGFP$^+$, OCT4-EGFP$^-$ and unsorted stably transfected ChaMel91 cells were injected into six NSR mice, respectively. Eight weeks after implantation, a difference in tumor growth between OCT4-EGFP$^+$ and OCT4-EGFP$^-$ cells as for CD133$^+$ and CD133$^-$ cells was examined. OCT4-EGFP$^+$ cells resulted in bigger tumors (**Figure 3.29**) in a shorter period of time after injection compared to OCT4-EGFP$^-$ and unsorted cells (**Figure 3.30**).

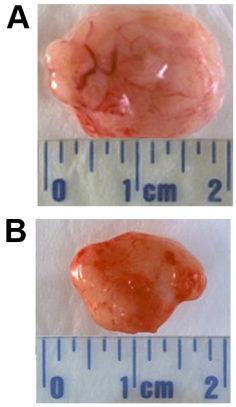

Figure 3.29: Excised tumors from NRS mice eight weeks after xenotransplantation.
Comparison of the tumors with the biggest volume developed after injection of 10^5 OCT4-EGFP$^+$ ChaMel91 (**A**) and 10^5 OCT4-EGFP$^-$ cells (**B**) into male NSR mice, respectively. On average, tumors of OCT4-EGFP$^+$ had a larger volume compared to the tumors of OCT4-EGFP$^-$ cells.

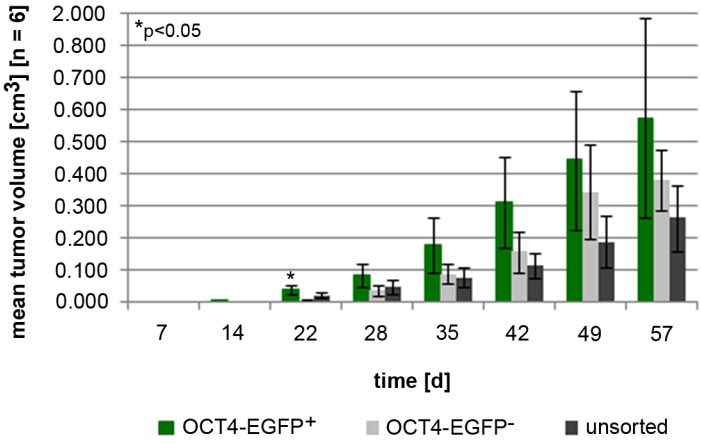

Figure 3.30: Tumor formation capability of OCT4-EGFP sorted ChaMel91 cells.
Tumor formation and growth capability of 10^5 OCT4-EGFP$^+$ cells injected into six NSR mice was higher than of OCT4-EGFP$^-$ or unsorted cells (monitored for 57 days). Error bars indicate the standard deviation among the group of six mice. p-values were determined for unpaired samples of OCT4-EGFP$^+$ and OCT4-EGFP$^-$ cells by Student's *t*-test.

3.4.4.3 Comparison of OCT4-EGFP$^+$ melanoma cells with partially and fully reprogrammed iPS cells

To determine if putative OCT4-EGFP$^+$ CSCs share similarities in gene expression not only with hESCs but also with induced pluripotent stem (iPS) cells we performed a meta-analysis of expression profiling data sets of partially and fully reprogrammed iPS cells and OCT4-EGFP$^+$ melanoma cells. The only available genome-wide expression data from partially and fully reprogrammed iPS cells are from a study of Mikkelsen *et al*. who reprogrammed mouse fibroblasts by ectopic expression of the four reprogramming factors Oct4, Sox2, Klf4 and c-Myc (Mikkelsen *et al.* 2008). Data from this study were downloaded from the NCBI GEO platform accession GSE10781. Comparison with my data from OCT4-EGFP$^+$ melanoma cells was enabled by mapping all probes to human gene symbols (probe sets of mouse genes were mapped to orthologous human gene symbols via Biomart version 62). Gene expression data were normalized and analyzed for significant differential gene expression differences (detection p-value <0.05, p-value <0.05).

We found an overlap in the expression of several hundred genes with known functions for stemness, epigenetic regulation, DNA repair as well as genes of important developmental pathways like TGF-β/BMP, Wnt and Notch. Also the master regulator of pluripotency OCT4A is expressed in partially and fully reprogrammed iPS cells and OCT4-EGFP$^+$

melanoma cells as shown in **Figure 3.31**. This comparison provides further evidence that melanoma cancer stem cells display features of partially/fully reprogrammed iPS cells and embryonic stem cells and vice versa.

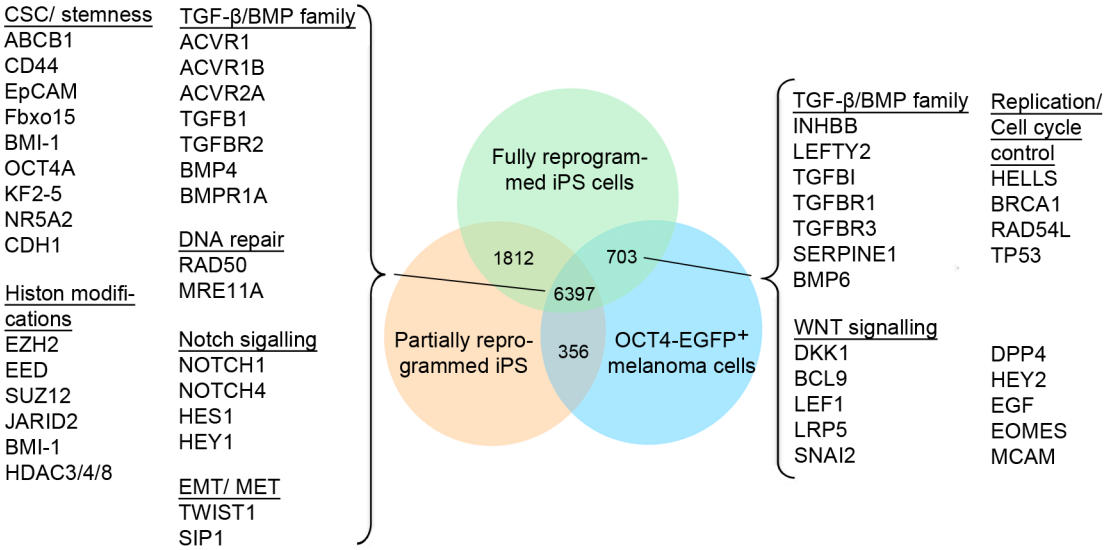

Figure 3.31: Comparison of expression profiles of OCT4-EGFP+ melanoma cells with partially and fully reprogrammed iPS cells.
Meta-analysis of microarray datasets from partially and fully reprogrammed iPSCs obtained from Mikkelsen *et al.* (Mikkelsen *et al.* 2008) and OCT4-EGFP+ melanoma cells. The Venn-diagram reflects commonly regulated genes of CSCs and embryonic stem cells like members of the TGF-β/ BMP, Wnt and Notch pathways, Histon modifiers, regulators of EMT/MET and components of the DNA repair machinery.

4 Discussion

There are three ways of identifying and sorting CSCs described in current literature. Interestingly, not a single publication evaluated and compared the methods in regards of conformity in results of the approaches. Therefore I started the project by comparing these current standard assays of CSC identification: “sphere formation analysis”, “dye exclusion assay” and “expression analysis of well described stem cell/CSC markers” on a cohort of ten patient derived low-passage melanoma cell lines.

By all methods, I identified subpopulations of melanoma cells with stem cell properties but there was no exact congruency in the outcome of these assays. E.g., nine of ten analyzed cell lines exhibited a side population (SP) by Hoechst staining but only six of these cell lines grew in spheres under hESC culture conditions. The low concordance between the three methods that I found in my work, as well as recent findings by other groups question the applicability of these current standards of CSC identification. Potential reasons for this low concruency and likely technical pitfals of these assays will be discussed below.

4.1.1 Sphere formation assays

Recently, the use of sphere formation assays to identify and enrich CSCs was put into question. Tumor spheres are defined as clonally derived non-adherent colonies of cells derived from a single tumor stem cell (Singh *et al.* 2003). Clarke *et al*. found out that the rate of sphere development in many *in vitro* models makes it unlikely that single cells solely through clonal expansion form those spheres. The difficulty of distinguishing the relative contributions of aggregation and proliferation in sphere formation represents the major hurdle to their use (Clarke *et al.* 2006). In my experiments spheres started to form after about five days. With an average doubling time of 32 h the cells would double four times in those five days. Some of the observed colonies were definitely composed of more than just 16 cells. Therefore we need to think of other mechanisms to explain formation of spheres. Given the fact that stem cells are highly dependent on their microenvironment, it is likely that different cell types attract each other to form the spheres as a highly robust and complex structure that helps to overcome harsh conditions. Another possible explanation could be that the cell cycle accelerates so that the spheres obtained in my experiments are after all generated from single cells by clonal expansion. Sorting at the single cell level would of course be the most reliable source of clonal growth. But we know from the stem cell research that single cell sorting leads to undesired differentiation of the cells making it impossible to analyze the stem cell properties. In the field of stem cell

research it therefore is a commonly used and accepted technique to pick colonies in order to propagate and maintain an undifferentiated stem cell culture.

To fathom the sphere forming mechanism one could use a strategy of "lineage tracing" where you use a DNA dye to mark the cells prior to the culture in hESC medium and analyze the formed spheres by flow cytometry. If spheres had formed by clonal expansion of single cells one would observe a measurable decrease of the DNA dye retained in the DNA double strand since each cell doubling halves the dye in the resulting daughter cells. On the other hand, if cells attract each other to form the spheres, an equal amount of DNA dye among the spheroid cells would be detected. Another technical difficulty of sphere formation assays is their sensitivity to the culturing method used (i.e., media composition, coating of the flasks with feeder cells or matrix and general cell culture handling techniques), making it difficult to compare experimental findings from different laboratories. Moreover, it has been shown that differentiated cells exhibit sphere-forming capability and because spheroid bodies themselves display marked cellular heterogeneity, experiments using spheres should be interpreted as studies of mixed cell populations, not purified stem cells (Schatton *et al.* 2010, Jensen *et al.* 2006). Ramgolam *et al*. showed that sphere forming cancer cells display higher capacity to differentiate along mesenchymal lineages. In their experiments they measured an increased expression of SOX2, NANOG, KLF4, and/or OCT4 transcription factors, but failed to show increased self-renewal or tumorigenicity of spheroid cells when compared to their adherent counterparts. They concluded that sphere formation assays are of limited efficiency for melanoma CSC identification, but rather predict an aggressive and heterogeneous phenotype which is likewise relevant to patients and clinical transferability (Ramgolam *et al.* 2011).

4.1.2 Dye exclusion assay

Stem cells are known to express ABC transporters. ABC transporters are used to actively eliminate small molecules from the cell. This trait evolved as a protection mechanism from chemically induced cell damage. High expression of ABC transporters is also observed in cancer cells and plays an important role in failure of chemotherapy. Hirschmann-Jax *et al*. showed that ABC transporter expression is not evenly distributed in the tumor cell population. High expression of ABC transporters is linked to only a few cells within the tumor, which they conclude could be potential cancer stem cells (Hirschmann-Jax *et al.* 2004).

Unfortunately, encouraging earlier findings of dye exclusion assays (compare 1.3.3.2) are accompanied by results from newer studies with thyroid, gastrointestinal, adrenocortical and glioma cancer cells, which question the possibility to identify CSCs by their efflux-

capacity. Functional studies depicted very well that SP and non-SP cells were similarly clonogenic *in vitro*, tumorigenic *in vivo*, and displayed similar differentiation potential *in vitro* and *in vivo.* Furthermore both fractions showed self-renewal capabilities, similar growth rates and chemoresistance (Burkert *et al.* 2008, Lichtenauer *et al.* 2008, Mitsutake *et al.* 2007, Platet *et al.* 2007).

My hypothesis is that these controversial results are in large parts due to inefficient and lenient sorting procedures that lead to false positive and negative sorted cells. Variations in the staining protocol (enzyme dissociation method, Hoechst and verapamil concentrations, incubation time) and FACS procedure (flow cytometer, nozzle size) do have enormous influence on the yield, viability and homogeneity of side population cells, affecting all later analyses performed on these cells. A good example of the influence of technical factors on the results is the comparison of studies from Kondo *et al*. and Patrawala *et al*. Both groups studied the same cell lines, but with variation in their protocols and of course in their technical equipment. The yield of SP cells varied by a magnitude of 10 (Kondo *et al.* 2004, Patrawala *et al.* 2005). In order to gain reproducible results, tissue dissociation to single cell suspension levels and cell counting needs to be optimized and standardized. Montanaro *et al*. showed that optimal Hoechst concentration should be independently determined for each new cell type studied and the optimal Hoechst concentration should be within the plateau region of retained SP cells (Montanaro *et al.* 2004). Remarkably, none of the researchers who has investigated SP cells tested for the optimal Hoechst concentration in the used cell type or modified the staining procedure although initial studies published the optimal concentration of Hoechst (Asakura *et al.* 2002, Bhattacharya *et al.* 2003, Dou *et al.* 2009, Fukaya *et al.* 2009, Grichnik *et al.* 2006, Haraguchi *et al.* 2006, Kondo *et al.* 2004, Mimeault *et al.* 2009). Moreover, it is more than likely that even different cell lines derived from the same tissue origin exhibit distinct sensitivities towards Hoechst since cell lines from different patients or various tumor grades probably have different amounts or activity of ABC transporters. Furthermore, it has been shown that various cell types are unequally sensitive to verapamil, which serves as an important control. A concentration of 50 µM verapamil is what seems to be the current standard without further determination of cell-line specific sensitivity towards verapamil prior to the SP sorting (Asakura *et al.* 2002, Grichnik *et al.* 2006, Patrawala *et al.* 2005). In addition to the variations in technical setup of FACS sorting, it has been demonstrated that the SP size depends on the density of cells in culture. SP cells preferentially survive at very low plating density, because such clonal growth favors the presence of CSCs (Mitsutake *et al.* 2007). Due to the wide range of parameters that can significantly influence SP analyses, results from such sorting experiments should be

compared very cautiously. Optimized and standardized protocols for each cell type as well as stringent cell culture and isolation settings are required to eliminate the risk of analyzing different SP cells.

Ultimately, the toxicity of Hoechst should be addressed and always kept in mind when applying this dye to isolating putative CSCs. As Hoechst binds to DNA, it can disrupt DNA replication during cell division. Consequently, it is potentially mutagenic and carcinogenic. Already in 1986, Siemann *et al.* evaluated the toxicity of this stain in cells derived from sarcomas. Hoechst toxicity increased with increasing exposure times resulting in 25- to 45-fold reduced survival in irradiated cells and 4- to 5-fold reduced survival in untreated cells. Furthermore, cytotoxic effects of Hoechst 33342 were found to be significantly greater in cells in the S-phase than in cells in G1- and G2-M-phases of the cell cycle (Siemann *et al.* 1986, Shen *et al.* 2008). This toxicity, particularly its cell cycle specificity, suggests a potentially severe limitation for the use of Hoechst dye in combination with fluorescence-activated cell sorting. Non-SP cells with lower capacity to efflux this dye will suffer more from its effects compared to putative CSCs of the SP. Hence, Wu *et al.* argued that SP cells may not represent stem-like cells, but rather, a population of cells that is able to escape the lethal effects of Hoechst staining (Wu *et al.* 2008). The alternative use of the non-cytotoxic Rhodamine 123 for identifying side populations of CSCs was previously discussed in more detail (Welte *et al.* 2010). Due to the controversial findings and technical hurdles of applying dye exclusion assays, it is doubtful if Hoechst staining and isolation of SP cells can be used to identify and isolate CSCs.

4.1.3 Expression of CSC markers

I used RT-PCR for confirmation of a selection of published putative markers of cancer stem cells, like *CD20* (Fang *et al.* 2005), *CD133* (Gedye *et al.* 2009, Monzani *et al.* 2007), *ABCB5* (Frank *et al.* 2005), *ABCG2* (Frank *et al.* 2005, Monzani *et al.* 2007) and *TNC* (Fukunaga-Kalabis *et al.* 2010). The expression of these markers was specifically described for melanoma. For the melanoma cell lines I used for this thesis, I showed the expression of all these markers except for *CD20*. Fang *et al*. were the first who described the expression the B-lymphocyte antigen CD20 also in melanoma cells. In their work they found that melanoma spheres, which in turn were more tumorigenic than their adherent counterparts, consistently express CD20. Furthermore, it was shown that this $CD20^+$ melanoma subpopulation was multipotent (Fang *et al.* 2005). Another group demonstrated that CD20 is a relevant marker to distinguish highly aggressive metastatic melanoma from malignant melanoma with better prognosis. This could guide to a prospective molecular classification of malignant melanoma (Bittner *et al.* 2000) (compare

1.2.3). Finally, different preclinical *in vivo* models confirmed that targeting CD20-expressing melanoma cells by cytotoxic T cells or cytotoxic anti-CD20 monoclonal antibody significantly reduces the growth of human melanoma xenografts in mice whereas targeting of any random 10% tumor cell subset is not effective (Schmidt *et al.* 2011, Wagner *et al.* 2010). Currently, a Phase II pilot study with patients diagnosed with unresectable stage IIIb, IIIc or stage IV melanoma assesses the effectivity of the human monoclonal anti-CD20 antibody ofatumumab as a first line treatment. In my work I did not detect the expression of *CD20* in melanoma cells, neither on enriched CSCs of melanoma spheres nor on $CD133^+$ or $OCT4A^+$ cells, although the cell lines that I have used for this work were derived from patients with highly aggressive stage III and IV melanoma. So I would assume that CD20 is more of a bystander finding and only a relatively small group of melanoma patients would benefit from a targeted anti-CD20 therapy. A comprehensive study is needed to investigate the abundance of $CD20^+$ melanomas.

In order to better compare cancer stem cells and normal stem cells, I investigated the expression of several markers of human embryonic stem cells as defined by the International Stem Cell Initiative (Adewumi *et al.* 2007) in melanoma cells as well as in normal melanocytes. These markers are also expressed in the embryonic carcinoma cell line NCCIT (Damjanov *et al.* 1993, Greber *et al.* 2007b), which I used as positive control for stem cell markers and characteristics. A study of Greber *et al*. demonstrated that human embryonic stem (hES) and embryonic carcinoma (hEC) cells share a number of properties such as surface antigen expression, growth characteristics, control of self-renewal and maintenance of the undifferentiated state by the same core transcription factors and autocrine FGF signaling (Greber *et al.* 2007b). In my studies NCCIT cells showed expression of stem cell factors e.g. *SOX2*, *OCT4A* and *GDF3*; alkaline phosphatase activity; anchorage-independent growth as well as migration and invasion capabilities. Thus, the ethically unobjectionable NCCIT cells served as suitable positive control and were an elegant alternative for hESCs.

The challenge with these markers is that their expression is not restricted to cancer stem cells, but they are also expressed on the surface of normal cells in healthy tissue (i.e. adult and neonatal melanocytes). Laga *et al*. have identified rare SOX2-immunoreactive cells in normal fetal and adult human skin co-located with the established stem cell niches (i.e. the follicular papilla, the basal layer of the epidermis, and the bulge region of the hair follicle), as well as in neural crest-derived tumors. Rare SOX2-immunoreactive cells also co-stained with MITF, suggesting that some precursors of melanocytes may be SOX2-positive (Laga *et al.* 2010). Also, EDNRB, CD166 and NANOG are expressed in normal melanocytes (Degen

et al. 1998, Saldana-Caboverde *et al.* 2010). EDNRB has been implicated in the de-differentiation of mature melanocytes, a process that takes place during malignant transformation. But also interaction of EDNRB and KIT signaling are specifically required in the final differentiation step of melanocytes (Saldana-Caboverde *et al.* 2010). This prevalent expression of putative CSC markers in malignant as well as normal tissue queries their use as molecular targets in cancer treatment.

I also investigated the expression of genes related to tumorigenesis (*C-MYC*, *C-KIT*, *BMI-1*, *TNC*, *MSI-1*) and drug resistance (ABC transporters) in melanoma cell lines to see if a set of markers or maybe even a single marker alone can be used to identify melanoma CSCs. I found a prevalent and heterogeneous expression pattern among all cell lines as well as melanocytes and NCCIT. There was no obvious marker combination present in all cancer cell lines I investigated and no expression of markers was found to be mutually exclusive.

My findings were coherent with reports that put the usefulness of single putative CSC markers into question (Quintana *et al.* 2008). Most notably, the applicability of ABC transporters and CD133 was discussed (Patrawala *et al.* 2005, Wang *et al.* 2008). Patrawala *et al.* compared $ABCG2^+$ and $ABCG2^-$ colon, breast and prostate cancer cells with respect to their tumorigenicity *in vivo*, but no significant difference in tumor incidence or latency periods comparing the two populations was observed (Patrawala *et al.* 2005). The most commonly used and widely accepted marker to identify CSCs in melanoma as well as certain other tumor entities is CD133 (refer to 1.3.3.1). Nevertheless controversial findings regarding CD133 as CSC marker are described in the literature. In fact, tumor cells that do not express CD133 are also capable of self-renewal, colony formation, differentiation and invasion, as well as resistance to chemotherapeutic drugs, and they are tumorigenic. This was demonstrated for human colon and lung cancer as well as glioma (Wang *et al.* 2008, Meng *et al.* 2009, Shmelkov *et al.* 2008).

Most contradictory were results published on C6 glioma cells: Whereas Zhou *et al.* have demonstrated that this cell line contains only a small population of cells that can form tumor spheres in serum-free stem cell medium and express stem cell markers CD133 and NESTIN (Zhou *et al.* 2009), Zheng *et al.* concluded that the C6 line is mainly composed of CSCs, although many of them are $CD133^-$ (Zheng *et al.* 2007). Each of the tested single C6 cells was able to generate a clone and subclones in serum-containing medium, which subsequently gave rise to a xenograft glioma in nude mice. The latter group confirmed these results the following year showing that most C6 cells are cancer stem-like cells with characteristics of self-renewal, multi-lineage differentiation potentials *in vitro*, and tumorigenic capacity *in vivo* irrespective of their CD133 expression (Shen *et al.* 2008).

To correlate the expression of CD133 with the level of differentiation of a certain cell type, the group of Huttner raised an antibody that recognizes CD133 independently of eventual posttranslational modifications. They found that the expression of CD133 is independent from the cell's state of differentiation, while posttranslational glycosylation negatively correlates with differentiation (Florek *et al.* 2005). Only AC133, the glycosylated epitope of CD133, is downregulated upon cell differentiation. Therefore it seems likely that upon dedifferentiation of cells as observed in oncogenesis, the glycosylation of CD133 (AC133) might also increase and serve as a marker for the tumorigenic potential of a cell. Keeping this in mind, one has to be cautious when interpreting results from experiments where it is unclear if the antibody used was directed against CD133 or AC133 as many groups in the field seem to use the term CD133 synonymously to AC133. This inattentiveness could lead to confusions in interpreting the results.

Despite the fact that not all groups concurrently used the anti-AC133 antibody to isolate $CD133^+$ cells, the choice of antibody specificity would explain these contradictory findings only to some extent. But even research groups that investigated the same cell type with the same type of antibody drew opposing conclusions regarding the use of CD133/AC133 as CSC marker (Shen *et al.* 2008, Zhou *et al.* 2009). Taken together, CD133/AC133 can be an indicator for defining a population of cells that may contain CSCs in solid tumors but CD133/AC133 should be seen as a necessary however insufficient criterion to identify CSCs in solid tumors. Quintana *et al.* examined the expression of more than 50 surface markers on melanoma cells and injected these cells into NOD/SCID mice lacking the interleukin-2 gamma receptor. In all animals, tumors arose from all populations of cells. No known marker distinguished tumorigenic from non-tumorigenic cells (Quintana *et al.* 2008).

Concluding these findings, it seems as if tumor-initiating cells are phenotypically heterogeneous and no single marker or set of markers has been found so far to identify CSCs in any solid tumor entity. Furthermore, the results of the different approaches described above suggest that there is not a single method so far known that allows to specifically depicting all cells with tumor initiating capacity in melanoma.

Because the phenotypic correlation of CD133 with asymmetric cell division seems to be widely accepted (Dubreuil *et al.* 2007), and AC133 the glycosylated epitope of CD133, is shown to be downregulated upon cell differentiation (Florek *et al.* 2005), I used AC133 to separate putative CSCs from the bulk. To avoid confusion, melanoma cells sorted with anti-AC133 antibody were nevertheless named $CD133^+$ and $CD133^-$ cells.

In addition to its role as a putative CSC marker, CD133 was described as an important therapeutic target for metastatic melanoma and potentially for other CD133-expressing cancer types. In 2008, Rappa *et al.* investigated the effects of CD133 downregulation in human metastatic melanoma, which resulted in reduced cell growth, less cell motility, decreased capacity to form spheres under stem cell-like growth conditions and reduced capacity of the cells to metastasize *in vivo*. Monoclonal antibodies directed against two different epitopes of the CD133 protein induced a specific, dose-dependent cytotoxic effect (Rappa *et al.* 2008). In further experiments I investigated the applicability to enrich CSC by CD133. First hints that CD133 is useful to enrich CSCs were obtained by western blot analysis and gene expression profiling.

4.2 CD133$^+$ melanoma cells comprise stem cell characteristics

In western blot analyses I demonstrated that, if cultivated in normal tumor medium, the phosphorylated form of ERK is only detectable in CD133$^+$ melanoma cells (refer to **Figure 3.9**). This is an indication for an activated TGF-β signaling pathway in CD133$^+$ melanoma cells. In hESCs the TGF-β pathway is known to be crucial to maintain the undifferentiated state (refer to 1.4.2). The same was observed in melanoma cells cultivated in hESC medium. This medium contains soluble FGF2, which was shown to promote self-renewal in hESCs by modulating the expression of TGF ligands (Greber *et al.* 2007a) and activating ERK via its phosphorylation (Kang *et al*. 2005).

Whereas FGF2 signaling participates in regulating self-renewal and maintenance of an undifferentiated state in hESCs, studies suggest that aberrant expression of FGF2 and its receptors in cancer cells increases their transforming activity, providing a growth advantage and self-renewal stimulation to CSCs (Dvorak *et al.* 2006). These data indicate that CD133$^+$ melanoma cells indeed comprise stem cell characteristics and sorting of CD133$^+$ cells is a useful tool to enrich CSCs. Such a constitutively activated MAPK pathway by phosphorylation of ERK has already been reported for CD133$^+$ hepatocellular carcinoma CSCs (Ding *et al.* 2009) as well as CD133$^+$ glioblastomas cells (Dong *et al.* 2010). Moreover, the latter group suggested that CD133 is involved in activation of the MAPK/ERK pathway since overexpression of CD133 in U87MG glioblastoma cells significantly increased levels of phosphorylated ERK (Dong *et al.* 2010). Mirmohammadsadegh *et al*. showed that the MAPK pathway is also activated in melanomas and that an activated MAPK pathway reduces the sensitivity of melanomas to cisplatin, a commonly used chemotherapeutic for melanoma treatment. They concluded that inhibition of ERK1/2 by MEK inhibitors such as U0126 in combination with selected

chemotherapeutic agents might hold promise for more effective therapy of melanoma (Mirmohammadsadegh et al. 2007).

Nevertheless, U0126 mediated inhibition of MEK1 located upstream of ERK in the MAPK pathway and responsible for its phosphorylation, did not have differential effects in $CD133^+$ and $CD133^-$ melanoma cell lines even though phosphorylated ERK was expressed at much higher levels in $CD133^+$ ChaMel91 and ChaMel47 cells (compare **Figure 3.9**). Both fractions responded within a comparable IC_{50} range when investigating the effects of U0126 on the cells' viability and no significant difference on apoptosis induction was observed. This argues in favor of a constitutive activation of ERK independent of MEK1. If this activation is directly influenced by CD133 as shown for glioblastomas cells, needs to be further investigated.

The amplification of upstream oncogenic drivers of ERK signaling was identified as one mechanism for MEK inhibitor resistance in cells with mutant BRAF or KRAS. ChaMel47 as well as ChaMel91 are heterozygous for BRAF mutations V600R and V600E, respectively. Increased abundance of BRAF or KRAS in response to prolonged drug treatment results in increased flux through the ERK pathway and restoration of ERK activity above the threshold required for cell growth (Poulikakos *et al.* 2011).

To determine the underlying mechanisms of differences in the TGF-β signaling pathway and to identify further distinct characteristics of $CD133^+$ and $CD133^-$ melanoma cells I analyzed genome-wide expression profiles of these populations. I found that genes involved in angiogenesis, inhibition of apoptosis, cell lineage determination, adhesion, cellular migration and invasion were most upregulated in the $CD133^+$ CSC fraction. In regards to the "hallmarks of cancer" proposed by Hannahan and Weinberg in 2001 and revised in 2011 these properties represent the foundation of tumorigenesis (Hanahan *et al.* 2000, Hanahan *et al.* 2011). This indicates that sorting for the surface marker CD133 can enrich melanoma CSCs. On the other hand, genome-wide expression profiling as well as validation by real-time PCR revealed that commonly used putative CSC markers described in literature are not differentially expressed between $CD133^+$ and $CD133^-$ melanoma cells (see 3.2.1). This is consistent with findings of Gedye *et al*. who also found that known CSC markers reported to be expressed in melanoma such as ABCB5, ABCG2, CD166, CD20 and NESTIN were not consistently differentially expressed in their CD133 sorted melanoma populations (Gedye *et al.* 2009). Consequently, these surrogate markers were unsuitable to identify CSCs in melanoma samples I worked with.

4.2.1 Rare differential SNPs between CD133+ and CD133- cells on transcript level

Between CD133+ and CD133- melanoma fractions I found only few differential single nucleotide polymorphisms (SNPs). SNPs, found in coding regions of genes, were mostly synonymous nucleotide exchanges. Only one non-synonymous mutation located in the coding region of the CoA synthase gene was SIFT (Sorting Intolerant From Tolerant) predicted to be damaging for the protein function (compare 3.2.3). CoA Synthase (COASY) is a mitochondria-associated enzyme, which facilitates the last two catalytic steps of *de novo* Coenzyme A (CoA) biosynthesis in mammalian cells. CoA and its derivatives play a key role in cell metabolism and also participate in regulatory processes. (Breus *et al.* 2009). Despite its role in metabolism, CoA synthase cannot account for differences between CD133+ and CD133- melanoma cells related to stemness since no correlation of this enzyme to developmental pathways or stem cell markers has been found. Furthermore, the detected SNP in the CoA synthase gene needs to be validated by single gene sequencing.

Most of the found SNPs were non-genic or located within the 5'UTR or 3'UTR of a gene. I investigated all cytosine and guanine-related SNPs of potentially regulatory regions like introns and 5'UTRs for their potential location in CpG islands. CpG islands are stretches within the genome with a high CG content (Gardiner-Garden *et al.* 1987) and frequent absence of DNA methylation. Methylation of CpG sites within the promoter of a gene could inhibit the expression of a gene. Therefore CpG islands are generically equipped to influence local chromatin structure and regulation of gene activity (Deaton *et al.* 2011). None of the non-genic SNPs found to be different between CD133+ and CD133- melanoma fractions was located in CpG islands. Thus, a potential influence of these non-genic SNPs by causing hypo- or hypermethylated DNA sequences is unlikely. Taken together, these results indicate that mutations on the transcriptome level are not responsible for the different expression pattern between CD133+ CSCs and CD133- non-CSCs in melanoma.

4.2.2 Epigenetic regulation of CD133

The tremendous varieties among gene expression patterns between CD133+ CSCs and CD133- non-CSCs in melanoma could not be credited to differences in coding mutations at the transcriptome level (refer to section 3.2.3). This argues in favor of epigenetic regulation and maintenance of the phenotype or alternative splicing. Epigenetic regulation of gene transcription by DNA methylation can be investigated using DNA methyltransferase inhibitors like 5-aza-2'-deoxycytidine. 5-aza-2'-deoxycytidine causes DNA demethylation or hypomethylation, which "opens" the chromatin structure and

allows transcription factors to bind to the promoter regions, assembly of the transcription complex, and gene expression.

Friel *et al*. showed that treatment of endometrial cancer cell lines for 72 h with 5 µM 5-aza-2'-deoxycytidine increases relative levels of CD133 suggesting a role for methylation in the regulation of CD133. To support this finding, they demonstrated that regions of the CD133 promoter were hypomethylated in malignant endometrial tissue relative to benign control tissue and that methylation of the CD133 promoter decreases over serial transplantation of endometrial tumor xenografts resulting in an increase of $CD133^+$ cells (Friel *et al.* 2010). The correlation of CD133 expression with promoter methylation was also observed in ovarian cancer cells via treatment with DNA methyltransferase inhibitors (Baba *et al.* 2009). Moreover, recent data from hepatocellular carcinoma cell lines link the TGF-β signaling pathway to CD133, since they show that TGF-β1 is able to regulate CD133 expression through inhibition of the DNA methyltransferases DNMT1 and DNMT3b expression and subsequent promoter demethylation (You *et al.* 2010). The importance of the TGF-β pathway for maintaining self-renewal and pluripotency in undifferentiated cells is defined more in detail in section 1.4.2.

Western blot analysis showed that already treatment with 0.1 µM 5-aza-2'-deoxycytidine reduced the DNMT1 expression to a level below the detection threshold in the melanoma cell lines I investigated. DNMT1 is the most abundant DNA methyltransferase in mammalian cells, and is considered to be the key maintenance methyltransferase in mammals. On the other hand, higher concentration of this agent remarkably reduced cell viability as determined by alamarBlue assays. This is why concentrations of 5 µM mostly used in experiments described in literature were not used in my experiments. Treating the melanoma cell line ChaMel91 with 0.1 µM 5-aza-2'-deoxycytidine did not result in an increase of CD133 expression. Rather, the CD133 expression was comparable to untreated cells during the first two days of the experiment. This was expected due to 5-aza-2'-deoxycytidine's mode of action as a cytidine analog. DNMT1 degrading effects of 5-aza-2'-deoxycytidine are dependent upon the incorporation of the inhibitor into DNA during DNA synthesis (Patel *et al.* 2010). 5-aza-2'-deoxycytidine incorporates into the progeny DNA strands only following DNA replication and results in depletion of the DNA methyltransferase. The unavailability of functional DNMTs prevents methylation of the newly replicated strand leading to DNA demethylation of genes and consecutive reexpression of corresponding proteins (Ghoshal *et al.* 2005). With the tested melanoma cells doubling time of 32 h no effects of 5-aza-2'-deoxycytidine on CD133 could have been observed before day three of the experiment. Three days after initial treatment these very

low concentrations of the DNA methyltransferase inhibitor resulted in a remarkably decreased CD133 expression, which further decreased during the next days of the experiment. This effect could not be linked to the demethylating property of 5-aza-2'-deoxycytidine since also the DNA crosslinker mitomycin reduced CD133 expression in ChaMel91 (compare **Figure 3.11**). Rather, these results suggested a potential correlation of CD133 expression with cell proliferation since the decline in CD133 expression was accompanied by a slow cell proliferation followed by a low cell density after seven days. In summary, I could not prove that in melanoma CD133 is influenced by DNA methylation and other regulating mechanism must therefore be investigated. One possibility could be the dynamic control of CD133 by chromatin condensation. Pellacani *et al*. showed that in benign and malignant prostate primary tissues, regulation of CD133 is independent of DNA methylation, but is under the dynamic control of chromatin condensation. Condensed chromatin was also associated with CD133 downregulation in prostate cell lines, and treatment with histone deacetylase inhibitors resulted in CD133 re-expression in both cell lines and primary samples (Pellacani *et al.* 2011).

4.3 Functional comparison of CD133$^+$ and CD133$^-$ cells

For the maintenance of a stem cell-like phenotype many factors, such as angiogenesis, invasion and migration, hypoxia, immune evasion, multiple drug resistance, and radioresistance are needed (Oishi *et al.* 2011). During my work I investigated some of these functional characteristics to directly link the expression of the cell surface marker CD133 to attributes known from stem cells and/or to cancer characteristics. I showed that ChaMel91 melanoma cells are able to grow anchorage-independently and have migrative as well as invasive capabilities. Using various functional *in vitro* assays no differences between CD133$^+$ and CD133$^-$ cells have been observed (see 3.2.5). Furthermore, I analyzed and compared alkaline phosphatase (AP) activity of melanoma with NCCIT cells. Alkaline phosphatase-positive staining is a sensitive, specific and quantitative indicator of undifferentiated human embryonic stem cells (O'Connor *et al.* 2008). But in contrast to NCCIT almost no AP activity was observed in ChaMel91 cells. Only a small number of melanoma cells stained positive for AP, which was very weak in contrast to NCCIT cells (compare **Figure 3.14**). This is concordant with published data where AP activity plays only a minor role in adult stem cells.

On the other hand, results by Prasmickaite *et al*. illustrated that not all fundamental properties of stem cells are also found in CSCs of all tumor entities: High ALDH1 activity is characteristic of normal stem cells of most human tissues investigated. Numerous cellular processes such as differentiation, proliferation, morphoregulation, and development, are

directly and/or indirectly regulated by the enzymatic activity of ALDH1 family members (Gires 2011). Recently, it appeared that ALDH may be able to fulfill the role as a marker for both normal and cancer stem cells since over-expression of ALDH1 was found in CSCs of breast, lung, head and neck, pancreas, cervix, prostate, liver, colon, and bladder cancer and is now widely used as a marker to identify and isolate various types of normal stem cells and CSCs (Ma *et al.* 2011,Gires 2011). But Prasmickaite *et al*. showed that although aggressive melanomas harbour a large, distinguishable $ALDH^+$ subpopulation, this marker does not define CSCs with tumor-initiating capabilities *in vivo*. These findings argue against ALDH as a ‘‘universal’’ marker (Prasmickaite *et al.* 2010). This example illustrates the ambiguity and ongoing debate of CSC research well. On the one hand, many markers that link to stem cells and their properties are found in rare tumor cells. On the other hand, not all the traits found in normal stem cells seem to play a role for the maintenance of a cancer stem cell population.

4.3.1 BRAF mutations and targeted therapy for malignant melanoma

The discovery of BRAF-activating mutations in 50-70% of human melanomas provides an attractive target for the therapy of malignant melanoma. Vemurafenib (PLX-4032) the currently most promising drug that specifically targets BRAF V600E mutant cells is well tolerated and induces high response rates and improved survival in patients with the BRAF V600E mutation (refer to section 1.2.4). 75% of the melanoma cell lines used in my work were BRAF mutated and as expected from literature the glutamic acid for valine substitution at position 600 (V600E) was also the most common BRAF mutation in these melanoma cell lines. Using *in vitro* cytotoxicity assays I analyzed the effects of two RAF kinase inhibitors on the heterozygous BRAF V600E mutant melanoma cell line ChaMel91, the heterozygous BRAF V600R mutant melanoma cell line ChaMel47 and the homozygous BRAF V600E mutant melanoma cell line Pat1T1k. Whereas treatment with sorafenib resulted in identical IC_{50} values in all three cell lines (9.7-9.9 µM), I observed different effects with PLX-4032. Most sensitive were Pat1T1k cells with an IC_{50} < 0.4 µM, followed by ChaMel91 with an IC_{50} of about 1 µM. Both of these cell lines carry the V600E mutation and lay within the sensitivity range for BRAF V600E mutants specified by the manufacturer. On the other hand, BRAF V600R mutant ChaMel47 cells showed a much higher resistance towards PLX-4032 with an IC_{50} > 4 µM. This is accordant with the high IC_{50} > 2.4 µM for BRAF wild type tumor cells indicated by the manufacturer. I conclude from these results that PLX-4032 is indeed very specific not only for BRAF mutant cells but specifically for the V600E mutation. In contrast to PLX-4032, the broad-spectrum

kinase inhibitor sorafenib, which acts more specific against CRAF than BRAF (Vultur *et al.* 2010) did not show an increased anti-tumorigenic effect on BRAF V600E mutant melanoma cells compared to others. Previous clinical trials also provided data that patients did not benefit when using sorafenib as a second-line treatment in combination with systemic chemotherapy (Hauschild *et al.* 2009). Therefore, selective targeting of BRAF mutant melanoma cells using vemurafenib seemed to be the only promising breakthrough in melanoma therapy. Unfortunately, recent findings query the use of vemurafenib for melanoma treatment. On the one hand, Lin *et al*. found that most primary melanomas harbor both BRAF wild type and BRAF mutant tumor cells and conclude that BRAF mutation is not a founder event, but may be one of the multiple clonal events in melanoma development (Lin *et al.* 2011). Further on, Halaban *et al*. showed that paradoxically, while PLX-4032 inhibits ERK1/2 in highly sensitive BRAF mutant cells it activates the pathway in the resistant BRAF wild type cells, via RAF1 activation, triggering downstream effectors and thus, ultimately increasing proliferation and mobility, while reducing cell adherence of BRAF wild type cells (Halaban *et al.* 2010, Joseph *et al.* 2010). These results illustrate the importance of selecting only patients with ideally homozygous mutant BRAF for vemurafenib treatment as well as frequently monitoring BRAF mutation status in any secondary or recurrent lesions of the patients to minimize potentially pro-tumorigenic effects of vemurafenib in BRAF wild type melanomas (Lee *et al.* 2010).

On the other hand, BRAF mutant tumor cells develop drug resistance frequently after initial responsiveness (Nazarian *et al.* 2010) (compare 1.2.4). Tumors with mutant BRAF and some with mutant RAS are dependent upon ERK signaling for proliferation, while their growth is suppressed by MAPK/ERK kinase (MEK) inhibitors (Joseph *et al.* 2010). For patients with BRAF mutant tumors, the results suggest that a combined BRAF/MEK inhibition may delay or overcome drug resistance (Paraiso *et al.* 2010, Poulikakos *et al.* 2011). Emery *et al*. showed that exposing BRAF-mutant melanoma cells to the allosteric MEK inhibitor AZD6244 and the BRAF inhibitor PLX-4720 in combination prevented emergence of resistant clones. These results confirm the importance of MEK dependency in BRAF-mutant melanomas and suggest novel mechanisms of resistance to MEK and BRAF inhibitors that may have important clinical implications (Emery *et al.* 2009). Further resistance mechanisms described include flexible switching among the three RAF isoforms, upregulation of the receptor tyrosine kinase, IGF-1R/PI3K signaling (Villanueva *et al.* 2010), and enrichment of a subpopulation of melanoma cells expressing a histone demethylase, JARID1B (Roesch *et al.* 2010). Taken together, it seems that melanoma cells are extremely plastic and can readily adapt to extreme selective pressures (Lee *et al.* 2010).

4.3.2 Drug resistance

As with PLX-4032, I did not detect significant differences in drug resistance between $CD133^+$ and $CD133^-$ melanoma cells following treatment with any of the tested kinase inhibitors. Moreover, apart from staurosporin no inhibitor specifically blocked proliferation or induced apoptosis in melanoma cells at nanomolar concentrations, which could be used *in vivo*. Only immense high concentrations at whose any kinase inhibitor induces toxic off-target effects were effective. For some inhibitors like PLX-4032 this was expected because they are specific for distinct mutations, which are not present in all melanoma cells. Furthermore, functional analysis of both subpopulations did not detect significant discrepancies in anchorage-independent growth capacity, alkaline phosphatase activity or migration and invasion potential. Possible reasons for these observations were discussed in previous parts of this work. But also the plasticity of cancer cells and interconversion between different cell states would explain that I could not observe any functional differences between $CD133^+$ and $CD133^-$ melanoma cells.

The first allusion to the existence of such plastic melanoma cells was provided by the influence of the kinase inhibitors sorafenib, SU5402 and GDC-0941 on the expression of CD133 in ChaMel91 cells. Within 48 h CD133 expression has been significantly altered in these melanoma cells, most notably in the $CD133^+$ fraction and following treatment with inhibitors that affect only a minor fraction of the melanoma population (SU5402 and GDC-0941).

4.4 Dynamic cell state transitions in tumors challenge cancer therapy concepts

Recently, Gupta *et al.* proposed a dynamic equilibrium between CSCs and non-CSCs within breast cancer. This equilibrium may be shifted in one direction or another by contextual signals within the tumor microenvironment that influence the probability of interconversion between the CSC and non-CSC compartments (Gupta *et al.* 2009). This could account for the varying amounts of putative cancer stem cells within the same tumor entity described by different groups.

Platet *et al*. and Lichtenauer *et al*. gave evidence for a conversion of CSC into non-CSCs and vice versa. Both groups found that non-SP cells in flow cytometric analyses after Hoechst staining are able to generate SP cells (Lichtenauer *et al.* 2008, Platet *et al.* 2007). In consequence, this finding would allow non-CSCs to convert into CSCs and explains the maintenance of the SP phenotype in long-term cell cultures. This dynamic equilibrium seems not to be a feature exclusively found in cancers. Switching cell fate was also

described for partially reprogrammed cells in the group of Rudolf Jaenisch where cells positive for SSEA1 as well as cells negative for this stem cell marker reverted to the heterogeneous state within 1-2 passages in cell culture (Mikkelsen *et al.* 2008). Recently, Gupta *et al*. showed that purified stem-like, basal and luminal subpopulations of breast cancer cells return towards equilibrium phenotypic proportions over time. These observations could be explained by a Markov model, a stochastic model, in which cells transition randomly between states with each proliferative cycle and transition probabilities depend only on a cell's current state, not on its prior states. The rapid rate of return to equilibrium proportions excluded the possibility of establishing equilibrium through differential growth alone (Gupta *et al.* 2011). Subsequently, this proposed Markov model predicted that breast cancer stem-like cells could arise *de novo* from non-stem-like cells. Gupta *et al.* validated this prediction *in vivo* with xenotransplantation experiments in mice. Also Chaffer *et al*. demonstrated that a subpopulation of basal-like human mammary epithelial cells spontaneously dedifferentiates into stem-like cells and that oncogenic transformation enhances this conversion of non-CSCs into CSCs *in vitro* and *in vivo* (Chaffer *et al.* 2011). These findings led these groups to the conclusion that the existing hierarchical model of cancer cell populations must be replaced by a stochastic model in which CSCs and non-CSCs can interconvert bidirectionally (Chaffer *et al.* 2011, Gupta *et al.* 2011).

In my experiments I investigated the cell state transition properties of $CD133^+$, $CD133^-$ and unsorted melanoma cells over a period of 38 days. Like Gupta *et al*. in breast cancer cells I found an interconversion of melanoma cells towards equilibrium proportions of $CD133^+$ and $CD133^-$ cells. But in contrast to Gupta's results even 38 days of cultivation were not enough for melanoma cells to return to their original CD133 equilibrium. Rather, CD133 expression in melanoma cells showed a consistent, non-trivial variation around a certain level. The length of one half-period from CD133 expression minimum to CD133 expression maximum differed between the three subpopulations and also within each subpopulation and ranged from three to eleven days. Gupta *et al*. observed conversions of sorted breast cancer cell populations only for six days and concluded that the cells reached a determined cell state equilibrium. Observing cells for a longer period of time revealed that cell states do not return to the equilibrium, at least not over such a short, defined period. It rather seems that cancer cells oscillate around a dynamic and not fixed equilibrium. Even in unsorted melanoma cells average CD133 expression varied by about 33%.

Like Chaffer *et al*. and Gupta *et al*. our observations in melanoma cell lines *in vitro* clearly show that also cells in CD133-depleted fractions give rise to CSCs expressing the CD133

marker. My observations indicate that this phenomenon is not caused by a lack in purity of the respective population by false positive or negative cells: There are only two possible explanations for the reappearance/reconstitution of the original amount of $CD133^+$ cells in the culture after only seven days. Either the small number of contaminating $CD133^+$ cells rapidly divided and expanded or $CD133^-$ cells switched their phenotype to $CD133^+$. The former would imply that the contaminating $CD133^+$ cells have to cycle far faster than $CD133^-$ cells to catch up. The cells would have needed to double about two times as fast as the $CD133^-$ cells. However, we measured no significant differences in doubling time between $CD133^+$ and $CD133^-$ cells, which would explain the reappearance the $CD133^+$ population in the short time span of the experiment. Also there are no indications that $CD133^+$ cells would be able to speed up their cell cycle in this way. Furthermore, the increase in $CD133^+$ cells is a self-limiting process that occurs in a wave-like pattern. If the increase in $CD133^+$ would be simply the result of one population overgrowing the other, an exponential increase in $CD133^+$ would be expected. Taken together, these observations strongly point to a mechanism independent from doubling time and the most likely mechanism to explain these findings is that $CD133^-$ cells can give rise to a population of $CD133^+$ cells. This conclusion is also supported by the cell cycle analysis, where we did not detect a correlation between the phases of the cell cycle and CD133 expression. This observation is adverse to the findings from Jaksch *et al*. where least CD133 reactive embryonic stem, colon cancer and melanoma cells were in the G1-G0 portion of the cell cycle. So they associated CD133 with actively cycling cells (Jaksch *et al.* 2008). In the melanoma cell lines of this work I could not confirm this correlation. So, the question for the underlying regulatory mechanisms, which drive the dynamic equilibrium between cell states, remains unsolved. Are the non-CSCs alone really able to de-differentiate into CSCs or do they obtain the priming signals to reconstitute the balance within the tumor microenvironment from the small part of CSCs or the tumor niche?

For explaining the dynamics between CSCs and non-CSCs the Markov model postulated by Gupta *et al*. assumes that interconversion rates depend only on a cell's current state and remain constant under fixed microenvironmental conditions. Furthermore, they suppose deviations from equilibrium proportions will be corrected even in the absence of any intercellular communication (Gupta *et al.* 2011). Modified iterations of the 38 days long-term experiment with ChaMel91 cells in my work supported the interpretation that cell state transitions likely depend on the tumor microenvironment as well as intercellular communication. Daily medium change during the long-term experiment or reduction of cell density prolonged the frequency remarkably but did not lead to an increase of the amplitude of the CD133 dynamic. Hence, I found no discrepancy when comparing this

finding with the results of the 5-aza-2'-deoxycytidine experiment (compare 3.2.4 and 4.2.2). Furthermore, results from anchorage-independent growth assays with ChaMel91 melanoma cells suggested how important tumor microenvironment and cell-cell-communication are for tumor cell growth *in vitro*. A minimum number of 10^4 tumor cells was required to form colonies in soft agar at all. Using fewer cells did not result in fewer colonies but prevented colony growth entirely, suggesting that a given threshold had to be exceeded. Therefore, explaining cell state transition by a stochastic process like the Markov model is not suitable in my opinion because it does not consider influences by a changing/variable microenvironment. Various speculations regarding the underlying regulatory mechanisms were made in the past e.g. the putative role of microRNAs in facilitating the equilibrium of CSCs and non-CSCs like they promote iPS cell formation by their regulatory effects on epigenetic and transcriptional modulation (Chen *et al.* 2009). This is also consistent with the plasticity of cancer because epigenetic modulations can efficiently be activated and reverted in short intervals. On the other hand, Iliopoulos *et al*. demonstrated that breast and prostate CSCs and non-CSCs do not represent distinct epigenetic states, and these CSCs do not behave as or arise from classic stem cells. Instead, tumor heterogeneity involves a dynamic equilibrium between CSCs and non-CSCs mediated by IL6 and activation of the inflammatory feedback loop required for oncogenesis (Iliopoulos *et al.* 2011). Summarizing these findings, I suppose that absent differences between $CD133^+$ and $CD133^-$ melanoma cells in functional assays like anchorage-independent growth assay and migration and invasion assays may also be explained by dynamic state transitions between $CD133^+$ and $CD133^-$ cells. Unfavorable microenvironment in softagar as well as serum-free medium in migration and invasion assays could have promoted the transition to more robust, mobile and tumorigenic melanoma cells, which would have prevented the observation of endogenous functional disparities.

Understanding how cell states coexist and evolve within tumors is of fundamental interest for the development of more effective cancer therapies. The study from Gupta *et al*. indicated that treatment of cancer patients could result in selective changes in phenotypic proportions within tumors since some cell states may be more resistant to the cancer therapy than others. Selectively targeting CSCs during anticancer therapies would result in *de novo* generation of CSCs from non-CSCs, which subsequently would lead to re-growth of the tumor after completion of therapy. Therefore, in order to be effective, cancer therapies will need to combine agents that are selectively toxic to CSCs with agents that either target the bulk non-CSC populations within tumors or inhibit transitions from non-CSC to CSC states (Gupta *et al.* 2011).

4.5 Expression of the pluripotency factor OCT4A in rare melanoma cells

In the final stages of my work, I focused on major stem cell properties such as self-renewal and pluripotency to identify additional common characteristics between normal stem cells and cancer stem cells that would allow a specific identification of CSCs in the future. Several studies show that OCT4A is the master regulator of the pluripotent state in mammalian cells (Buitrago *et al.* 2007, Nichols *et al.* 1998), therefore I investigated a putative OCT4A expression in melanoma cells.

4.5.1 Data misconception

In the past, various authors illustrated the risk of data misinterpretation when analyzing OCT4 expression on transcriptome as well as protein level. The presence of several pseudogenes and alternatively spliced transcripts, which show high homology to the *OCT4A* sequence, can be a potential source of false positive results and might be misinterpreted in RT-PCR experiments addressing *OCT4* expression (Atlasi *et al.* 2008).

Many studies have used nonspecific primers that detect transcripts from the *OCT4* gene as well as from pseudogenes or splice variants. This could be a major reason for measuring expression of *OCT4* in a broad extent of cells and tissues. In addition, the presence of intronless pseudogenes, which are not transcribed can result in false positive artifacts, if DNA contamination is present in RNA preparations (de Jong *et al.* 2006). Furthermore, de Jong *et al*. indicated that probe sets used in microarray expression profiling such as the Affymetrix chips are not specific for the *OCT4A* transcript, but also detect at least some of the pseudogenes (de Jong *et al.* 2006).

The design of primers for PCR that specifically anneal to polymorphic regions of the sequence, which are unique for the *OCT4A* transcript, followed by cloning and sequencing, is mandatory. *OCT4A* polymorphisms are located at position 48, 234 and 353 within exon 1 starting at the transcriptional start codon *AUG* and can discriminate between *OCT4A* and its pseudogenes. Furthermore, this region of the sequence is not present in the predominant alternative splice variant *OCT4B* (Liedtke *et al.* 2008). In my studies I exclusively used primer pairs that anneal to the 5'coding region of exon 1, so amplification of *OCT4B*, which does not sustain stem cell properties is avoided. Furthermore, used primer pairs flank *OCT4A* polymorphisms within the first exon. Thus, subsequent Sanger-sequencing and restriction digest confirmed expression of *OCT4A* in melanoma cells as well as melanocytes beyond doubt.

The published reports for OCT4 expression in differentiated cells are ambiguous not only on the transcriptome level, but also on the protein level. Many of the antibodies used in these studies are not specific for OCT4A because they bind to the C-terminal part of the proteins which is identical in all known splice variants of *OCT4* or they are polyclonal which increases the likeliness of background fluorescence by unspecific binding (Liedtke *et al.* 2008). In FACS analyses results from such unspecific antibodies can never be interpreted correctly. In western blot experiments the resulting signals can and should be discriminated by protein size. OCT4B has a lower molecular weight than OCT4A. Nevertheless, Liedtke *et al*. recommend using a blocking peptide to confirm the identity of a western blot signal, because the size of a protein itself might not be accurate enough to ensure its identity, taking into account that even the buffer system used for western blot experiments influences the resulting band size of the analyzed protein (Liedtke *et al.* 2008). In immunohistochemical analysis only a precisely localized nuclear signal can be regarded as derived from OCT4A protein expression and responsible for stem cell properties. All cytoplasmic staining is solely caused by splice variant OCT4B or nonspecific artifacts (de Jong *et al.* 2006, Liedtke *et al.* 2008). Summarizing these facts, a careful analysis of the pluripotency factor OCT4A is strongly advised.

To confirm that OCT4-EGFP$^+$ melanoma cells express nuclear OCT4A, I performed immunocytological staining with an anti-OCT4A-specific antibody. Results showed a strong nuclear staining pattern for OCT4A in OCT4-EGFP$^+$ melanoma cells whereas OCT4-EGFP$^-$ melanoma cells were only weakly and unspecificly stained all over the cell body. If this diffuse staining was due to expression of OCT4B or nonspecific artifacts was not further determined. The results of this experiment clearly show that EGFP expression in stably transfected ChaMel91 cells correlates with nucleic expression of constitutively expressed OCT4A. Furthermore, immunocytological staining showed that on protein level OCT4A is not expressed in neonatal melanocytes. This was the first time OCT4A expression has been shown on transcript as well as protein level in melanoma cells whereas authors that previously described OCT4 expression in melanoma did not specifically analyze OCT4A (Cheli *et al.* 2011, Ramgolam *et al.* 2011).

4.5.2 OCT4-EGFP$^+$ melanoma cells overrepresent stem cell related pathways

From annotation analysis we learned that crucial regulatory pathways related to stemness such as Wnt, Hedgehog (Hh) and Notch signaling are significantly more activated in the OCT4-EGFP$^+$ population compared to OCT4-EGFP$^-$ melanoma cells, thus suggesting that the expression of OCT4A plays a crucial role in maintaining cancer stem-like properties in

melanoma-derived cells. In embryonic stem cells processes that govern development, self-renewal and cell fate are in large part regulated by the Wnt, Notch and Hedgehog pathways (Curtin *et al.* 2010). These pathways are also found to be frequently aberrant in many types of cancers and will therefore be discussed in more detail in this section.

Under normal conditions, HH signaling plays an important role in the embryonic development as well as adult tissue regeneration of many cell types and organs including the brain, bone, skin, gonads and lungs. A surprising number of apparently unrelated human diseases, including familial and sporadic cancers and a number of syndromes and malformations, seem to be associated with abnormal function of the HH signaling pathway (Ruiz i Altaba 1999,Varjosalo *et al.* 2008). Notch signaling also regulates numerous processes in both embryonic development and in adult tissue renewal. In the adult organism, Notch governs the fate of hematopoietic stem cells and gastrointestinal stem cells, as well is playing a role in angiogenesis. Like HH signaling aberrant Notch signaling has been observed in several tumor types (Curtin *et al.* 2010). Mounting experimental data support a role for Notch in regulating cell differentiation and growth arrest at the boundary between the basal layer cluster of progenitor cells and the adjacent cells. Whether Notch dys-regulation has a role in the pathogenesis of certain types of human skin cancer remains speculative (Allenspach *et al.* 2002). Weijzen *et al*. showed for the first time a correlation of oncogenic Ras signaling and Notch signaling in human fibroblast and epithelial transformed cell lines. They demonstrated that wild type NOTCH-1 is necessary to maintain the neoplastic phenotype in RAS-transformed human cells *in vitro* and *in vivo*. Oncogenic RAS increases levels and activity of the intracellular form of wild type NOTCH-1, and upregulates NOTCH-associated proteins. These observations place Notch signaling among key downstream effectors of oncogenic RAS and suggest that it might be a novel therapeutic target (Weijzen *et al.* 2002).

Wild type Wnt signaling is crucial for tissue homeostasis, self-renewal, cell polarization, differentiation and proliferation in a variety of adult tissues as well as embryonic development and hematopoiesis (Espada *et al.* 2009, Gat *et al.* 1998). Haegebarth *et al*. showed that stem cells in the small intestine and the skin are regulated by Wnt signaling. Wnt ligands activate the canonical Wnt signaling pathway resulting in subsequent stabilization of β-catenin. β-catenin translocates to the nucleus, where it binds to TCF transcription factors, thus activating Wnt target genes (Haegebarth *et al.* 2009).

Additionally, WNT has been implicated as being one of the drivers of oncogenesis in various organs (Korinek *et al.* 1998, Larue *et al.* 2006, Taipale *et al.* 2001). The relevance of Wnt signaling in human cancers is highlighted by the frequency with which this

pathway is aberrantly activated across a vast range of malignancies. The first described, and perhaps best understood role for Wnt/β-catenin signaling is in colon cancer, where β-catenin mutations are commonly observed. Furthermore, the Wnt pathway regulates epithelial-mesenchymal transition (EMT), an important component of metastasis (Curtin *et al.* 2010).

Interestingly, growing evidence illustrates a critical role of β-catenin in CSCs. For example, stem-like colon cells with a high activation of Wnt/β-catenin signaling have a much greater tumorigenic potential than counterpart cells with low Wnt/β-catenin signaling. Wnt stimulation may occur in an autocrine fashion due to Wnt secretion by CSCs, and may be potentiated by secreted factors from cells within the CSC microenvironment (Curtin *et al.* 2010). Malanchi *et al*. described Wnt/β-catenin signaling as being essential in sustaining the CSC phenotype in early epidermal tumors. Ablation of the β-catenin gene resulted in the loss of CSCs and complete tumor regression (Malanchi et al. 2008). Microarray analysis of human metastatic melanoma cells with downregulated CD133 expression by Rappa *et al*. revealed that Wnt inhibitors are upregulated in this non-CSC fraction suggesting an interaction between CD133 and the canonical Wnt pathway in melanoma and supporting the role of CD133 as a CSC marker (Rappa *et al.* 2008). The link between CD133 and the Wnt pathway was further supported by the findings of Katoh *et al*. who identified tandem T-cell factor/ lymphoid enhancer factor (TCF/LEF) binding sites in the CD133 gene suggesting it as a target of canonical Wnt signal activation (Katoh *et al.* 2007). Also, a link of the Notch pathway with CD133 was found recently. Fan *et al*. showed that inhibition of Notch reduced $CD133^+$ cells significantly, abolished the side population and blocked engraftment in embryonal brain tumors (Fan *et al.* 2006).

Recent results of various groups and of different tumor entities (retinoblastoma, lung cancer, brain astrocytoma, neck squamous cell carcinoma and breast cancer) demonstrated an overexpression and activation of Wnt, Notch and Hedgehog pathways in putative CSCs of the Hoechst side population indicating that these cascades control tumor formation, self-renewal and metastasis by regulating the CSC population (Balbuena *et al.* 2011, Kruger *et al.* 2006, Salcido *et al.* 2010, Silva *et al.* 2010, Song *et al.* 2010, Tian *et al.* 2011). Inhibiting these pathways resulted in reduced SPs and reduced tumor growth. Fodde *et al*. postulated that both intrinsic (tumor cell-autonomous) and extrinsic (secreted by the tumor microenvironment) factors are likely to influence cancer stemness, epithelial-mesenchymal transition, local invasion and metastasis by differentially modulating Wnt and other signaling pathways such as Notch, TGF-β and Hedgehog since

they found an upregulation of Wnt signaling in tumor cells at the invasive front and in those migrating into the adjacent stromal tissues (Fodde *et al.* 2007).

These findings and the similarities between normal adult stem cells and CSCs, suggest that the Wnt, Hedgehog, and Notch signaling pathways involved in regulating somatic stem cell maintenance are also involved in the regulation of CSCs (Merchant *et al.* 2010, Pannuti *et al.* 2010, Takahashi-Yanaga *et al.* 2010). The results of my work provide further evidences that Wnt, Notch and Hedgehog pathways might maintain stem cell characteristics of melanoma CSCs. Thus targeting Wnt, Notch, and Hedgehog pathways in CSCs especially in combination with classic chemotherapeutic agents is a plausible therapeutic strategy (Takebe *et al.* 2011). A cytotoxic agent such as cisplatin may target the bulk of a tumor but not the putative chemoresistant CSCs. However, if the CSCs were targeted in parallel with a Wnt, Notch, and/or Hedgehog pathway inhibitor, a better curative response might be achieved (Curtin *et al.* 2010). Recent results of *in vitro* and *in vivo* models already showed that pharmacological blockade of Hedgehog signaling most notably following chemotherapy inhibited the growth of SCLC and CML (Mar *et al.* 2011, Park *et al.* 2011). On the other hand, shared key signaling molecules by both CSCs and normal stem cells, add further challenges for designing molecularly targeted strategies specific to CSCs but sparing normal stem cells to avoid side effects (Oishi *et al.* 2011).

4.6 Tumorigenic abilities of CSCs in *in vivo* experiments

The first immunodeficient mouse model of cancer to be developed was based on athymic nude mice, which support the growth of solid human tumors since they lack functioning T cells. This prevents nude mice from rejecting not only allografts, but they cannot even reject most xenografts, that is, transplants of tissue or cells from another species. In the following, severe combined immunodeficiency (SCID) mice, which have severely reduced numbers of mature T and B cell lymphocytes were shown to support disseminated tumor growth for a number of human tumors, particularly hematologic disorders and malignant melanoma, and were used preferentially for the investigation of such malignancies. But tumor growth was limited by high levels of host natural killer (NK) cell activity (Becker *et al.* 2009, Mueller *et al.* 1991). Thus, NOD-SCID mice were developed and are nowadays used in most laboratories. In these mice the SCID mutation has been transferred onto non-obese diabetic (NOD) mice with absent hemolytic complement system, reduced dendritic cell function, and defective macrophage activity. Furthermore, it was observed that NK-cell activity is reduced in NOD-SCID mice what allowed even the growth of melanoma cell lines that grew poorly or not at all in SCID mice (Shultz *et al.* 2007). Until two years ago, it seemed that only few cells isolated from a tumor have the ability to initiate tumor growth

in transplantation experiments. But in 2008 Quintana *et al.* put this dogma of rare CSCs at least for melanoma into question. They found out that melanoma-initiating cells are only rare in NOD/SCID mice if monitoring tumor formation for a short term, like most researcher do, and using the common assays described in literature. But this frequency could be significantly increased by following melanoma formation for more than eight weeks, using NOD/SCID IL2Rγ^{null} mice that lack natural killer cell activity compared to NOD/SCID mice and injecting melanoma cells together with matrigel, a mixture of structural proteins and growth factors. Overall, after injection of single, unselected melanoma cells, 27% initiated a tumor suggesting that so far the frequency of melanoma-initiating cells was significantly underestimated (Quintana *et al.* 2008).

This is concordant with results from the xenotransplantation experiments I did in collaboration with EPO GmbH. All melanoma subpopulations tested (i.e. CD133$^+$, CD133$^-$, OCT4$^+$, OCT4$^-$) were tumorigenic. Nevertheless, both positive fractions were more tumorigenic after injecting 10^5 cells. They induced faster growing tumors and OCT4-EGFP$^+$ melanoma cells initiated tumors earlier compared to OCT4-EGFP$^-$ cells. However, not for every time point differences in tumor volume between marker-positive and marker-negative cells were significant. Post sorting stress response is one possible explanation that I did not observe greater differences. The CD133-specific magnetic sorting as well as the FACS-sorting of OCT4-EGFP-transfected melanoma cells induces greater stress to the marker-positive CSC fractions. During the MACS procedure CD133$^+$ cells are labeled with anti-CD133 antibody and magnetic beads and remain in the sorting-columns for a longer period compared to CD133$^-$ cells. Furthermore, it is known from *in vitro* experiments that the magnetic beads can stay bound to the cells for several weeks, which may negatively influence the viability and tumorigenicity of CD133$^+$ cells. The same is true for OCT4-EGFP$^+$ cells. Here of course the stress during FACS-sorting was equal to all cells and to recover from sorting stress OCT4-EGFP-transfected cells were cultured for five days after FACS before they were used for xenotransplantation. But the expression of EGFP in OCT4-EGFP$^+$ cells eventually reduced their viability. In 1999 Liu *et al*. showed for the first time that expression of EGFP can induce apoptosis in human cell lines (Liu *et al.* 1999). This would have disadvantaged OCT4-EGFP$^+$ melanoma cells during xenotransplantation experiments.

The amount of tumor-initiating cells is influenced by the experimental setup like enzyme treatment during the preparation of the cell suspensions. Detachment of adherent cells might decrease the viability of tumor cells and modify protein expression, thereby affecting the population into which the cells are sorted and the ability of these proteins to

play a role in tumor formation following transplantation (Hill 2006). By the use of accutase instead of the widely used trypsin in my experiments I tried to minimize these potentially negative effects. According to the manufacturer PAA accutase is a mixture of enzymes, which more gently detaches adherent cells without decreasing cell viability but protecting surface epitopes. However, also the use of accutase cannot entirely exclude negative influences on cell viability and tumorigenicity. These might be explanations for our unsuccessful attempts of xenotransplantations with fewer than 10^5 injected cells. Those experiments resulted in delayed tumor development and large variances of tumor volumes among the replicate of each subpopulation and could not be evaluated. Nevertheless, with 10^5 injected cells per xenotransplantion we established an efficient mouse model together with EPO Gbmh, which is currently commercially used for pre-clinical *in vivo* drug testings.

The fact that marker-positive as well as marker-negative cells induced tumors in NSR mice can also be explained by the dynamic equilibrium between CSCs and non-CSCs. Observations in breast cancer lines by Gupta *et al*. as well as my long-term observations of the CD133 fluctuations in melanoma cells *in vitro* indicate that cells in CSC-depleted fractions give rise to cells expressing marker profiles of CSCs (see 4.4). If a similar interconversion occurs after *in vivo* injection, a prediction would be that CSC-depleted fractions would give rise to tumors if they survived long enough at the site of implantation to regenerate CSCs (Gupta *et al.* 2011). The use of severely immunosuppressive NSR mice in our experiments could facilitate the survival of injected tumor cells and the cell state transition necessary to produce tumorigenic CSCs. Furthermore, we diluted tumor cell suspensions 1:1 with matrigel prior to injection as described by Quintana *et al*. (Quintana *et al.* 2008). Matrigel represents a rich store of matrix proteins as well as angiogenic and growth factors, which promote tumor growth and metastasis (Kleinman *et al.* 2005).

With this modified assay Quintana *et al.* provided a good example of the importance of interactions between tumor cells and their extracellular matrix and how they dictate whether or not a tumor develops from a mutated cell. But still the aberrant extracellular matrix of immunodeficient mice cannot substitute for all factors of the human microenvironment, and the stem cell niche which is crucial to initiate tumor growth is not reconstituted in xenotransplantation models (Bissell *et al.* 2005). This is supported by studies, which show that the frequency of cells that sustain tumor growth was dramatically increased using allograft transplantation models (Kelly *et al.* 2007).

After all, one has to bear in mind that all these experiments and findings about CSCs are based on *in vitro* models, which might not reflect the complexity of the human body. In

2009 Schatton and Frank proposed that CSCs in human melanoma that express the chemoresistance mediator ABCB5 might be responsible for melanoma immune evasion (Schatton *et al.* 2009a). Recently, the results of Di Tomaso *et al*. indicated lower immunogenicity and higher suppressive activity of glioblastoma CSCs compared to their non-CSC counterparts (Di Tomaso *et al.* 2010). Thus, immunomodulation might represent the key mechanism by which CSCs promote tumorigenic growth.

4.7 Categorization of CSCs

A far more trans-disciplinary approach to learn about the early events in tumorigenesis could be the analysis and comparison of CSCs and induced pluripotent stem (iPS) cells. In 2006 Takahashi and Yamanaka were the first who successfully reversed differentiated mouse embryonic or adult fibroblasts into pluripotent stem cells by introducing only the four factors Oct3/4, Sox2, c-Myc and Klf4 and named these reprogrammed cells which exhibit the morphology and growth properties of embryonic stem (ES) cells and express ES cell marker genes, induced pluripotent stem cells (Takahashi *et al.* 2006). After inducing somatic cells with these four "Yamanaka factors", Mikkelsen and colleagues found out that about 20% of the cells stained positive for the stem-cell marker SSEA1, but only about 1.2% were fully reprogrammed. Whereas fully reprogrammed cells showed gene expression and epigenetic states similar to that of ES cells, gene expression profiling revealed that partially reprogrammed cells reactivated only a small group of genes related to stem cell renewal and maintenance, but yet these cells are not pluripotent. Instead they exhibit a downregulation of structural genes and regulatory factors expressed in differentiated cells and upregulation of some lineage-specific and proliferative genes not expressed in iPS cells (Mikkelsen *et al.* 2008). Potentially, the same is true for cancer stem cells. Probably they represent an intermediate state between stem cells and differentiated tumor cells like partially reprogrammed cells do between iPS cells and differentiated cells (compare **Figure 4.1**). Mikkelsen *et al.* showed that these differences are due to epigenetic events like persistent DNA hypermethylation at pluripotency- and germ-cell-specific loci (Mikkelsen *et al.* 2008). DNA de-methylation is an inefficient step in the transition to pluripotency. Several groups demonstrated that treatment with small molecules like the histone deacetylase inhibitor valproic acid, the DNA methyltransferase inhibitor 5-aza-cytidine or the kinase inhibitor kenpaullone can improve the overall efficiency of the reprogramming process by modeling epigenetic information (Huangfu *et al.* 2008, Lyssiotis *et al.* 2009, Wernig *et al.* 2008).

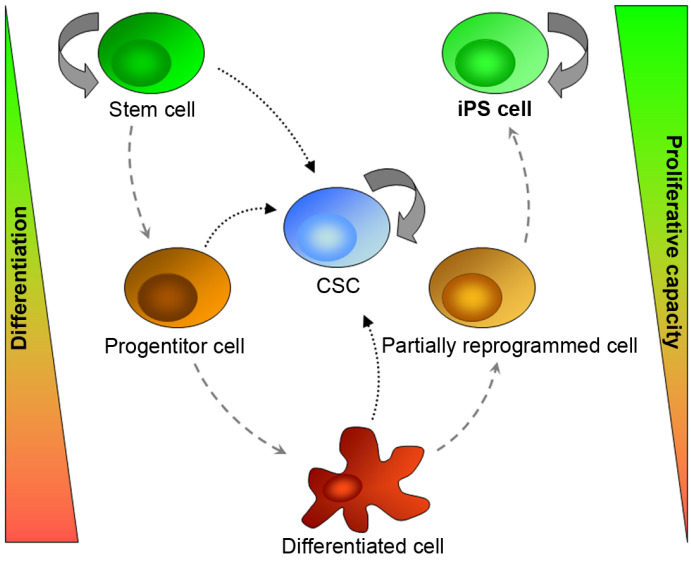

Figure 4.1: Relationship between stem cell species. Stem cells are characterized by their ability to form many different types of tissues and their capacity to self-renew. With increasing level of differentiation from progenitor cell to differentiated cell, the plasticity reduces, as does the proliferative capacity. Cancer stem cells form at the interface between stem cell and progenitor cells. This phenomenon has lately also been credited to iPS cells and their partially reprogrammed precursors.

In my work this 'intermediate' state of CSCs is indicated by the expression and activation of some crucial stem cell genes and pathways like shown for OCT4A and the TGF-β signaling cascade but absence of other important stem cell characteristics like expression of *GDF3* and *LIN28*. Furthermore, OCT4^{+} melanoma cells comprise both the characteristics of stem-like cells and malignant tumors as indicated by high tumor-initiating and migratory capabilities as well as the ability to grow anchorage-independent. My findings provide evidence that cancer cells oscillate between different states in a dynamic equilibrium as shown by fluctuations of CD133 expression. This observation is concordant with the transient state of partially reprogrammed cells. Epigenetic modeling of cancer cells might guide directed transition between CSC- and non stem-like states as observed for iPS cells. Additional investigations are needed to classify CSCs in melanoma and other tumors and further characterize them.

5 Conclusion and perspectives

In my work I identified OCT4$^+$ melanoma cells, which comprise both the characteristics of stem-like cells and malignant tumors and provide strict criteria for self-renewal and asymmetric cell division to hold up the term of stem cell-like cells in solid tumors. My findings provide further evidence to what has already been published on cancer stem cells and the shift in paradigms related hereto. Until today the origin of cancer stem cells and their defining properties remain elusive, but at least for melanomas defining CSCs by the expression of the pluripotency factor OCT4A might be possible.

Among the properties specific for OCT4$^+$ melanoma cells I identified Wnt, Notch and Hedgehog pathways, which associate with the maintenance of stem cell characteristics in OCT4$^+$ melanoma CSCs. Targeting these pathways in CSCs in combination with "classic" chemotherapeutic agents might be an effective therapeutic strategy. *In vitro* down-regulation of Wnt, Notch and Hedgehog signaling using siRNAs could give first hints about the influence of these pathways on viability and apoptosis of melanoma CSCs. Challenging for the development of new therapies is the heterogeneous and dynamic behavior of tumor cell populations that can substantially hamper successful intervention based on chemotherapy and targeted therapies. The results of my work indicate that a strict top-down organization of stem cell-like populations, which determines tumor fate in a strictly hierarchical order, does not exist. Instead, a dynamic equilibrium between stem cell-like and non-stem cell populations seems to replace the unidirectional process of enlargement and development in melanoma. This plasticity could facilitate tumor survival even under unfavorable environmental conditions and allows for rapid adaptation to changes in tumor microenvironment. Accurate characterization of tumor cell dynamics and interconversion between cell populations will be an important prerequisite for a lasting prevention of tumor recurrence and metastasis. For our further research this calls for a careful investigation of xenograft tumors regarding the presence of CSC-related proteins as OCT4A and CD133 as well as activation of oncogenic drivers like Wnt and Hedgehog signaling.

Future experiments should focus on two main aspects: (a) further investigation of the regulatory mechanisms that influence and control the dynamic cell state transitions. Reversible modifications on the epigenetic level are of particular interest to explain fate switching or cyclic processes between different cellular subpopulations. In addition to DNA methylation also chromatin condensation, histone modification or acetylation of proteins can influence tumor heterogeneity. Furthermore, regulation by microRNAs might play a significant role in tumor cell plasticity and the metastatic phenotype. They have

been shown to be incorporated into a large regulatory network to control the self-renewal of stem cells e.g. by regulating key pluripotency factors like OCT4 and that they function as regulators of signal transduction in cancer. (b) exploitation of key regulatory signaling pathways for therapeutic intervention. I found a number of potentially significant signaling molecules overactivated in putative CSCs, including Wnt signaling molecules as well as CD133 and OCT4A. Molecules involved in these pathways could potentially make good targets in gene therapy together with classical chemotherapeutic agents to circumvent the escape mechanisms of tumor cells by interconversion between stem cell-like and non-stem cell populations. In order to apply inhibitors against the above named targets, one has to envision an application strategy that is more localized than today's treatment options. One way to precisely target cutaneous melanomas is the jet-injection technology. Jet-injection is gaining increasing acceptance as nonviral gene delivery technology (Mitragotri 2006). The principle is based on the use of fluid jets at high velocity and it allows gene transfer with deep penetration of the naked DNA and high transfer efficiencies (Walther *et al.* 2009). The results of a phase I-study demonstrate that the use of jet-injection could be employed for the treatment of patients with skin metastases of malignant melanoma (Walther *et al.* 2008). It has also been shown that intratumoral jet-injection of shRNA expressing vectors targeting ABCB1 is sufficient to reconvert drug resistant tumors into chemo sensitive tumors (Stein *et al.* 2008). Local application of shRNA expressing vectors targeting Wnt signaling molecules, CD133 or OCT4A in tumor lesions in combination with chemotherapeutics could improve future melanoma therapy.

In conclusion, my approach of combining knowledge and experiments from stem cell and cancer research enabled the identification of cancer stem cells and provided new insights into how melanomas develop, propagate and potentially evade treatment. I am confident that consequent use of this interdisciplinary approach will provide us with new understandings that in the future might lead to new therapeutic strategies to fight cancer.

References

Adewumi O, Aflatoonian B, Ahrlund-Richter L *et al*. Characterization of human embryonic stem cell lines by the International Stem Cell Initiative**.** *Nat Biotechnol.* **2007**, 25(7)**:**803-816.

Allenspach EJ, Maillard I, Aster JC *et al*. Notch signaling in cancer**.** *Cancer biology & therapy.* **2002**, 1(5)**:**466-476.

Amit M, Carpenter MK, Inokuma MS *et al*. Clonally derived human embryonic stem cell lines maintain pluripotency and proliferative potential for prolonged periods of culture**.** *Dev Biol.* **2000**, 227(2)**:**271-278.

Amit M, Shariki C, Margulets V *et al*. Feeder layer- and serum-free culture of human embryonic stem cells**.** *Biol Reprod.* **2004**, 70(3)**:**837-845.

Asakura A, Rudnicki MA. Side population cells from diverse adult tissues are capable of in vitro hematopoietic differentiation**.** *Exp Hematol.* **2002**, 30(11)**:**1339-1345.

Atlasi Y, Mowla SJ, Ziaee SA *et al*. OCT4 spliced variants are differentially expressed in human pluripotent and nonpluripotent cells**.** *Stem Cells.* **2008**, 26(12)**:**3068-3074.

Baba T, Convery PA, Matsumura N *et al*. Epigenetic regulation of CD133 and tumorigenicity of CD133+ ovarian cancer cells**.** *Oncogene.* **2009**, 28(2)**:**209-218.

Balbuena J, Pachon G, Lopez-Torrents G *et al*. ABCG2 is required to control the sonic hedgehog pathway in side population cells with stem-like properties**.** *Cytometry Part A : the journal of the International Society for Analytical Cytology.* **2011**, 79(9)**:**672-683.

Balch CM, Soong S, Ross MI *et al*. Long-term results of a multi-institutional randomized trial comparing prognostic factors and surgical results for intermediate thickness melanomas (1.0 to 4.0 mm). Intergroup Melanoma Surgical Trial**.** *Ann Surg Oncol.* **2000**, 7(2)**:**87-97.

Balch CM, Soong SJ, Atkins MB *et al*. An evidence-based staging system for cutaneous melanoma**.** *CA Cancer J Clin.* **2004**, 54(3)**:**131-149; quiz 182-134.

Balch CM, Wilkerson JA, Murad TM *et al*. The prognostic significance of ulceration of cutaneous melanoma**.** *Cancer.* **1980**, 45(12)**:**3012-3017.

Bandarchi B, Ma L, Navab R *et al*. From melanocyte to metastatic malignant melanoma**.** *Dermatol Res Pract.* **2010**, 2010(

Becker JC, Houben R, Schrama D *et al*. Mouse models for melanoma: a personal perspective**.** *Exp Dermatol.* **2009**, 19(2)**:**157-164.

Bertolini G, Roz L, Perego P *et al*. Highly tumorigenic lung cancer CD133+ cells display stem-like features and are spared by cisplatin treatment**.** *Proc Natl Acad Sci U S A.* **2009**, 106(38)**:**16281-16286.

Bhattacharya S, Jackson JD, Das AV *et al*. Direct identification and enrichment of retinal stem cells/progenitors by Hoechst dye efflux assay**.** *Invest Ophthalmol Vis Sci.* **2003**, 44(6)**:**2764-2773.

Bissell MJ, Labarge MA. Context, tissue plasticity, and cancer: are tumor stem cells also regulated by the microenvironment? *Cancer Cell.* **2005**, 7(1)**:**17-23.

Bittner M, Meltzer P, Chen Y *et al*. Molecular classification of cutaneous malignant melanoma by gene expression profiling**.** *Nature.* **2000**, 406(6795)**:**536-540.

Blanpain C, Mohrin M, Sotiropoulou PA *et al*. DNA-damage response in tissue-specific and cancer stem cells**.** *Cell Stem Cell.* **2011**, 8(1)**:**16-29.

Boyer LA, Lee TI, Cole MF *et al.* Core transcriptional regulatory circuitry in human embryonic stem cells**.** *Cell.* **2005**, 122(6)**:**947-956.

Bradford PT, Goldstein AM, McMaster ML *et al.* Acral lentiginous melanoma: incidence and survival patterns in the United States, 1986-2005**.** *Arch Dermatol.* **2009**, 145(4)**:**427-434.

Breslow A. Tumor thickness, level of invasion and node dissection in stage I cutaneous melanoma**.** *Ann Surg.* **1975**, 182(5)**:**572-575.

Breus O, Panasyuk G, Gout IT *et al.* CoA synthase is in complex with p85alphaPI3K and affects PI3K signaling pathway**.** *Biochem Biophys Res Commun.* **2009**, 385(4)**:**581-585.

Buitrago W, Roop DR. Oct-4: the almighty POUripotent regulator? *J Invest Dermatol.* **2007**, 127(2)**:**260-262.

Burkert J, Otto WR, Wright NA. Side populations of gastrointestinal cancers are not enriched in stem cells**.** *J Pathol.* **2008**, 214(5)**:**564-573.

Buttner P, Garbe C, Bertz J *et al.* Primary cutaneous melanoma. Optimized cutoff points of tumor thickness and importance of Clark's level for prognostic classification**.** *Cancer.* **1995**, 75(10)**:**2499-2506.

Chaffer CL, Brueckmann I, Scheel C *et al.* Normal and neoplastic nonstem cells can spontaneously convert to a stem-like state**.** *Proc Natl Acad Sci U S A.* **2011**, 108(19)**:**7950-7955.

Chapman PB, Hauschild A, Robert C *et al.* Improved survival with vemurafenib in melanoma with BRAF V600E mutation**.** *N Engl J Med.* **2011**, 364(26)**:**2507-2516.

Chaudhary PM, Roninson IB. Expression and activity of P-glycoprotein, a multidrug efflux pump, in human hematopoietic stem cells**.** *Cell.* **1991**, 66(1)**:**85-94.

Cheli Y, Giuliano S, Botton T *et al.* Mitf is the key molecular switch between mouse or human melanoma initiating cells and their differentiated progeny**.** *Oncogene.* **2011**, 30(20)**:**2307-2318.

Chen L, Liu L. Current progress and prospects of induced pluripotent stem cells**.** *Sci China C Life Sci.* **2009**, 52(7)**:**622-636.

Chiba T, Kita K, Zheng YW *et al.* Side population purified from hepatocellular carcinoma cells harbors cancer stem cell-like properties**.** *Hepatology.* **2006**, 44(1)**:**240-251.

Cho YR, Chiang MP. Epidemiology, staging (new system), and prognosis of cutaneous melanoma**.** *Clin Plast Surg.* **2010**, 37(1)**:**47-53.

Clark WH, Jr., Elder DE, Guerry Dt *et al.* A study of tumor progression: the precursor lesions of superficial spreading and nodular melanoma**.** *Hum Pathol.* **1984**, 15(12)**:**1147-1165.

Clark WH, Jr., Elder DE, Van Horn M. The biologic forms of malignant melanoma**.** *Hum Pathol.* **1986**, 17(5)**:**443-450.

Clark WH, Jr., From L, Bernardino EA *et al.* The histogenesis and biologic behavior of primary human malignant melanomas of the skin**.** *Cancer Res.* **1969**, 29(3)**:**705-727.

Clarke MF, Dick JE, Dirks PB *et al.* Cancer stem cells--perspectives on current status and future directions: AACR Workshop on cancer stem cells**.** *Cancer Res.* **2006**, 66(19)**:**9339-9344.

Corbeil D, Roper K, Hellwig A *et al.* The human AC133 hematopoietic stem cell antigen is also expressed in epithelial cells and targeted to plasma membrane protrusions**.** *J Biol Chem.* **2000**, 275(8)**:**5512-5520.

Cress RD, Holly EA. Incidence of cutaneous melanoma among non-Hispanic whites, Hispanics, Asians, and blacks: an analysis of california cancer registry data, 1988-93**.** *Cancer Causes Control.* **1997**, 8(2)**:**246-252.

Cui R, Widlund HR, Feige E *et al*. Central role of p53 in the suntan response and pathologic hyperpigmentation**.** *Cell.* **2007**, 128(5)**:**853-864.

Curtin JA, Fridlyand J, Kageshita T *et al*. Distinct sets of genetic alterations in melanoma**.** *N Engl J Med.* **2005**, 353(20)**:**2135-2147.

Curtin JC, Lorenzi MV. Drug discovery approaches to target Wnt signaling in cancer stem cells**.** *Oncotarget.* **2010**, 1(7)**:**563-577.

Damjanov I, Horvat B, Gibas Z. Retinoic acid-induced differentiation of the developmentally pluripotent human germ cell tumor-derived cell line, NCCIT**.** *Lab Invest.* **1993**, 68(2)**:**220-232.

de Jong J, Looijenga LH. Stem cell marker OCT3/4 in tumor biology and germ cell tumor diagnostics: history and future**.** *Crit Rev Oncog.* **2006**, 12(3-4)**:**171-203.

Deaton AM, Bird A. CpG islands and the regulation of transcription**.** *Genes Dev.* **2011**, 25(10)**:**1010-1022.

Degen WG, van Kempen LC, Gijzen EG *et al*. MEMD, a new cell adhesion molecule in metastasizing human melanoma cell lines, is identical to ALCAM (activated leukocyte cell adhesion molecule)**.** *Am J Pathol.* **1998**, 152(3)**:**805-813.

Di Tomaso T, Mazzoleni S, Wang E *et al*. Immunobiological characterization of cancer stem cells isolated from glioblastoma patients**.** *Clin Cancer Res.* **2010**, 16(3)**:**800-813.

Diepgen TL. [Epidemiology of chronic UV-damage]**.** *J Dtsch Dermatol Ges.* **2005**, 3 Suppl 2(S32-35.

Ding W, Mouzaki M, You H *et al*. CD133+ liver cancer stem cells from methionine adenosyl transferase 1A-deficient mice demonstrate resistance to transforming growth factor (TGF)-beta-induced apoptosis**.** *Hepatology.* **2009**, 49(4)**:**1277-1286.

Dong L, Qi N, Ge RM *et al*. Overexpression of CD133 promotes the phosphorylation of Erk in U87MG human glioblastoma cells**.** *Neurosci Lett.* **2010**, 484(3)**:**210-214.

Dou J, Wen P, Hu W *et al*. Identifying tumor stem-like cells in mouse melanoma cell lines by analyzing the characteristics of side population cells**.** *Cell Biol Int.* **2009**, 33(8)**:**807-815.

Du P, Kibbe WA, Lin SM. lumi: a pipeline for processing Illumina microarray**.** *Bioinformatics.* **2008**, 24(13)**:**1547-1548.

Dubreuil V, Marzesco AM, Corbeil D *et al*. Midbody and primary cilium of neural progenitors release extracellular membrane particles enriched in the stem cell marker prominin-1**.** *J Cell Biol.* **2007**, 176(4)**:**483-495.

Dvash T, Ben-Yosef D, Eiges R. Human embryonic stem cells as a powerful tool for studying human embryogenesis**.** *Pediatr Res.* **2006**, 60(2)**:**111-117.

Dvorak P, Dvorakova D, Hampl A. Fibroblast growth factor signaling in embryonic and cancer stem cells**.** *FEBS Lett.* **2006**, 580(12)**:**2869-2874.

Eigentler TK, Meier F, Keilholz U *et al*. Systemic therapy of metastized melanoma**.** *Der Onkologe.* Springer-Verlag; **2010**, 16(12)**:**1160-1166.

Elwood JM, Gallagher RP, Worth AJ *et al*. Etiological differences between subtypes of cutaneous malignant melanoma: Western Canada Melanoma Study**.** *J Natl Cancer Inst.* **1987**, 78(1)**:**37-44.

Emery CM, Vijayendran KG, Zipser MC *et al.* MEK1 mutations confer resistance to MEK and B-RAF inhibition**.** *Proc Natl Acad Sci U S A.* **2009**, 106(48)**:**20411-20416.

Espada J, Calvo MB, Diaz-Prado S *et al.* Wnt signalling and cancer stem cells**.** *Clin Transl Oncol.* **2009**, 11(7)**:**411-427.

Fan X, Matsui W, Khaki L *et al.* Notch pathway inhibition depletes stem-like cells and blocks engraftment in embryonal brain tumors**.** *Cancer research.* **2006**, 66(15)**:**7445-7452.

Fang D, Nguyen TK, Leishear K *et al.* A tumorigenic subpopulation with stem cell properties in melanomas**.** *Cancer Res.* **2005**, 65(20)**:**9328-9337.

Ferlay J, Parkin DM, Steliarova-Foucher E. Estimates of cancer incidence and mortality in Europe in 2008**.** *Eur J Cancer.* **2010a**, 46(4)**:**765-781.

Ferlay J, Shin HR, Bray F *et al*. GLOBOCAN 2008 v1.2, Cancer Incidence and Mortality Worldwide: IARC CancerBase No. 10 [Internet]. Lyon, France: International Agency for Research on Cancer; 2010 Available from: http://globocan.iarc.fr, accessed on 20/07/2011

Florek M, Haase M, Marzesco AM *et al.* Prominin-1/CD133, a neural and hematopoietic stem cell marker, is expressed in adult human differentiated cells and certain types of kidney cancer**.** *Cell Tissue Res.* **2005**, 319(1)**:**15-26.

Fodde R, Brabletz T. Wnt/beta-catenin signaling in cancer stemness and malignant behavior**.** *Current opinion in cell biology.* **2007**, 19(2)**:**150-158.

Forman SB, Ferringer TC, Peckham SJ *et al.* Is superficial spreading melanoma still the most common form of malignant melanoma? *J Am Acad Dermatol.* **2008**, 58(6)**:**1013-1020.

Frank NY, Margaryan A, Huang Y *et al.* ABCB5-mediated doxorubicin transport and chemoresistance in human malignant melanoma**.** *Cancer Res.* **2005**, 65(10)**:**4320-4333.

Friel AM, Zhang L, Curley MD *et al.* Epigenetic regulation of CD133 and tumorigenicity of CD133 positive and negative endometrial cancer cells**.** *Reprod Biol Endocrinol.* **2010**, 8(147.

Frosina G. The bright and the dark sides of DNA repair in stem cells**.** *J Biomed Biotechnol.* **2010**, 2010(845396.

Fukaya R, Ohta S, Yamaguchi M *et al.* Isolation of cancer stem-like cells from a side population of a human glioblastoma cell line, SK-MG-1**.** *Cancer Lett.* **2009**.

Fukunaga-Kalabis M, Martinez G, Liu ZJ *et al.* CCN3 controls 3D spatial localization of melanocytes in the human skin through DDR1**.** *J Cell Biol.* **2006**, 175(4)**:**563-569.

Fukunaga-Kalabis M, Martinez G, Nguyen TK *et al.* Tenascin-C promotes melanoma progression by maintaining the ABCB5-positive side population**.** *Oncogene.* **2010**, 29(46)**:**6115-6124.

Fusi A, Busse A, Ochsenreiter S *et al*. Expression of stem cell markers in circulating melanoma cells. In *2009 ASCO Annual Meeting Proceedings (Post-Meeting Edition)*. J Clin Oncol 27, No 15S (May 20 Supplement), **2009: e22056** e22056.

Gao Y, Wang X, Han J *et al.* The novel OCT4 spliced variant OCT4B1 can generate three protein isoforms by alternative splicing into OCT4B**.** *J Genet Genomics.* **2010**, 37(7)**:**461-465.

Garbe C, Hauschild A, Volkenandt M *et al*. Deutsche Leitlinie: Malignes Melanom. In *Interdisziplinäre Leitlinien zur Diagnostik und Behandlung von*

Hauttumoren. Edited by Garbe C. Stuttgart, New York: Georg Thieme Verlag; **2005**: 23-25.

Garbe C, Hauschild A, Volkenandt M *et al*. Evidence and interdisciplinary consense-based German guidelines: diagnosis and surveillance of melanoma**.** *Melanoma Res.* **2007**, 17(6)**:**393-399.

Garbe C, Schadendorf D, Stolz W *et al*. Short German guidelines: malignant melanoma**.** *J Dtsch Dermatol Ges.* **2008**, 6 Suppl 1(S9-S14.

Gardiner-Garden M, Frommer M. CpG islands in vertebrate genomes**.** *Journal of molecular biology.* **1987**, 196(2)**:**261-282.

Garibyan L, Fisher DE. How sunlight causes melanoma**.** *Curr Oncol Rep.* **2010**, 12(5)**:**319-326.

Gat U, DasGupta R, Degenstein L *et al*. De Novo hair follicle morphogenesis and hair tumors in mice expressing a truncated beta-catenin in skin**.** *Cell.* **1998**, 95(5)**:**605-614.

Gedye C, Quirk J, Browning J *et al*. Cancer/testis antigens can be immunological targets in clonogenic CD133+ melanoma cells**.** *Cancer immunology, immunotherapy : CII.* **2009**, 58(10)**:**1635-1646.

Gentleman RC, Carey VJ, Bates DM *et al*. Bioconductor: open software development for computational biology and bioinformatics**.** *Genome Biol.* **2004**, 5(10)**:**R80.

Gerrard L, Zhao D, Clark AJ *et al*. Stably transfected human embryonic stem cell clones express OCT4-specific green fluorescent protein and maintain self-renewal and pluripotency**.** *Stem Cells.* **2005**, 23(1)**:**124-133.

Gershenwald JE, Soong SJ, Balch CM. 2010 TNM staging system for cutaneous melanoma...and beyond**.** *Ann Surg Oncol.* **2010**, 17(6)**:**1475-1477.

Ghoshal K, Datta J, Majumder S *et al*. 5-Aza-deoxycytidine induces selective degradation of DNA methyltransferase 1 by a proteasomal pathway that requires the KEN box, bromo-adjacent homology domain, and nuclear localization signal**.** *Mol Cell Biol.* **2005**, 25(11)**:**4727-4741.

Gires O. Lessons from common markers of tumor-initiating cells in solid cancers**.** *Cellular and molecular life sciences : CMLS.* **2011**.

Gola Isasi A, Garcia Zapirain B, Mendez Zorrilla A. Melanomas non-invasive diagnosis application based on the ABCD rule and pattern recognition image processing algorithms**.** *Comput Biol Med.* **2011**.

Goodell MA, Brose K, Paradis G *et al*. Isolation and functional properties of murine hematopoietic stem cells that are replicating in vivo**.** *J Exp Med.* **1996**, 183(4)**:**1797-1806.

Greber B, Lehrach H, Adjaye J. Fibroblast growth factor 2 modulates transforming growth factor beta signaling in mouse embryonic fibroblasts and human ESCs (hESCs) to support hESC self-renewal**.** *Stem Cells.* **2007a**, 25(2)**:**455-464.

Greber B, Lehrach H, Adjaye J. Silencing of core transcription factors in human EC cells highlights the importance of autocrine FGF signaling for self-renewal**.** *BMC Dev Biol.* **2007b**, 7(46.

Greber B, Lehrach H, Adjaye J. Control of early fate decisions in human ES cells by distinct states of TGFbeta pathway activity**.** *Stem Cells Dev.* **2008**, 17(6)**:**1065-1077.

Grichnik JM, Burch JA, Burchette J *et al*. The SCF/KIT pathway plays a critical role in the control of normal human melanocyte homeostasis**.** *J Invest Dermatol.* **1998**, 111(2)**:**233-238.

Grichnik JM, Burch JA, Schulteis RD *et al.* Melanoma, a tumor based on a mutant stem cell? *J Invest Dermatol.* **2006**, 126(1)**:**142-153.

Grskovic B, Ruzicka K, Karimi A *et al.* Cell cycle analysis of the CD133+ and CD133- cells isolated from umbilical cord blood**.** *Clin Chim Acta.* **2004**, 343(1-2)**:**173-178.

Gupta PB, Chaffer CL, Weinberg RA. Cancer stem cells: mirage or reality? *Nat Med.* **2009**, 15(9)**:**1010-1012.

Gupta PB, Fillmore CM, Jiang G *et al.* Stochastic State Transitions Give Rise to Phenotypic Equilibrium in Populations of Cancer Cells**.** *Cell.* **2011**, 146(August 19)**:**633–644.

Hadnagy A, Gaboury L, Beaulieu R *et al.* SP analysis may be used to identify cancer stem cell populations**.** *Exp Cell Res.* **2006**, 312(19)**:**3701-3710.

Haegebarth A, Clevers H. Wnt signaling, lgr5, and stem cells in the intestine and skin**.** *Am J Pathol.* **2009**, 174(3)**:**715-721.

Halaban R, Zhang W, Bacchiocchi A *et al.* PLX4032, a selective BRAF(V600E) kinase inhibitor, activates the ERK pathway and enhances cell migration and proliferation of BRAF melanoma cells**.** *Pigment Cell Melanoma Res.* **2010**, 23(2)**:**190-200.

Hamburger A, Salmon SE. Primary bioassay of human myeloma stem cells**.** *J Clin Invest.* **1977a**, 60(4)**:**846-854.

Hamburger AW, Salmon SE. Primary bioassay of human tumor stem cells**.** *Science.* **1977b**, 197(4302)**:**461-463.

Hanahan D, Weinberg RA. The hallmarks of cancer**.** *Cell.* **2000**, 100(1)**:**57-70.

Hanahan D, Weinberg RA. Hallmarks of cancer: the next generation**.** *Cell.* **2011**, 144(5)**:**646-674.

Hansis C, Grifo JA, Krey LC. Oct-4 expression in inner cell mass and trophectoderm of human blastocysts**.** *Mol Hum Reprod.* **2000**, 6(11)**:**999-1004.

Haraguchi N, Utsunomiya T, Inoue H *et al.* Characterization of a side population of cancer cells from human gastrointestinal system**.** *Stem Cells.* **2006**, 24(3)**:**506-513.

Hauschild A, Agarwala SS, Trefzer U *et al.* Results of a phase III, randomized, placebo-controlled study of sorafenib in combination with carboplatin and paclitaxel as second-line treatment in patients with unresectable stage III or stage IV melanoma**.** *J Clin Oncol.* **2009**, 27(17)**:**2823-2830.

Hill RP. Identifying cancer stem cells in solid tumors: case not proven**.** *Cancer Res.* **2006**, 66(4)**:**1891-1895; discussion 1890.

Hirschmann-Jax C, Foster AE, Wulf GG *et al.* A distinct "side population" of cells in human tumor cells: implications for tumor biology and therapy**.** *Cell Cycle.* **2005**, 4(2)**:**203-205.

Hirschmann-Jax C, Foster AE, Wulf GG *et al.* A distinct "side population" of cells with high drug efflux capacity in human tumor cells**.** *Proc Natl Acad Sci U S A.* **2004**, 101(39)**:**14228-14233.

Hittelman WN, Liao Y, Wang L *et al.* Are cancer stem cells radioresistant? *Future Oncol.* **2010**, 6(10)**:**1563-1576.

Hoath SB, Leahy DG. The organization of human epidermis: functional epidermal units and phi proportionality**.** *J Invest Dermatol.* **2003**, 121(6)**:**1440-1446.

Hoffman LM, Carpenter MK. Characterization and culture of human embryonic stem cells**.** *Nat Biotechnol.* **2005**, 23(6)**:**699-708.

Huangfu D, Maehr R, Guo W *et al.* Induction of pluripotent stem cells by defined factors is greatly improved by small-molecule compounds**.** *Nat Biotechnol.* **2008**, 26(7)**:**795-797.

Hussein D, Punjaruk W, Storer LC *et al.* Pediatric brain tumor cancer stem cells: cell cycle dynamics, DNA repair, and etoposide extrusion**.** *Neuro Oncol.* **2011**, 13(1)**:**70-83.

Ieta K, Tanaka F, Haraguchi N *et al.* Biological and genetic characteristics of tumor-initiating cells in colon cancer**.** *Ann Surg Oncol.* **2008**, 15(2)**:**638-648.

Ihaka R, Gentleman R. R: A Language for Data Analysis and Graphics**.** *J Comput Graph Stat.* **1996**, 5(3)**:**299-314.

Iliopoulos D, Hirsch HA, Wang G *et al.* Inducible formation of breast cancer stem cells and their dynamic equilibrium with non-stem cancer cells via IL6 secretion**.** *Proc Natl Acad Sci U S A.* **2011**, 108(4)**:**1397-1402.

Jacob F. Expression of embryonic characters by malignant cells**.** *Ciba Found Symp.* **1983**, 96(4-27.

Jaksch M, Munera J, Bajpai R *et al.* Cell cycle-dependent variation of a CD133 epitope in human embryonic stem cell, colon cancer, and melanoma cell lines**.** *Cancer Res.* **2008**, 68(19)**:**7882-7886.

Jensen JB, Parmar M. Strengths and limitations of the neurosphere culture system**.** *Mol Neurobiol.* **2006**, 34(3)**:**153-161.

Jiang L, Li J, Song L. Bmi-1, stem cells and cancer**.** *Acta Biochim Biophys Sin (Shanghai).* **2009**, 41(7)**:**527-534.

Jimbow K, Lee SK, King MG *et al.* Melanin pigments and melanosomal proteins as differentiation markers unique to normal and neoplastic melanocytes**.** *J Invest Dermatol.* **1993**, 100(3)**:**259S-268S.

Joseph EW, Pratilas CA, Poulikakos PI *et al.* The RAF inhibitor PLX4032 inhibits ERK signaling and tumor cell proliferation in a V600E BRAF-selective manner**.** *Proc Natl Acad Sci U S A.* **2010**, 107(33)**:**14903-14908.

Kähler KC, Egberts F, Hauschild F *et al.* Adjuvante systemische Therapie des Melanoms. *Hautarzt.* Springer-Verlag; **2011**, 62(414-422.

Kanehisa M, Goto S, Furumichi M *et al.* KEGG for representation and analysis of molecular networks involving diseases and drugs**.** *Nucleic Acids Res.* **2010**, 38(Database issue)**:**D355-360.

Kang HB, Kim JS, Kwon HJ *et al.* Basic fibroblast growth factor activates ERK and induces c-fos in human embryonic stem cell line MizhES1**.** *Stem Cells Dev.* **2005**, 14(4)**:**395-401.

Kaplan DH. In vivo function of Langerhans cells and dermal dendritic cells**.** *Trends Immunol.* **2010**, 31(12)**:**446-451.

Katoh Y, Katoh M. Comparative genomics on PROM1 gene encoding stem cell marker CD133**.** *International journal of molecular medicine.* **2007**, 19(6)**:**967-970.

Keilholz U, Tilgen W, Hohenberger W. Systemische Therapie des metastasierten Melanoms: Ergebnisse randomisierter Studien der letzten zehn Jahre**.** *Deutsches Ärzteblatt.* **2003**, 100(16)**:**A-1054.

Kelly PN, Dakic A, Adams JM *et al.* Tumor growth need not be driven by rare cancer stem cells**.** *Science.* **2007**, 317(5836)**:**337.

Keshet GI, Goldstein I, Itzhaki O *et al.* MDR1 expression identifies human melanoma stem cells**.** *Biochem Biophys Res Commun.* **2008**, 368(4)**:**930-936.

Klein WM, Wu BP, Zhao S *et al.* Increased expression of stem cell markers in malignant melanoma**.** *Mod Pathol.* **2007**, 20(1)**:**102-107.

Kleinman HK, Martin GR. Matrigel: basement membrane matrix with biological activity**.** *Semin Cancer Biol.* **2005**, 15(5)**:**378-386.

Kobari L, Giarratana MC, Pflumio F *et al*. CD133+ cell selection is an alternative to CD34+ cell selection for ex vivo expansion of hematopoietic stem cells**.** *J Hematother Stem Cell Res.* **2001**, 10(2)**:**273-281.

Kondo T, Setoguchi T, Taga T. Persistence of a small subpopulation of cancer stem-like cells in the C6 glioma cell line**.** *Proc Natl Acad Sci U S A.* **2004**, 101(3)**:**781-786.

Korinek V, Barker N, Moerer P *et al*. Depletion of epithelial stem-cell compartments in the small intestine of mice lacking Tcf-4**.** *Nat Genet.* **1998**, 19(4)**:**379-383.

Krivtsov AV, Twomey D, Feng Z *et al*. Transformation from committed progenitor to leukaemia stem cell initiated by MLL-AF9**.** *Nature.* **2006**, 442(7104)**:**818-822.

Kruger JA, Kaplan CD, Luo Y *et al*. Characterization of stem cell-like cancer cells in immune-competent mice**.** *Blood.* **2006**, 108(12)**:**3906-3912.

Kukekov VG, Laywell ED, Thomas LB *et al*. A nestin-negative precursor cell from the adult mouse brain gives rise to neurons and glia**.** *Glia.* **1997**, 21(4)**:**399-407.

Laga AC, Lai CY, Zhan Q *et al*. Expression of the embryonic stem cell transcription factor SOX2 in human skin: relevance to melanocyte and merkel cell biology**.** *Am J Pathol.* **2010**, 176(2)**:**903-913.

Langmead B, Trapnell C, Pop M *et al*. Ultrafast and memory-efficient alignment of short DNA sequences to the human genome**.** *Genome Biol.* **2009**, 10(3)**:**R25.

Larue L, Delmas V. The WNT/Beta-catenin pathway in melanoma**.** *Front Biosci.* **2006**, 11(733-742.

LeBoit PE, Burg G, Weedon D *et al*. (Eds.) World Health Organization Classification of Tumours: Pathology & Genetics of Skin Tumours. *IARC Press*: Lyon **2006**.

Lee J, Kim HK, Rho JY *et al*. The human OCT-4 isoforms differ in their ability to confer self-renewal**.** *J Biol Chem.* **2006**, 281(44)**:**33554-33565.

Lee JT, Li L, Brafford PA *et al*. PLX4032, a potent inhibitor of the B-Raf V600E oncogene, selectively inhibits V600E-positive melanomas**.** *Pigment Cell Melanoma Res.* **2010**, 23(6)**:**820-827.

Legg J, Jensen UB, Broad S *et al*. Role of melanoma chondroitin sulphate proteoglycan in patterning stem cells in human interfollicular epidermis**.** *Development.* **2003**, 130(24)**:**6049-6063.

Lessard J, Sauvageau G. Bmi-1 determines the proliferative capacity of normal and leukaemic stem cells**.** *Nature.* **2003**, 423(6937)**:**255-260.

Li H, Handsaker B, Wysoker A *et al*. The Sequence Alignment/Map format and SAMtools**.** *Bioinformatics.* **2009**, 25(16)**:**2078-2079.

Lichtenauer UD, Shapiro I, Geiger K *et al*. Side population does not define stem cell-like cancer cells in the adrenocortical carcinoma cell line NCI h295R**.** *Endocrinology.* **2008**, 149(3)**:**1314-1322.

Liedtke S, Stephan M, Kogler G. Oct4 expression revisited: potential pitfalls for data misinterpretation in stem cell research**.** *Biol Chem.* **2008**, 389(7)**:**845-850.

Lim YC, Oh SY, Cha YY *et al.* Cancer stem cell traits in squamospheres derived from primary head and neck squamous cell carcinomas**.** *Oral oncology.* **2011**, 47(2)**:**83-91.

Lin J, Goto Y, Murata H *et al.* Polyclonality of BRAF mutations in primary melanoma and the selection of mutant alleles during progression**.** *Br J Cancer.* **2011**, 104(3)**:**464-468.

Liu G, Yuan X, Zeng Z *et al.* Analysis of gene expression and chemoresistance of CD133+ cancer stem cells in glioblastoma**.** *Mol Cancer.* **2006**, 5(67.

Liu HS, Jan MS, Chou CK *et al.* Is green fluorescent protein toxic to the living cells? *Biochem Biophys Res Commun.* **1999**, 260(3)**:**712-717.

Lucarz A, Brand G. Current considerations about Merkel cells**.** *Eur J Cell Biol.* **2007**, 86(5)**:**243-251.

Lyssiotis CA, Foreman RK, Staerk J *et al.* Reprogramming of murine fibroblasts to induced pluripotent stem cells with chemical complementation of Klf4**.** *Proc Natl Acad Sci U S A.* **2009**, 106(22)**:**8912-8917.

Ma I, Allan AL. The role of human aldehyde dehydrogenase in normal and cancer stem cells**.** *Stem Cell Rev.* **2011**, 7(2)**:**292-306.

Makino S. The role of tumor stem-cells in regrowth of the tumor following drastic applications**.** *Acta Unio Int Contra Cancrum.* **1959**, 15(Suppl 1)(196-198.

Malanchi I, Peinado H, Kassen D *et al.* Cutaneous cancer stem cell maintenance is dependent on beta-catenin signalling**.** *Nature.* **2008**, 452(7187)**:**650-653.

Mar BG, Amakye D, Aifantis I *et al.* The controversial role of the Hedgehog pathway in normal and malignant hematopoiesis**.** *Leukemia : official journal of the Leukemia Society of America, Leukemia Research Fund, UK.* **2011**, 25(11)**:**1665-1673.

McGovern VJ, Shaw HM, Milton GW *et al.* Ulceration and prognosis in cutaneous malignant melanoma**.** *Histopathology.* **1982**, 6(4)**:**399-407.

Meng X, Li M, Wang X *et al.* Both CD133+ and CD133- subpopulations of A549 and H446 cells contain cancer-initiating cells**.** *Cancer Sci.* **2009**, 100(6)**:**1040-1046.

Merchant AA, Matsui W. Targeting Hedgehog--a cancer stem cell pathway**.** *Clin Cancer Res.* **2010**, 16(12)**:**3130-3140.

Mikkelsen TS, Hanna J, Zhang X *et al.* Dissecting direct reprogramming through integrative genomic analysis**.** *Nature.* **2008**, 454(7200)**:**49-55.

Mimeault M, Batra SK. Characterization of nonmalignant and malignant prostatic stem/progenitor cells by Hoechst side population method**.** *Methods Mol Biol.* **2009**, 568(139-149.

Mirmohammadsadegh A, Mota R, Gustrau A *et al.* ERK1/2 is highly phosphorylated in melanoma metastases and protects melanoma cells from cisplatin-mediated apoptosis**.** *J Invest Dermatol.* **2007**, 127(9)**:**2207-2215.

Mitragotri S. Current status and future prospects of needle-free liquid jet injectors**.** *Nature reviews Drug discovery.* **2006**, 5(7)**:**543-548.

Mitsutake N, Iwao A, Nagai K *et al.* Characterization of side population in thyroid cancer cell lines: cancer stem-like cells are enriched partly but not exclusively**.** *Endocrinology.* **2007**, 148(4)**:**1797-1803.

Moitra K, Lou H, Dean M. Multidrug efflux pumps and cancer stem cells: insights into multidrug resistance and therapeutic development**.** *Clinical pharmacology and therapeutics.* **2011**, 89(4)**:**491-502.

Montanaro F, Liadaki K, Schienda J *et al.* Demystifying SP cell purification: viability, yield, and phenotype are defined by isolation parameters**.** *Exp Cell Res.* **2004**, 298(1)**:**144-154.

Monzani E, Facchetti F, Galmozzi E *et al.* Melanoma contains CD133 and ABCG2 positive cells with enhanced tumourigenic potential**.** *Eur J Cancer.* **2007**, 43(5)**:**935-946.

Morris RJ. Keratinocyte stem cells: targets for cutaneous carcinogens**.** *J Clin Invest.* **2000**, 106(1)**:**3-8.

Mueller BM, Reisfeld RA. Potential of the scid mouse as a host for human tumors**.** *Cancer Metastasis Rev.* **1991**, 10(3)**:**193-200.

Nading MA, Balch CM, Sober AJ. Implications of the 2009 American Joint Committee on Cancer Melanoma Staging and Classification on dermatologists and their patients**.** *Semin Cutan Med Surg.* **2010**, 29(3)**:**142-147.

Navysany S, Löser C, Dippel E. Surgical treatment of malignant melanoma of the skin**.** *Der Onkologe.* Springer-Verlag; **2010**, 16(12)**:**1131-1139.

Nazarian R, Shi H, Wang Q *et al.* Melanomas acquire resistance to B-RAF(V600E) inhibition by RTK or N-RAS upregulation**.** *Nature.* **2010**, 468(7326)**:**973-977.

Ng PC, Henikoff S. Predicting the effects of amino acid substitutions on protein function**.** *Annual review of genomics and human genetics.* **2006**, 7(61-80.

Nichols J, Zevnik B, Anastassiadis K *et al.* Formation of pluripotent stem cells in the mammalian embryo depends on the POU transcription factor Oct4**.** *Cell.* **1998**, 95(3)**:**379-391.

Noggle SA, James D, Brivanlou AH. A molecular basis for human embryonic stem cell pluripotency**.** *Stem Cell Rev.* **2005**, 1(2)**:**111-118.

O'Connor MD, Kardel MD, Iosfina I *et al.* Alkaline phosphatase-positive colony formation is a sensitive, specific, and quantitative indicator of undifferentiated human embryonic stem cells**.** *Stem Cells.* **2008**, 26(5)**:**1109-1116.

Ohsie SJ, Sarantopoulos GP, Cochran AJ *et al.* Immunohistochemical characteristics of melanoma**.** *Journal of cutaneous pathology.* **2008**, 35(5)**:**433-444.

Oishi N, Wang XW. Novel therapeutic strategies for targeting liver cancer stem cells**.** *International journal of biological sciences.* **2011**, 7(5)**:**517-535.

Orlow SJ. Melanosomes are specialized members of the lysosomal lineage of organelles**.** *J Invest Dermatol.* **1995**, 105(1)**:**3-7.

Ossowski L, Aguirre-Ghiso JA. Dormancy of metastatic melanoma**.** *Pigment Cell Melanoma Res.* **2009**.

Palmieri G, Capone M, Ascierto ML *et al.* Main roads to melanoma**.** *J Transl Med.* **2009**, 7(86.

Pannuti A, Foreman K, Rizzo P *et al.* Targeting Notch to target cancer stem cells**.** *Clin Cancer Res.* **2010**, 16(12)**:**3141-3152.

Paraiso KH, Fedorenko IV, Cantini LP *et al.* Recovery of phospho-ERK activity allows melanoma cells to escape from BRAF inhibitor therapy**.** *Br J Cancer.* **2010**, 102(12)**:**1724-1730.

Park CH, Bergsagel DE, McCulloch EA. Mouse myeloma tumor stem cells: a primary cell culture assay**.** *J Natl Cancer Inst.* **1971**, 46(2)**:**411-422.

Park KS, Martelotto LG, Peifer M *et al.* A crucial requirement for Hedgehog signaling in small cell lung cancer**.** *Nat Med.* **2011**, 17(11)**:**1504-1508.

Patel K, Dickson J, Din S *et al.* Targeting of 5-aza-2'-deoxycytidine residues by chromatin-associated DNMT1 induces proteasomal degradation of the free enzyme**.** *Nucleic Acids Res.* **2010**, 38(13)**:**4313-4324.

Patnana M, Bronstein Y, Szklaruk J *et al.* Multimethod imaging, staging, and spectrum of manifestations of metastatic melanoma**.** *Clin Radiol.* **2011**, 66(3)**:**224-236.

Patrawala L, Calhoun T, Schneider-Broussard R *et al.* Side population is enriched in tumorigenic, stem-like cancer cells, whereas ABCG2+ and ABCG2- cancer cells are similarly tumorigenic**.** *Cancer Res.* **2005**, 65(14)**:**6207-6219.

Pellacani D, Packer RJ, Frame FM *et al.* Regulation of the stem cell marker CD133 is independent of promoter hypermethylation in human epithelial differentiation and cancer**.** *Mol Cancer.* **2011**, 10(1)**:**94.

Perego M, Tortoreto M, Tragni G *et al.* Heterogeneous phenotype of human melanoma cells with in vitro and in vivo features of tumor-initiating cells**.** *J Invest Dermatol.* **2010**, 130(7)**:**1877-1886.

Pfenninger CV, Roschupkina T, Hertwig F *et al.* CD133 is not present on neurogenic astrocytes in the adult subventricular zone, but on embryonic neural stem cells, ependymal cells, and glioblastoma cells**.** *Cancer Res.* **2007**, 67(12)**:**5727-5736.

Platet N, Mayol JF, Berger F *et al.* Fluctuation of the SP/non-SP phenotype in the C6 glioma cell line**.** *FEBS Lett.* **2007**, 581(7)**:**1435-1440.

Poulikakos PI, Solit DB. Resistance to MEK inhibitors: should we co-target upstream? *Science signaling.* **2011**, 4(166)**:**pe16.

Prasmickaite L, Engesaeter BO, Skrbo N *et al.* Aldehyde dehydrogenase (ALDH) activity does not select for cells with enhanced aggressive properties in malignant melanoma**.** *PLoS ONE.* **2010**, 5(5)**:**e10731.

Quintana E, Shackleton M, Sabel MS *et al.* Efficient tumour formation by single human melanoma cells**.** *Nature.* **2008**, 456(7222)**:**593-598.

Quirbt I, Verma S, Petrella T *et al.* Temozolomide for the treatment of metastatic melanoma**.** *Curr Oncol.* **2007**, 14(1)**:**27-33.

Quirici N, Soligo D, Caneva L *et al.* Differentiation and expansion of endothelial cells from human bone marrow CD133(+) cells**.** *Br J Haematol.* **2001**, 115(1)**:**186-194.

R Development Core Team. *R: A language and environment for statistical computing.* Vienna Austria: R Foundation for Statistical Computing; **2008**.

Radovic-Kovacevic V, Pekmezovic T, Adanja B *et al.* [Survival analysis in patients with cutaneous malignant melanoma]**.** *Srp Arh Celok Lek.* **1997**, 125(5-6)**:**132-137.

Ramgolam K, Lauriol J, Lalou C *et al.* Melanoma spheroids grown under neural crest cell conditions are highly plastic migratory/invasive tumor cells endowed with immunomodulator function**.** *PLoS ONE.* **2011**, 6(4)**:**e18784.

Rao BM, Zandstra PW. Culture development for human embryonic stem cell propagation: molecular aspects and challenges**.** *Curr Opin Biotechnol.* **2005**, 16(5)**:**568-576.

Rappa G, Fodstad O, Lorico A. The stem cell-associated antigen CD133 (Prominin-1) is a molecular therapeutic target for metastatic melanoma**.** *Stem Cells.* **2008**, 26(12)**:**3008-3017.

Regenbrecht CR, Lehrach H, Adjaye J. Stemming Cancer: Functional Genomics of Cancer Stem Cells in Solid Tumors**.** *Stem Cell Rev.* **2008**.

Reya T, Clevers H. Wnt signalling in stem cells and cancer**.** *Nature.* **2005**, 434(7035)**:**843-850.

Reya T, Morrison SJ, Clarke MF *et al*. Stem cells, cancer, and cancer stem cells**.** *Nature.* **2001**, 414(6859)**:**105-111.

Reynolds BA, Tetzlaff W, Weiss S. A multipotent EGF-responsive striatal embryonic progenitor cell produces neurons and astrocytes**.** *J Neurosci.* **1992a**, 12(11)**:**4565-4574.

Reynolds BA, Weiss S. Generation of neurons and astrocytes from isolated cells of the adult mammalian central nervous system**.** *Science.* **1992b**, 255(5052)**:**1707-1710.

Robinson JT, Thorvaldsdottir H, Winckler W *et al*. Integrative genomics viewer**.** *Nat Biotechnol.* **2011**, 29(1)**:**24-26.

Roesch A, Fukunaga-Kalabis M, Schmidt EC *et al*. A temporarily distinct subpopulation of slow-cycling melanoma cells is required for continuous tumor growth**.** *Cell.* **2010**, 141(4)**:**583-594.

Romano E, Schwartz GK, Chapman PB *et al*. Treatment implications of the emerging molecular classification system for melanoma**.** *Lancet Oncol.* **2011**.

Ropolo M, Daga A, Griffero F *et al*. Comparative analysis of DNA repair in stem and nonstem glioma cell cultures**.** *Mol Cancer Res.* **2009**, 7(3)**:**383-392.

Rosner MH, Vigano MA, Ozato K *et al*. A POU-domain transcription factor in early stem cells and germ cells of the mammalian embryo**.** *Nature.* **1990**, 345(6277)**:**686-692.

Rozen S, Skaletsky H. Primer3 on the WWW for general users and for biologist programmers**.** *Methods Mol Biol.* **2000**, 132(365-386.

Ruiz i Altaba A. Gli proteins and Hedgehog signaling: development and cancer**.** *Trends in genetics : TIG.* **1999**, 15(10)**:**418-425.

Salcido CD, Larochelle A, Taylor BJ *et al*. Molecular characterisation of side population cells with cancer stem cell-like characteristics in small-cell lung cancer**.** *British journal of cancer.* **2010**, 102(11)**:**1636-1644.

Saldana-Caboverde A, Kos L. Roles of endothelin signaling in melanocyte development and melanoma**.** *Pigment Cell Melanoma Res.* **2010**, 23(2)**:**160-170.

Scharenberg CW, Harkey MA, Torok-Storb B. The ABCG2 transporter is an efficient Hoechst 33342 efflux pump and is preferentially expressed by immature human hematopoietic progenitors**.** *Blood.* **2002**, 99(2)**:**507-512.

Schatton T, Frank MH. Antitumor immunity and cancer stem cells**.** *Ann N Y Acad Sci.* **2009a**, 1176(154-169.

Schatton T, Frank MH. The in vitro spheroid melanoma cell culture assay: cues on tumor initiation? *J Invest Dermatol.* **2010**, 130(7)**:**1769-1771.

Schatton T, Frank NY, Frank MH. Identification and targeting of cancer stem cells**.** *Bioessays.* **2009b**, 31(10)**:**1038-1049.

Schatton T, Murphy GF, Frank NY *et al*. Identification of cells initiating human melanomas**.** *Nature.* **2008**, 451(7176)**:**345-349.

Schinkel AH, Smit JJ, van Tellingen O *et al*. Disruption of the mouse mdr1a P-glycoprotein gene leads to a deficiency in the blood-brain barrier and to increased sensitivity to drugs**.** *Cell.* **1994**, 77(4)**:**491-502.

Schmidt P, Kopecky C, Hombach A *et al*. Eradication of melanomas by targeted elimination of a minor subset of tumor cells**.** *Proc Natl Acad Sci U S A.* **2011**, 108(6)**:**2474-2479.

Schubert A. [Malignant Melanoma of the Skin: Does Screening for Cancer Influence the Incidence and Mortality?]**.** *Gesundheitswesen.* **2011**.

Scolyer RA, Long GV, Thompson JF. Evolving concepts in melanoma classification and their relevance to multidisciplinary melanoma patient care**.** *Mol Oncol.* **2011**, 5(2)**:**124-136.

Shen G, Shen F, Shi Z *et al*. Identification of cancer stem-like cells in the C6 glioma cell line and the limitation of current identification methods**.** *In Vitro Cell Dev Biol Anim.* **2008**, 44(7)**:**280-289.

Shirakata Y. Regulation of epidermal keratinocytes by growth factors**.** *J Dermatol Sci.* **2010**, 59(2)**:**73-80.

Shmelkov SV, Butler JM, Hooper AT *et al*. CD133 expression is not restricted to stem cells, and both CD133+ and CD133- metastatic colon cancer cells initiate tumors**.** *J Clin Invest.* **2008**, 118(6)**:**2111-2120.

Shultz LD, Ishikawa F, Greiner DL. Humanized mice in translational biomedical research**.** *Nat Rev Immunol.* **2007**, 7(2)**:**118-130.

Siemann DW, Keng PC. Cell cycle specific toxicity of the Hoechst 33342 stain in untreated or irradiated murine tumor cells**.** *Cancer Res.* **1986**, 46(7)**:**3556-3559.

Silva AK, Yi H, Hayes SH *et al*. Lithium chloride regulates the proliferation of stem-like cells in retinoblastoma cell lines: a potential role for the canonical Wnt signaling pathway**.** *Mol Vis.* **2010**, 16(36-45.

Singh SK, Clarke ID, Terasaki M *et al*. Identification of a cancer stem cell in human brain tumors**.** *Cancer Res.* **2003**, 63(18)**:**5821-5828.

Singh SK, Hawkins C, Clarke ID *et al*. Identification of human brain tumour initiating cells**.** *Nature.* **2004**, 432(7015)**:**396-401.

Song J, Chang I, Chen Z *et al*. Characterization of side populations in HNSCC: highly invasive, chemoresistant and abnormal Wnt signaling**.** *PLoS ONE.* **2010**, 5(7)**:**e11456.

Stein U, Walther W, Stege A *et al*. Complete in vivo reversal of the multidrug resistance phenotype by jet-injection of anti-MDR1 short hairpin RNA-encoding plasmid DNA**.** *Molecular therapy : the journal of the American Society of Gene Therapy.* **2008**, 16(1)**:**178-186.

Storey JD. A direct approach to false discovery rates**.** *Journal of the Royal Statistical Society Series B-Statistical Methodology.* **2002**, 64(479-498.

Szotek PP, Pieretti-Vanmarcke R, Masiakos PT *et al*. Ovarian cancer side population defines cells with stem cell-like characteristics and Mullerian Inhibiting Substance responsiveness**.** *Proc Natl Acad Sci U S A.* **2006**, 103(30)**:**11154-11159.

Taipale J, Beachy PA. The Hedgehog and Wnt signalling pathways in cancer**.** *Nature.* **2001**, 411(6835)**:**349-354.

Takahashi K, Yamanaka S. Induction of pluripotent stem cells from mouse embryonic and adult fibroblast cultures by defined factors**.** *Cell.* **2006**, 126(4)**:**663-676.

Takahashi-Yanaga F, Kahn M. Targeting Wnt signaling: can we safely eradicate cancer stem cells? *Clin Cancer Res.* **2010**, 16(12)**:**3153-3162.

Takebe N, Harris PJ, Warren RQ *et al*. Targeting cancer stem cells by inhibiting Wnt, Notch, and Hedgehog pathways**.** *Nat Rev Clin Oncol.* **2011**, 8(2)**:**97-106.

Takeda J, Seino S, Bell GI. Human Oct3 gene family: cDNA sequences, alternative splicing, gene organization, chromosomal location, and expression at low levels in adult tissues**.** *Nucleic Acids Res.* **1992**, 20(17)**:**4613-4620.

Thomson JA, Odorico JS. Human embryonic stem cell and embryonic germ cell lines**.** *Trends Biotechnol.* **2000**, 18(2)**:**53-57.

Tian F, Mysliwietz J, Ellwart J *et al*. Effects of the Hedgehog pathway inhibitor GDC-0449 on lung cancer cell lines are mediated by side populations**.** *Clin Exp Med.* **2011**.

Ting W, Schultz K, Cac NN *et al*. Tanning bed exposure increases the risk of malignant melanoma**.** *Int J Dermatol.* **2007**, 46(12)**:**1253-1257.

Tirino V, Desiderio V, d'Aquino R *et al*. Detection and characterization of CD133+ cancer stem cells in human solid tumours**.** *PLoS ONE.* **2008**, 3(10)**:**e3469.

Toma JG, Akhavan M, Fernandes KJ *et al*. Isolation of multipotent adult stem cells from the dermis of mammalian skin**.** *Nat Cell Biol.* **2001**, 3(9)**:**778-784.

Uong A, Zon LI. Melanocytes in development and cancer**.** *J Cell Physiol.* **2010**, 222(1)**:**38-41.

Vallier L, Alexander M, Pedersen RA. Activin/Nodal and FGF pathways cooperate to maintain pluripotency of human embryonic stem cells**.** *J Cell Sci.* **2005**, 118(Pt 19)**:**4495-4509.

Varjosalo M, Taipale J. Hedgehog: functions and mechanisms**.** *Genes Dev.* **2008**, 22(18)**:**2454-2472.

Villanueva J, Vultur A, Lee JT *et al*. Acquired resistance to BRAF inhibitors mediated by a RAF kinase switch in melanoma can be overcome by cotargeting MEK and IGF-1R/PI3K**.** *Cancer Cell.* **2010**, 18(6)**:**683-695.

Virchow R. *Die Cellularpathologie in ihrer Begrundung auf physiologische und pathologische Gewebelehre.* Berlin: August Hirschwald **1858**.

Vultur A, Villanueva J, Herlyn M. BRAF inhibitor unveils its potential against advanced melanoma**.** *Cancer Cell.* **2010**, 18(4)**:**301-302.

Wagner SN, Somasundaram R, Pinc A *et al*. CD20-immunotargeting of malignant melanoma. In *2010 ASCO Annual Meeting* J Clin Oncol 28:15s, **2010** (suppl; abstr 8565)

Walther W, Fichtner I, Schlag PM *et al*. Nonviral jet-injection technology for intratumoral in vivo gene transfer of naked DNA**.** *Methods Mol Biol.* **2009**, 542(195-208.

Walther W, Siegel R, Kobelt D *et al*. Novel jet-injection technology for nonviral intratumoral gene transfer in patients with melanoma and breast cancer**.** *Clin Cancer Res.* **2008**, 14(22)**:**7545-7553.

Wang J, Guo LP, Chen LZ *et al*. Identification of cancer stem cell-like side population cells in human nasopharyngeal carcinoma cell line**.** *Cancer Res.* **2007**, 67(8)**:**3716-3724.

Wang J, Sakariassen PO, Tsinkalovsky O *et al*. CD133 negative glioma cells form tumors in nude rats and give rise to CD133 positive cells**.** *Int J Cancer.* **2008**, 122(4)**:**761-768.

Wang X, Zhao Y, Xiao Z *et al*. Alternative translation of OCT4 by an internal ribosome entry site and its novel function in stress response**.** *Stem Cells.* **2009a**, 27(6)**:**1265-1275.

Wang XY, Penalva LO, Yuan H *et al*. Musashi1 regulates breast tumor cell proliferation and is a prognostic indicator of poor survival**.** *Mol Cancer.* **2010**, 9(221.

Wang YH, Li F, Luo B *et al*. A side population of cells from a human pancreatic carcinoma cell line harbors cancer stem cell characteristics**.** *Neoplasma.* **2009b**, 56(5)**:**371-378.

Weijzen S, Rizzo P, Braid M *et al.* Activation of Notch-1 signaling maintains the neoplastic phenotype in human Ras-transformed cells**.** *Nat Med.* **2002**, 8(9)**:**979-986.

Welte Y, Adjaye J, Lehrach HR *et al.* Cancer stem cells in solid tumors: elusive or illusive? *Cell Commun Signal.* **2010**, 8(1)**:**6.

Wernig M, Lengner CJ, Hanna J *et al.* A drug-inducible transgenic system for direct reprogramming of multiple somatic cell types**.** *Nat Biotechnol.* **2008**, 26(8)**:**916-924.

Wu C, Alman BA. Side population cells in human cancers**.** *Cancer Lett.* **2008**, 268(1)**:**1-9.

Wysocki AB. Skin anatomy, physiology, and pathophysiology**.** *Nurs Clin North Am.* **1999**, 34(4)**:**777-797, v.

You H, Ding W, Rountree CB. Epigenetic regulation of cancer stem cell marker CD133 by transforming growth factor-beta**.** *Hepatology.* **2010**, 51(5)**:**1635-1644.

Zabierowski SE, Fukunaga-Kalabis M, Li L *et al.* Dermis-derived stem cells: a source of epidermal melanocytes and melanoma? *Pigment Cell Melanoma Res.* **2011**, 24(3)**:**422-429.

Zhao S, Yuan Q, Hao H *et al.* Expression of OCT4 pseudogenes in human tumours: lessons from glioma and breast carcinoma**.** *J Pathol.* **2011**, 223(5)**:**672-682.

Zheng X, Shen G, Yang X *et al.* Most C6 cells are cancer stem cells: evidence from clonal and population analyses**.** *Cancer Res.* **2007**, 67(8)**:**3691-3697.

Zhou S, Morris JJ, Barnes Y *et al.* Bcrp1 gene expression is required for normal numbers of side population stem cells in mice, and confers relative protection to mitoxantrone in hematopoietic cells in vivo**.** *Proc Natl Acad Sci U S A.* **2002**, 99(19)**:**12339-12344.

Zhou S, Schuetz JD, Bunting KD *et al.* The ABC transporter Bcrp1/ABCG2 is expressed in a wide variety of stem cells and is a molecular determinant of the side-population phenotype**.** *Nat Med.* **2001**, 7(9)**:**1028-1034.

Zhou XD, Wang XY, Qu FJ *et al.* Detection of cancer stem cells from the C6 glioma cell line**.** *J Int Med Res.* **2009**, 37(2)**:**503-510.

Appendix

Publications

Welte Y, Davies C, Schäfer R, Regenbrecht CR, "Patient derived cell culture and isolation of $CD133^+$ putative cancer stem cells from melanoma" J Vis Exp, 2013 Mar 13;(73):e50200. DOI: 10.3791/50200

Welte Y, Faust A, Greinert R, Volkmer B, Schäfer R, Regenbrecht CR, "Keep the fate: Malignant melanoma cells can spontaneously acquire a stem cell-like state *in vitro*" Cell Commun Signal, submitted

Welte Y, Wruck W, Fichtner I, Regenbrecht CR, "The role of Oct-4 in melanoma stem cells", Mol Cancer Res, submitted

Jarmalavicius S, **Welte Y**, Walden P, "High immunogenicity of the human leukocyte antigen peptidomes of melanoma tumor cells" J Biol Chem, 2012 Sep 28;287(40):33401-11

Welte Y, Adjaye J, Lehrach HR, Regenbrecht CR, "Cancer stem cells in solid tumors: elusive or illusive?" Cell Commun Signal. 2010 May 11;8(1):6

Regenbrecht CRA, **Welte Y**, Jödicke A, Hugel R, Walden P, Jung M, Lehrach H, Adjaye J, "Molecular characterization of signaling pathways in cancer stem cells", ecancermedicalscience DOI: 10.3332/ecancer.2008.115

Regenbrecht CRA, **Welte Y**, Hugel R, Trefzer U, Losch FO, Adjaye J & Walden P, "Cancer Stem Cells in Melanoma", ecancermedicalscience DOI: 10.3332/ecancer.2008.114

Curriculum vitae

For reasons of data protection, the curriculum vitae is not included in the online version.

Supplementary tables

Table S 1: List of GOs enriched in CD133$^+$ melanoma cells.

Shown are interesting GOs (e.g. related to cancer development), which were significantly (p-value <0.05) overrepresented in CD133$^+$ Pat1T1k melanoma cells compared to CD133$^-$ cells. Count: number of upregulated genes in CD133$^+$ cells assigned to the respective biological process; Size: total number of genes generally assigned to the respective biological process.

GO Biological Process	Count	Size	p-value
translation	56	410	3.49e-25
cellular component organization	129	3254	4.28e-08
gene expression	141	3750	2.01e-07
mitotic cell cycle checkpoint	13	122	1.60e-05
mitotic cell cycle G1/S transition checkpoint	10	74	1.94e-05
G1/S transition checkpoint	10	74	1.94e-05
regulation of G1/S transition of mitotic cell cycle	10	77	2.76e-05
response to copper ion	5	16	3.87e-05
translational initiation	9	66	4.70e-05
mitotic cell cycle G1/S transition DNA damage checkpoint	9	66	4.70e-05
cell cycle arrest	21	316	7.57e-05
S phase of mitotic cell cycle	12	125	9.46e-05
S phase	12	131	1.48e-04
regulation of cell cycle arrest	16	218	1.76e-04
M/G1 transition of mitotic cell cycle	9	78	1.76e-04
G1/S transition of mitotic cell cycle	13	155	1.93e-04
interphase of mitotic cell cycle	20	315	2.06e-04
regulation of mitotic cell cycle	17	247	2.40e-04
cell death	56	1353	2.60e-04
apoptosis	52	1230	2.67e-04
death	56	1355	2.70e-04
interphase	20	323	2.87e-04
programmed cell death	52	1239	3.18e-04
negative regulation of cell cycle	22	376	3.19e-04
transcription	101	2861	3.44e-04
cell cycle checkpoint	15	209	3.55e-04
regulation of cell cycle	29	575	4.66e-04
anti-apoptosis	16	238	4.72e-04
cell cycle	48	1140	5.14e-04
DNA damage response, signal transduction by p53 class mediator	9	94	7.17e-04
DNA integrity checkpoint	10	114	7.37e-04
DNA damage response, signal transduction by p53 class mediator resulting in cell cycle arrest	7	59	7.80e-04
signal transduction involved in cell cycle checkpoint	7	59	7.80e-04
signal transduction involved in DNA integrity checkpoint	7	59	7.80e-04
signal transduction involved in G1/S transition checkpoint	7	59	7.80e-04
signal transduction involved in mitotic cell cycle checkpoint	7	59	7.80e-04
signal transduction involved in DNA damage checkpoint	7	59	7.80e-04
signal transduction involved in mitotic cell cycle G1/S transition DNA damage checkpoint	7	59	7.80e-04
signal transduction involved in mitotic cell cycle G1/S checkpoint	7	59	7.80e-04
negative regulation of programmed cell death	23	431	8.46e-04

positive regulation of cell cycle arrest	7	62	1.05e-03
negative regulation of cell death	23	443	1.22e-03
angiogenesis involved in wound healing	3	9	1.28e-03
wound healing	27	559	1.38e-03
regulation of programmed cell death	41	987	1.73e-03
cellular copper ion homeostasis	3	10	1.79e-03
regulation of cell cycle process	18	323	1.89e-03
mitotic cell cycle	29	634	2.10e-03
regulation of cell death	41	999	2.16e-03
regulation of apoptosis	40	977	2.55e-03
cell cycle phase	31	702	2.56e-03
cell cycle process	36	856	2.69e-03
copper ion homeostasis	3	12	3.17e-03
negative regulation of apoptosis	21	426	3.63e-03
vascular wound healing	2	4	3.86e-03
regulation of vascular wound healing	2	4	3.86e-03
positive regulation of cell cycle process	8	101	4.62e-03
response to wounding	37	917	4.67e-03
regulation of cell division	5	54	1.26e-02
positive regulation of ERK1 and ERK2 cascade	4	38	1.62e-02
germ cell migration	2	8	1.68e-02
cellular homeostasis	22	533	2.10e-02
glial cell migration	2	9	2.13e-02
leukocyte migration	10	184	2.14e-02
cell aging	4	43	2.45e-02
negative regulation of DNA repair	1	1	2.58e-02
negative regulation of calcium-dependent cell-cell adhesion	1	1	2.58e-02
cell adhesion molecule production	1	1	2.58e-02
regulation of cell adhesion molecule production	1	1	2.58e-02
positive regulation of cell adhesion molecule production	1	1	2.58e-02
negative regulation of vascular wound healing	1	1	2.58e-02
negative regulation of wound healing	1	1	2.58e-02
negative regulation of smooth muscle cell-matrix adhesion	1	1	2.58e-02
regulation of interferon-gamma production	4	44	2.64e-02
induction of apoptosis by extracellular signals	7	113	2.72e-02
'de novo' posttranslational protein folding	4	45	2.85e-02
positive regulation of apoptosis	20	491	3.04e-02
positive regulation of programmed cell death	20	495	3.27e-02
regulation of ERK1 and ERK2 cascade	4	47	3.27e-02
epidermal growth factor receptor signaling pathway	6	95	3.64e-02
positive regulation of cell death	20	502	3.70e-02
'de novo' protein folding	4	50	3.98e-02
cell-substrate adhesion	8	150	4.10e-02
vascular endothelial growth factor receptor signaling pathway	3	30	4.15e-02
developmental process	107	3568	4.17e-02
induction of apoptosis	15	355	4.30e-02
induction of programmed cell death	15	357	4.48e-02
cell migration	21	551	4.92e-02

Table S 2: Differential SNPs in coding regions of CD133 sorted melanoma cells.

Using whole transcriptome mRNA sequencing various SNPs were found to be different between CD133+ and CD133- ChaMel91 cells. From all SNPs, which are located in coding sequences only the nucleotide substitution in the COASY gene was SIFT predicted to be damaging for the protein function. Nonsyn: nonsynonymous; Syn: synonymous; NP: not predicted; Tol: tolerated; Dam: damaging.

Coordinates	Sub-stitution	Region	SNP Type	Pre-diction	Gene	SNP details
14,23312594,1	D273N	EXON CDS	Nonsyn	TOL	MMP14	REF:G;CD133+:A/A;CD133-:G/G
1,89449029,1	S161P	EXON CDS	Nonsyn	Tol	RBMXL1	REF:A;CD133+:A/G;CD133-:G/G
1,155186246,1	G188S	EXON CDS	Nonsyn	Tol	GBAP1	REF:C;CD133+:T/T;CD133-:C/T
10,93135,1	T365T	EXON CDS	Syn	Tol	TUBB8	REF:C;CD133+:C/T;CD133-:T/T
12,49297467,1	V203V	EXON CDS	Syn	Tol	ARF3	REF:C;CD133+:C/T;CD133-:T/T
14,70793058,1	T105P	EXON CDS	Nonsyn	Tol	COX16	REF:T;CD133+:G/G;CD133-:T/G
14,81712743,1	H55H	EXON CDS	Syn	Tol	DYNLL1P1	REF:G;CD133+:G/A;CD133-:A/A
16,21847857,1	N617N	EXON CDS	Syn	Tol	RP11-645C24.1	REF:G;CD133+:A/A;CD133-:G/A
17,40714804,1	S55Y	EXON CDS	Nonsyn	Dam	COASY	REF:C;CD133+:A/A;CD133-:C/A
17,66039350,1	V267V	EXON CDS	Syn	Tol	KPNA2	REF:A;CD133+:A/G;CD133-:G/G
2,86756381,1	A189A	EXON CDS	Syn	Tol	FLJ58988	REF:T;CD133+:T/G;CD133-:G/G
2,107039743,1	F1560F	EXON CDS	Syn	Tol	RGPD3	REF:A;CD133+:G/G;CD133-:A/G
2,130832120,1	H975H	EXON CDS	Syn	Tol	POTEF	REF:A;CD133+:G/G;CD133-:A/G
2,130832213,1	D944D	EXON CDS	Syn	Tol	POTEF	REF:A;CD133+:G/G;CD133-:A/G
2,130832669,1	N792N	EXON CDS	Syn	Tol	POTEF	REF:G;CD133+:A/A;CD133-:G/A
2,131221241,1	N792N	EXON CDS	Syn	Tol	POTEI	REF:G;CD133+:A/A;CD133-:G/A
2,131221265,1	K784K	EXON CDS	Syn	Tol	POTEI	REF:C;CD133+:T/T;CD133-:C/T
2,131221349,1	K756N	EXON CDS	Nonsyn	Tol	POTEI	REF:C;CD133+:G/G;CD133-:C/G
2,179406191,1	R23665H	EXON CDS	Nonsyn	NP	TTN	REF:C;CD133+:C/T;CD133-:T/T
20,42089511,1	P281P	EXON CDS	Syn	Tol	SRSF6	REF:T;CD133+:C/C;CD133-:T/C
22,43036027,1	T85M	EXON CDS	Nonsyn	Tol	ATP5L2	REF:G;CD133+:G/A;CD133-:A/A
22,43036061,1	L74V	EXON CDS	Nonsyn	Tol	ATP5L2	REF:A;CD133+:A/C;CD133-:C/C
6,34212743,1	H113R	EXON CDS	Nonsyn	Tol	HMGA1	REF:A;CD133+:G/G;CD133-:A/G
X,134930703,1	Q120R	EXON CDS	Nonsyn	Tol	CT45A4	REF:T;CD133+:C/C;CD133-:T/C

Table S 3: List of GOs enriched in OCT4-EGFP+ melanoma cells.

Shown are interesting GOs (e.g. related to cancer development), which were significantly (p-value <0.05) overrepresented in OCT4-EGFP+ ChaMel91 melanoma cells compared to OCT4-EGFP- cells. Count: number of upregulated genes in OCT4-EGFP+ cells assigned to the respective biological process; Size: total number of genes generally assigned to the respective biological process.

GO Biological Process	Count	Size	p-value
translational elongation	12	103	5.96e-11
translation	19	410	1.44e-09
translational termination	10	92	5.05e-09
cellular process involved in reproduction	14	349	1.41e-06
cellular protein metabolic process	43	2720	1.14e-05
protein metabolic process	46	3182	5.19e-05
cellular metabolic process	85	7636	6.85e-05
ATP metabolic process	7	124	8.54e-05
ATP catabolic process	5	66	2.34e-04
cell cycle phase	16	702	2.68e-04

cell cycle process	18	856	2.91e-04
metabolic process	90	8540	3.11e-04
gene expression	49	3750	3.62e-04
posttranscriptional regulation of gene expression	9	263	3.88e-04
reproductive process	19	964	4.38e-04
reproduction	19	969	4.67e-04
regulation of translational initiation	4	44	5.06e-04
M/G1 transition of mitotic cell cycle	5	78	5.10e-04
cell cycle	21	1140	5.22e-04
regulation of epidermal growth factor receptor activity	3	20	6.03e-04
regulation of cellular protein metabolic process	18	910	6.04e-04
mitotic cell cycle	14	634	9.05e-04
regulation of protein metabolic process	18	968	1.23e-03
regulation of epidermal growth factor receptor signaling pathway	4	56	1.27e-03
ATP biosynthetic process	4	63	1.96e-03
G1/S transition of mitotic cell cycle	6	155	2.91e-03
regulation of translation	6	155	2.01e-03
regulation of receptor activity	3	30	2.02e-03
translational initiation	4	66	2.33e-03
regulation of cell cycle	12	575	3.38e-03
S phase of mitotic cell cycle	5	125	4.14e-03
S phase	5	131	5.05e-03
interphase of mitotic cell cycle	8	315	5.24e-03
T cell mediated immune response to tumor cell	1	1	8.45e-03
regulation of T cell mediated immune response to tumor cell	1	1	8.45e-03
positive regulation of T cell mediated immune response to tumor cell	1	1	8.45e-03
intracellular copper ion transport	1	1	8.45e-03
epidermal growth factor receptor signaling pathway	4	95	8.54e-03
regulation of metabolic process	47	4141	1.11e-02
developmental cell growth	3	56	1.18e-02
DNA damage checkpoint	4	107	1.28e-02
M phase	9	445	1.31e-02
DNA damage response, signal transduction by p53 class mediator resulting in cell cycle arrest	3	59	1.35e-02
signal transduction involved in cell cycle checkpoint	3	59	1.35e-02
signal transduction involved in DNA integrity checkpoint	3	59	1.35e-02
signal transduction involved in G1/S transition checkpoint	3	59	1.35e-02
signal transduction involved in mitotic cell cycle checkpoint	3	59	1.35e-02
signal transduction involved in DNA damage checkpoint	3	59	1.35e-02
signal transduction involved in mitotic cell cycle G1/S transition DNA damage checkpoint	3	59	1.35e-02
signal transduction involved in mitotic cell cycle G1/S checkpoint	3	59	1.35e-02
positive regulation of cell cycle arrest	3	62	1.55e-02
DNA integrity checkpoint	4	114	1.58e-02
canonical Wnt receptor signaling pathway involved in positive regulation of epithelial to mesenchymal transition	1	2	1.68e-02
negative regulation of translational elongation	1	2	1.68e-02
negative regulation of ubiquitin-protein ligase activity involved in mitotic cell cycle	3	65	1.76e-02
cell cycle arrest	7	316	1.77e-02

mitotic cell cycle G1/S transition DNA damage checkpoint	3	66	1.83e-02
regulation of mitotic cell cycle	6	247	1.83e-02
transcription	34	2861	1.90e-02
regulation of cell cycle process	7	323	1.97e-02
positive regulation of ubiquitin-protein ligase activity involved in mitotic cell cycle	3	69	2.06e-02
mitotic cell cycle G1/S transition checkpoint	3	74	2.47e-02
G1/S transition checkpoint	3	74	2.47e-02
regulation of cilium movement	1	3	2.51e-02
cilium movement involved in cell motility	1	3	2.51e-02
regulation of cilium movement involved in cell motility	1	3	2.51e-02
regulation of cilium beat frequency involved in ciliary motility	1	3	2.51e-02
regulation of ubiquitin-protein ligase activity involved in mitotic cell cycle	3	75	2.55e-02
regulation of G1/S transition of mitotic cell cycle	3	77	2.73e-02
developmental growth involved in morphogenesis	3	78	2.83e-02
cell cycle checkpoint	5	209	3.21e-02
regulation of phosphorylation	10	606	3.23e-02
DNA-dependent DNA replication initiation	2	35	3.51e-02
regulation of canonical Wnt receptor signaling pathway	3	85	3.52e-02
negative regulation of epidermal growth factor receptor signaling pathway	2	36	3.70e-02
regulation of cell cycle arrest	5	218	3.75e-02
transmembrane receptor protein tyrosine kinase signaling pathway	9	542	4.00e-02
negative regulation of cell cycle	7	376	4.02e-02
negative regulation of epidermal growth factor receptor activity	1	5	4.15e-02
ciliary cell motility	1	5	4.15e-02
DNA damage response, signal transduction by p53 class mediator	3	94	4.53e-02
sensory cilium assembly	1	6	4.96e-02
copper ion transmembrane transport	1	6	4.96e-02

Table S 4: List of KEGG pathways enriched in OCT4-EGFP$^+$ melanoma cells.
Shown are interesting KEGG pathways (e.g. related to cancer development), which were overrepresented in OCT4-EGFP$^+$ ChaMel91 melanoma cells compared to OCT4-EGFP$^-$ cells. Count: number of upregulated genes in OCT4-EGFP$^+$ cells assigned to the respective pathway; Size: total number of genes generally assigned to the respective pathway.

KEGG generic term	KEGG pathway	Count	Size	p-value
Translation	Ribosome	11	88	2.06e-11
Signal Transduction	Wnt signaling pathway	6	149	5.63e-04
Translation	RNA transport	5	140	2.77e-03
Cell Growth & Death	Oocyte meiosis	4	111	7.12e-03
Cell Growth & Death	Cell cycle	4	122	9.86e-03
Replication & Repair	DNA replication	2	36	2.51e-02
Signal Transduction	Notch signaling pathway	2	47	4.10e-02
Transcription	Spliceosome	3	124	5.33e-02
Metabolism	Metabolic pathways	12	1086	6.85e-02
Folding, Sorting & Degradation	RNA degradation	2	69	8.09e-02
Translation	mRNA surveillance pathway	2	78	0.10
Cell Growth and Death	Apoptosis	2	88	0.12

Cell Communication	Gap junction	2	89	0.12
Cancers	Pathways in cancer	4	322	0.18
Signal Transduction	Hedgehog signaling pathway	1	55	0.31
Xenobiotics Biodegradation & Metabolism	Drug metabolism - cytochrome P450	1	70	0.38
Translation	Ribosome biogenesis in eukaryotes	1	72	0.39
Cell Communication	Adherens junction	1	72	0.39
Signal Transduction	Phosphatidylinositol signaling system	1	78	0.41
Signal Transduction	ErbB signaling pathway	1	86	0.45
Signaling Molecules and Interaction	Cell adhesion molecules (CAMs)	1	128	0.59
Development	Axon guidance	1	129	0.59
Signal Transduction	Jak-STAT signaling pathway	1	153	0.65
Signal Transduction	Calcium signaling pathway	1	174	0.70
Cell Communication	Focal adhesion	1	197	0.74
Cell Motility	Regulation of actin cytoskeleton	1	211	0.77
Signal Transduction	MAPK signaling pathway	1	261	0.84